공학박사 학위논문

Study on ECH-assisted start-up using trapped particle configuration in KSTAR and application to ITER

KSTAR 장치에서 입자가둠 구조와 전자공명가열을 활용한 플라즈마 시동 연구 및 ITER로의 응용

2017 년 2 월

서울대학교 대학원

에너지시스템공학부

이 정 원

Study on ECH-assisted start-up using trapped particle configuration in KSTAR and application to ITER

지도 교수 나 용 수

이 논문을 공학박사 학위논문으로 제출함
2016 년 10 월

서울대학교 대학원
에너지시스템공학부
이 정 원

이 정 원의 공학박사 학위논문을 인준함
2016 년 12 월

위 원 장 황 용 석 (인)

부위원장 나 용 수 (인)

위 원 함 택 수 (인)

위 원 최 원 호 (인)

위 원 김 재 현 (인)

Abstract

Study on ECH-assisted start-up using trapped particle configuration in KSTAR and application to ITER

Lee, Jeongwon

Department of Energy System Engineering

(Fusion & Plasma Engineering)

The Graduate School

Seoul National University

Efficient and reliable ECH (Electron Cyclotron resonance Heating)-assisted start-up using TPC (trapped particle configuration) is demonstrated in conventional, superconducting tokamak, KSTAR and analyzed by a plasma start-up simulator. Characteristics of TPC start-up under the start-up conditions of the magnetic field quality and the prefill pressure are studied. Stable plasma start-up under ITER-relevant condition is achieved in KSTAR and the ITER start-up scenario using TPC is proposed to replace FNC (field null configuration). ECH-assisted plasma start-up

has been proposed to overcome the difficulties of plasma initiation phase in future tokamaks, such as JT60-SA and ITER. Due to the limitation of superconducting solenoid coil operations, the toroidal electric field applied by an inductive way is lower than that of present tokamak devices. And large eddy current and complex ferromagnetic structure makes it difficult to control the poloidal magnetic field. So tokamak plasma initiation with ECH-assistance has been studied to supplement the limited inductive input power and to relax the criteria related to the poloidal magnetic field quality. Many researches have shown that the poloidal magnetic structure makes an efficient ECH-assisted start-up, instead of the conventional FNC. The TPC, recently developed in VEST (Versatile Experiment Spherical Torus), has shown enhanced confinement of ECH pre-ionization plasmas and based on them, efficient tokamak plasma formation with an expanded operation window is achieved. Applicability of TPC needs to be demonstrated to large, conventional, and SC tokamaks. It is noticed that TPC could help to overcome the defects of start-up based on FNC in JT60-SA or ITER, but it needs to be validated. However, there are some concerns when applying TPC to large, conventional, and SC (superconducting) tokamaks such as KSTAR. First, the PF (Poloidal Field) coils to generate the TPC field structure need to be carefully chosen with consideration of the initial charging current of PF coils. Second, the reduced particle trapping fraction effect due to the intrinsically low magnetic mirror ratio of large aspect ratio tokamaks need to be tested. Third, the operation window of the TPC poloidal field strength and initial deuterium prefill pressure needs to be identified. The plasma start-up experiments using TPC has been conducted in KSTAR for feasibility study and finding the operation regime of TPC. The plasma start-up

scenario based on FNC is replaced by TPC by overlapping the mirror-like structure on the null. The 2nd harmonic, X-mode ECH system is used for pre-ionization of plasmas. 170 GHz of wave frequency with injection power of 600 kW is applied with toroidal injection angle of 20 degree, co-current direction. Applicability of TPC in conventional tokamak with improved efficiency than FNC is clearly demonstrated by experiments. The feasibility of TPC in low particle trapping ratio is analyzed through 0-d modeling, TECHP0D. The plasma confinement model is improved to represent the reduced convective loss due to the mirror effect. Based on this model, 35 % reduction of the convective loss along the magnetic field line is required to reproduce the experimental pre-ionization condition. The reduction fraction is similar value of the trapped particle fraction which is calculated by the guiding center averaged single particle calculation. Then, operation window of the TPC start-up is identified in KSTAR 2015 and 2016 campaign. With 16 shots using TPC, an operation diagram in terms of the magnetic pitch which represent magnetic field quality and the deuterium prefill pressure is obtained. The diagram shows a broader operation range of TPC for both magnetic pitch and prefill pressure than that of FNC. The magnetic pitch and the prefill pressure can be increased by 5 times and 1.5 times, respectively, compared to conventional FNC. All shots using the TPC scheme in KSTAR 2015 and 2016 campaign are used to find the operation limits of TPC. The diagram in terms of the magnetic pitch and the deuterium prefill pressure shows two operation limits of TPC; a high prefill limit that is independent of the magnetic pitch and a low prefill limit that is linearly dependent on the magnetic pitch have been found. The parameter scan experiment shows two conditions in which the plasma start-up is failed. One is in a low

ionization rate state and the other is in a low ionization density state. The operation limits are analyzed by the TECHP0D code. Low pre-ionization density case, the high electron temperature is achieved due to the reduced radiation loss. The radiative barrier is overcome by only the ECH power. However, the high electron temperature makes shorter confinement time than the closed flux surface formation time and the plasma start-up is failed. These conditions are confirmed by the experimental data with a low ionization density. The low ionization rate makes energy loss by ionization reaction after solenoid swing down. The energy loss delays the rise of the electron temperature and increases the plasma resistance. As a result, the plasma start-up was failed. Applicability of TPC start-up to ITER is studied. TPC start-up with a reduced toroidal electric field to ITER-level is conducted and successful plasma formation is observed, whereas with FNC, the start-up is failed. ECH power of 700 kW is used, and the toroid electric field during the entire start-up phase is kept less than the target value of ITER of 0.3 V / m. The TPC structure can be generated by ITER PF coils of #1 and #6, even though the up-down asymmetry of position and turn-number of coils. The newly developed start-up scenario using TPC is proposed to ITER and compared to the conventional FNC based scenario. Saving the solenoid flux and stable superconducting coil operation will be expected.

Keyword: Nuclear fusion, Plasma start-up, Trapped particle configuration, KSTAR, ITER

Student Number: 2012-30266

Table of Contents

List of tables

List of Figures

Chapter 1. Introduction

As a future energy resource, nuclear fusion is the most attractive and fascinating way to address the world-widely growing energy demand. The nuclear fusion realizes the way the sun makes energy on earth. In the sun, light nuclei fuse together to produce energy. There are many types of fusion reactions, but the most promising is the reaction between deuterium and tritium [1];

$$ {}_{1}^{2}D + {}_{1}^{3}T = {}_{2}^{4}He\left(3.5\ MeV\right) + {}_{0}^{1}n\left(14.1\ MeV\right) \tag{1.1} $$

The energy required to fuse the two nuclei is tens of *keV*, which is much lower than the energy calculated by Coulomb barrier due to the quantum-mechanical tunneling effect. This is called *thermonuclear fusion* because the nuclei are heated to a temperature sufficient to cause a fusion reaction. At the temperature for thermonuclear fusion, the fuel atoms are ionized and the fuel is in a plasma state.

For a commercial fusion reactor, the energy from the fusion reaction must be greater than the energy required to sustain the fusion reaction. For sustained fusion reactions, the energy carried by alpha particles is used to maintain the plasma temperature with external heating, and the energy carried by neutrons is converted to electrical energy. If the plasma is maintained solely by energy from alpha particle, then this state is called *ignition*. In this state, no external heating is required to maintain the plasma temperature, and the plasma is self-ignited. To make this state, the following conditions must be satisfied[1];

$$nT\tau_E > 3\times10^{21}\ m^{-3}\cdot keV\cdot s \tag{1.2}$$

where n, T, and τ_E are plasma density, temperature and energy confinement time, respectively. In this condition, the density and temperature profile is assumed to be flat. If both the energy by alpha particle and neutron are needed to sustain the plasma, it is called *breakeven*.

As an expected fusion reactor concept, the magnetic confinement devices have been studied and developed. The basic idea of magnetic confinement is that the magnetic field makes the high-energy charges particles to move circularly by Lorentz force so that they are not randomly scattered. Among the magnetic confinement devices, the torus-shaped magnetic confinement tokamak has been the most successful. The tokamak has toroidal and poloidal magnetic field made by external coils and plasma current. The schematic diagram of plasma and magnetic field structure in tokamak is presented in figure 1.1. As alternative concepts of magnetic confined torus-shaped devices, stellarator [2] and spherical torus [3] are also under researched.

ITER (International Thermonuclear Experimental Reactor) is the largest tokamak device currently under construction and is being built in Cadarache, France through collaboration of USA, EU, Russia, India, Japan, China, and Korea to provide the production of fusion energy and to verify its engineering effectiveness. The target energy multiplication factor is 10 under H-mode operation. In addition to studying plasmas, proving that the self-generation and safe management of tritium and the energy carried by neutrons to thermal energy is one of the important goals.

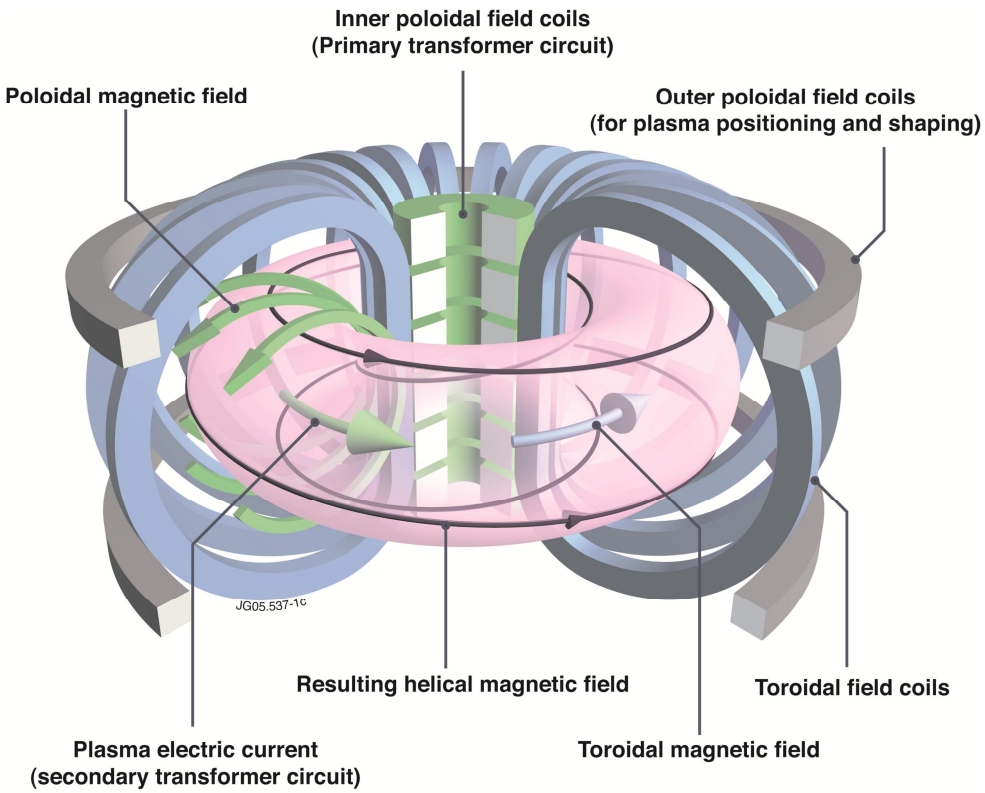

Figure 1.1 Schematic of plasma and magnetic field structure in tokamak. ***Image: EUROfusion (www.euro-fusion.org)***

1.1. Tokamak start-up

The plasma start-up in the tokamak consists of three phase, avalanche, burn-through, and plasma current ramp-up. The tokamak start-up depends mainly on the toroidal electric field induced by the central solenoid coils. This is similar to a transformer, where solenoid coils corresponds to primary winding, and plasma corresponds to secondary loop. The toroidal electric field is used not only for plasma avalanche but also for the plasma current formation and maintenance in the tokamak.

In tokamak, the seed electrons present in the gas are used for the plasma avalanche process. The seed electrons are accelerated by the external toroidal electric field and ionize the prefilled gas molecules. For hydrogen, the energy required for ionization is 13.6 eV. The seed electrons as well as the electrons generated by ionization reaction are accelerated and contribute to the ionization reaction. The process is known as Townsend avalanche theory. The growth rate of electron density along the electron pass is called as the first Townsend coefficient.

Electron confinement during avalanche process is essential for a successful plasma start-up. The electron travels through two mechanisms, one to move along the magnetic field line with a termination speed, and the other to drift motion by magnetic field gradient and curvature. The first of these is the primary mechanism for electron confinement. Therefore, it is necessary to maximize magnetic connection length by making poloidal field null configuration improve the electron confinement. Because the poloidal magnetic field is created by the solenoid coils to create the toroidal electric field, it must be compensated for using the external PF coils. However, this is not easy because the eddy currents which is

induced in the tokamak structure by the external coils, also contributes to the poloidal magnetic field. Development of a code that optimizes the magnetic field structure considering the tokamak geometry is essential for reliable plasma start-up.

After the avalanche phase, the burn-through phase starts. To raise the electron temperature, it is necessary to exceed the radiative barrier by impurities in the vacuum vessel. The rise of the electron temperature is important for reducing the plasma resistance and raising the plasma current. The radiative power loss by impurities are determined by impurity density, electron density, and cooling rate, which is a function of electron temperature and impurity species.

Recently, the plasma breakdown studies have been carried out in consideration of plasma response as well as external electromagnetic fields. By using PIC(particle-in-cell)-MCC(MonteCarlo Collision) simulation, the studies show that electric potential due to charge distribution during discharging, as well as external electromagnetic field conditions, play an important role during the plasma formation phase [4, 5].

1.2. ECH-assisted start-up

The ECH-assisted plasma start-up is initially proposed by Y-K. M. Peng[6] to get the cost efficiency of tokamak fusion reactor by moderating the ohmic heating power supply system. The required reduction of loop voltage was demonstrated in ISX [6], and related researches were performed in tokamaks such as FT-1 [7], WT-1 [8], WT-2, WT-3 [9], ISX-B [10], JFT-2 [11] and CLEO [12], as well as the stellarator, Tokapole-II [13]. Based on these results, study was conducted on various experimental conditions in DIII-D device [14].

Especially in the results at DIII-D, the various advantages of ECH-assisted start-up have been experimentally demonstrated in mid-size tokamak [14]. The loop voltage for plasma initiation was reduced to 0.15 V/m, which is lower than the target value of ITER, 0.3 V/m. The poloidal field strength to 50 G was overcome and the resistive volt-second consumptions decreases of 30 %. This shows that the ITER design of the 1990's was possible with reliable ECH-assisted plasma start-up.

Since the 2000's, the ECH-assisted start-up study was conducted under high harmonic ECH condition. A reduction of the magnetic field was applied as an alternative method for high-β operation with limited heating power. Therefore the ECH resonance condition changes from fundamental to second harmonic. The experiments were performed in JT60-U [15], DIII-D [16], Tore Supra [17], ASDEX-U [18], KSTAR [19] and FTU [20]. Especially ECH-assisted start-up contributes to the first plasma of KSTAR[21]. The experiments focused on the reliable ECH-assistance with reduced high harmonic ECH and reducing loop voltage below the ITER limitation in the mid-size tokamak.

The theoretical expectation for second harmonic assisted start-up is proposed with experimental results in DIII-D [22]. The single particle simulation of collisionless heating phase with second harmonic ECH shows that electrons can be heated up to several tens of eV, which is effective for the ionization reaction regardless of the initial energy, but when the $L_{heat} >> L_{n\text{-}e\ col} + L_{ionization}$ condition is satisfied. And the perpendicular energy growth rate, $\beta = 0.5 k_0 E_0 / B_t$, proposed in this study is used to compare the efficiency of different 2nd harmonic ECH.

A study of ECH-assisted start-up experiment under ITER-like conditions

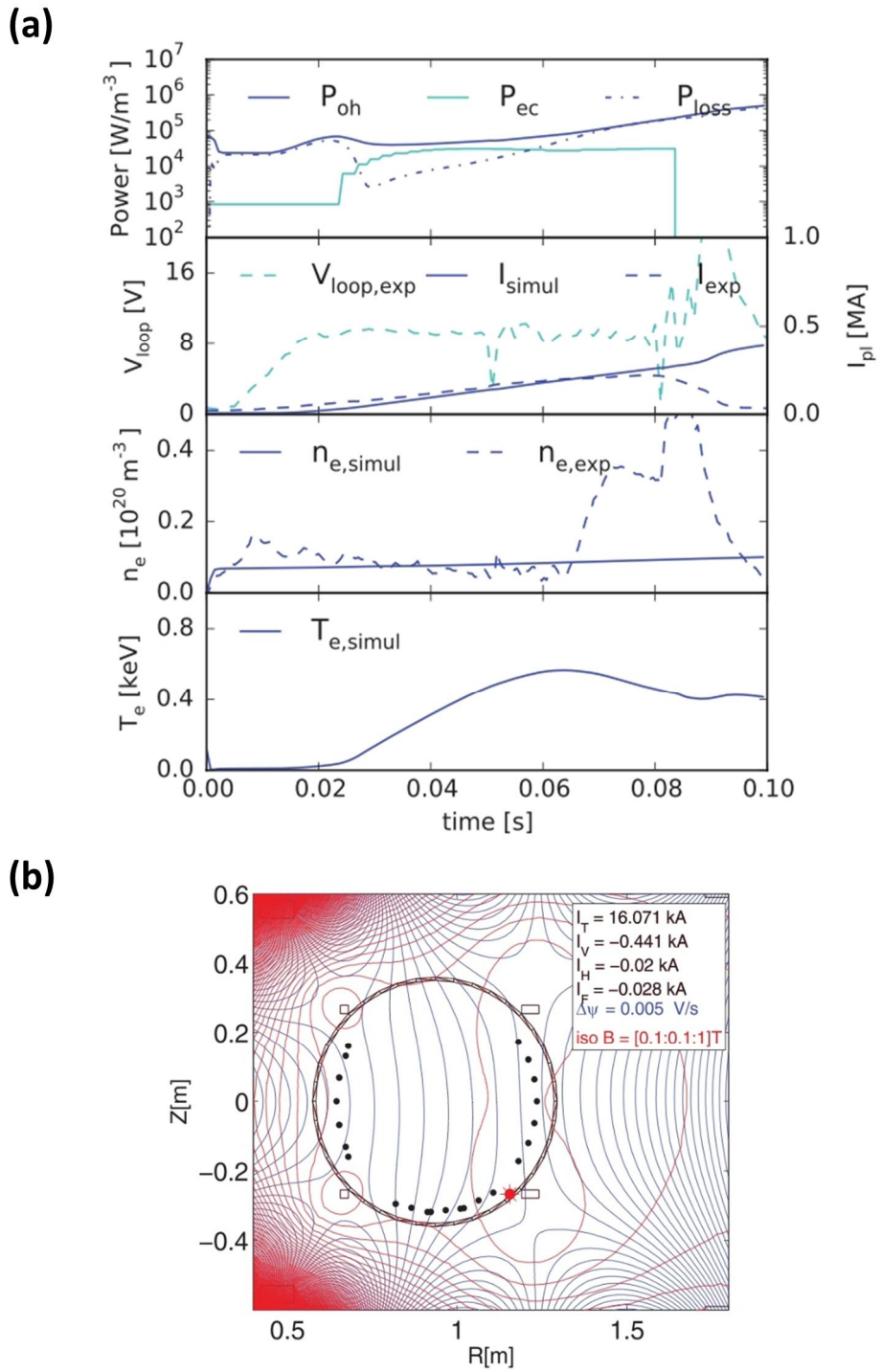

Figure 1.2 The experimental results in FTU tokamak with different ECH injection mode (a), and the poloidal magnetic field structure at the error field of 85 G (b) [20].

in FTU is studied [20]. In this research, the identical ECH frequency and toroidal magnetic condition of ITER are applied and the operation limit of toroidal electric field and poloidal error field are explored. With 2nd harmonic extraordinary ECH injection of 350 kW and toroidal injection angle of 20˚, reliable plasma start-up with error field up to 9.52 mT is achieved with 0.5 V/m of toroidal electric field. In this case, the toroidal magnetic field is 2.7 T and the connection length is 85 m. The experimental results are analyzed by BKD0 plasma evolution code with ECH ray tracing calculation by GRAY code [23].

The effect of the poloidal field on the open-field pre-ionization plasma confinement, especially the vertical poloidal magnetic field, has been studied through theory and experimental methods. A plasma start-up with a vertical field of 40 G showed better pre-ionization plasma performance and current ramp-up performance than the conventional FNC (field null configuration) in DIII-D [16]. The experimental result with vertical magnetic field is shown in figure 1.3. Theoretical studies on the vertical magnetic field effect on open field plasma confinement has been conducted [24, 25]. The charge accumulation by the drift motions is neutralized by the current flowing along the magnetic field line, and therefore the radial plasma loss by *ExB* drift is reduced. However, because the poloidal field reduces magnetic connection length and exacerbates the parallel loss, optimal vertical field strength exists.

1.3. Trapped particle configuration start-up

Efficient ECH-assisted plasma start-up at mirror-like TPC (Trapped Particle Configuration) has been developed in VEST (Versatile Experiment Spherical

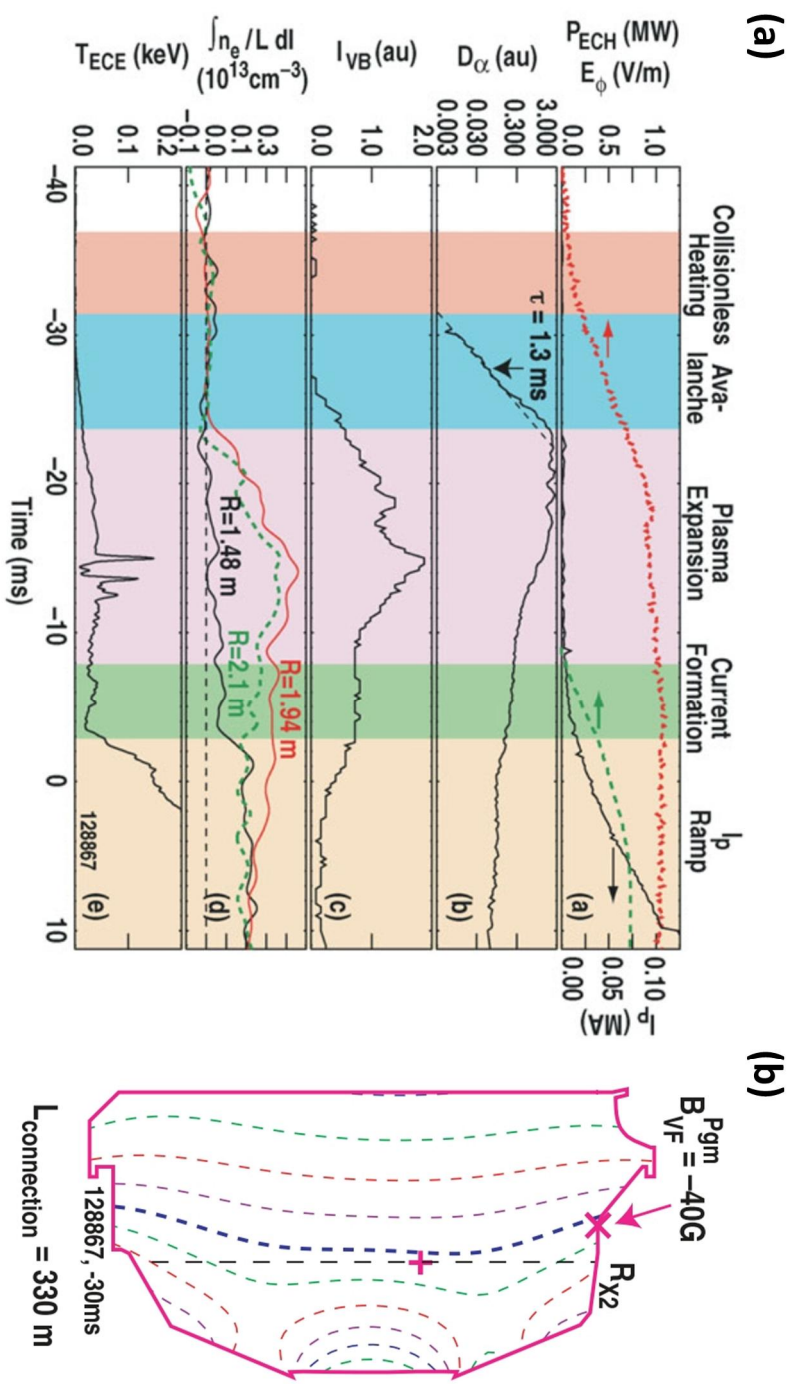

Figure 1.3 Time evolution of plasma parameters with five different phases of ECH-assisted start-up (a), and 2-dimensional magnetic field configuration of -40 G vertical field case (b) [16].

Torus) [26]. The mirror-like curved magnetic field structure has shown that it is more efficient and robust to plasma start-up performance than the vertical field case like DIII-D and FNC. The TPC has a wider operation range for the electromagnetic condition, the ECH input power, and the prefill pressure.

For pre-ionization plasma formation, the fundamental, extraordinary ECH power of up to 6 kW is applied. In VEST pre-ionization plasmas, studies related to EBW (Electron Bernstein Wave) heating are also being conducted. Electron density and temperature of the pre-ionization plasma are measured by the movable triple Langmuir probe at the mid-plane. Total plasma current is measured by the Rogowski coil installed inside of the vacuum chamber, and the plasma evolution is shown by the fast visible camera images.

The electron density and temperature of the TF only, FNC and TPC are shown in figure 1.4 (a). The left figure shows the TPC generated by the PF#3 and PF#4. The plasma equilibrium field is supplied by the PF#8 and PF#9 with plasma current initiation. The magenta dot line shows the resonance layer of 2.45 GHz ECH fundamental resonance layer with toroidal field of 0.05 T at the machine center. The red solid line shows the single particle trajectory according to the magnetic field structure.

TPC shows an improved confinement of ECH pre-ionization plasma in open field condition. The electron density and temperature profiles show the enhanced plasma confinement than FNC, and even though pure TF (perfect field null) case. Especially the density is higher than both FNC and pure TF at the whole region and the temperature is especially higher at outer region. The particle

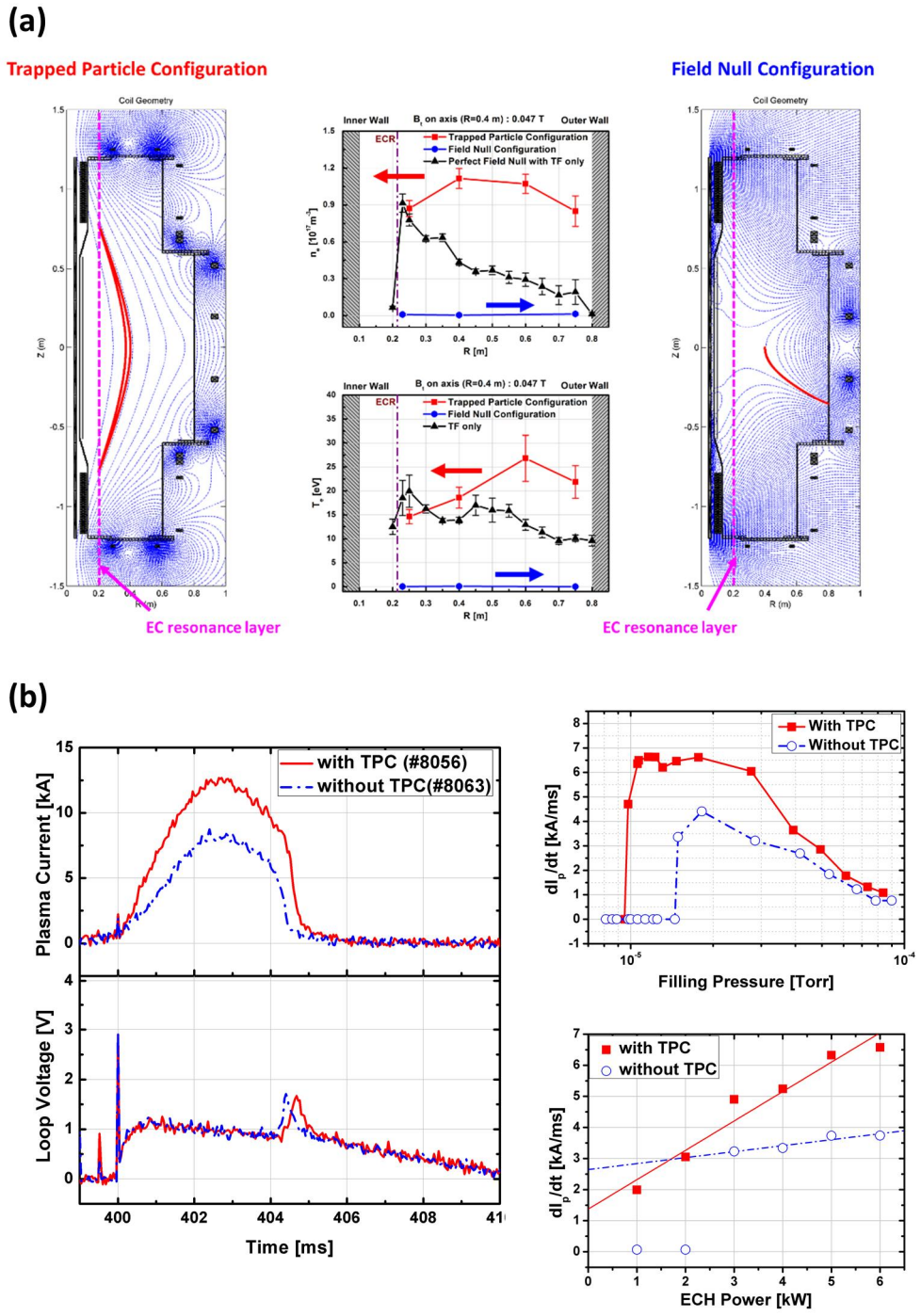

Figure 1.4 Pre-ionization plasma density and temperature profiles at the mid-plane under the magnetic field of pure TF, TPC, and FNC (a), and plasma start-up performance of TPC and FNC (b) in VEST [26].

confinement time measured by the exponential decay rate of the electron density after ECH termination was found to be 3 times higher in TPC than that of pure TF case.

The improved ECH plasma contribute to efficient and reliable plasma current formation. At the same loop voltage, higher maximum plasma current was achieved with a faster ramp-up rate at TPC than at FNC. TPC is capable of reliable plasma start-up under broader operating conditions for prefill pressure, ECH injection power and electromagnetic conditions. Additionally, the intrinsically favorable magnetic field curvature for plasma position stability also results in immediate plasma current formation.

Plasma breakdown condition is represented by the electromagnetic condition, E_t*B_t/B_p, also called *Lloyd condition*, not only in ohmic but also in ECH-assisted start-up. In this condition, the toroidal electric field represents the electron multiplication capability and the B_t/B_p expresses the magnetic connection length related to the electron confinement. Although the criteria of the electromagnetic condition is released with ECH pre-ionization, but the physical concept does not changed. However TPC achieves a more efficient plasma start-up through improved pre-ionization plasma, even though the connection length is reduced.

The TPC is expected to enable reliable plasma start-up in superconducting tokamak like ITER and spherical torus. The superconducting tokamaks have a limitation of toroidal electric field because of the limitation of current slew rate of the solenoid coils. Additionally, the large eddy current of conducting structure makes lowers the poloidal field control performance. Spherical torus has a low flux supply capability due to the small cross section of the solenoid coils. An efficient

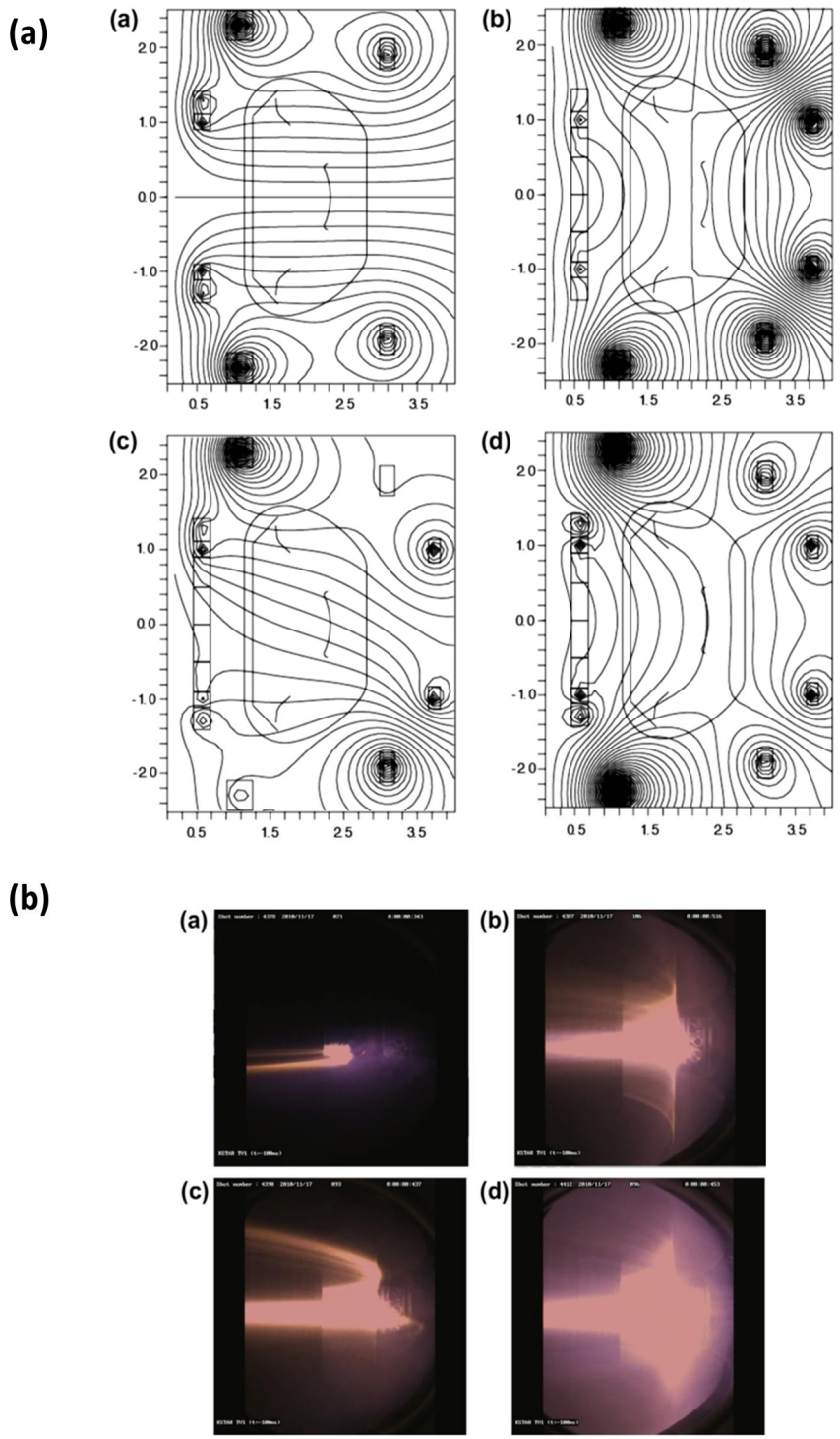

Figure 1.5 The various poloidal magnetic field structure (a), and the ECH plasma images (b) for inter-shot wall conditioning in KSTAR [27].

start-up using TPC can help overcome the problems in the plasma initiation phase.

It has been studied that the curved poloidal field configuration can improve plasma confinement performance in wall conditioning by ECH plasmas between the plasma discharges in KSTAR [27] as well as in start-up. Among the various poloidal field structure, the mirror-like poloidal magnetic field structure showed the most expanded ECH plasma in vertical and horizontal directions with density of 2.3×10^{19} m^{-3}. Successful wall recovery after the disruption is demonstrated by the wall conditioning plasmas. The various magnetic field structure and the ECH plasmas for wall conditioning is shown in figure 1.5.

1.4. Objectives and outline of this research

In this research, the efficient and improved ECH-assisted start-up using TPC is studied in conventional, superconducting tokamak, KSTAR. The feasibility of TPC will be studied by experiments and improved 0-dimensional start-up modeling. The characteristics of TPC operation in KSTAR will be explored and analyzed. Finally, ITER-relevant operation will be performed and scenario development using TPC for ITER will be proposed.

The plasma start-up scenario of KSTAR based on the FNC has inherent difficulties in controlling the poloidal magnetic field. PF coils for solenoid have a ferromagnetic material in coil jacket. This makes a serious distortion to the poloidal magnetic field structure, especially trying to generate the magnetic field null. Since 2011, the start-up scenario has been developed with PF and eddy currents as well as ferromagnetic effect. However, the ferromagnetic calculation has error to affect the plasma start-up, which is confirmed by the measured magnetic probe. In order

to optimize a scenario, the calculation and experiment have been carried out, simultaneously.

In addition, prefill pressure control has difficulties in reliable plasma start-up. The prefill pressure is affected by the neutralizer of the NBI (Neutral Beam Injection) system. The pressure at the neutralizer needs to rise 5 second prior to NBI operation and require about 10^2 times higher than the prefill pressure. In KSTAR, there is one NBI box consists of 3 neutral beam lines. Each beam line has its own neutralizer, and the main chamber prefill pressure is increased by 4×10^{-6} mbar per each neutralizer. The prefill pressure effect from a single NBI box is controllable to around 1×10^{-5} *mbar*. However, when a newly developed NBI system is installed, the two NBI boxes create a high pressure factor of 2 over the normal operation range.

Low toroidal electric field operation using TPC is the final issue of KSTAR start-up. NBI is inject in the direction of co-current when the normal experiments. But counter-current injection experiments are also needed for other physics researches such as resonant magnetic perturbation or plasma rotation. For counter-current operation, the plasma current direction must be reversed because the NBI system cannot move. However, since the BRIS (Blip Resistor Insert Circuit) circuit cannot be used to increase the slew-down rate of the solenoid coil currents, the toroid electric field in the start-up phase for reversed plasma current operation is limited. The low toroidal electric field scenario with FNC was developed in 2012, but it is very unstable. In this case, the toroidal electric field is reduced to ITER target level of less than *0.3 V/m*. Thus, development of low toroidal electric field start-up scenario can help not only to various physics

researches in KSTAR but also ITER-relevant start-up researches.

In ITER, it is well-known problem that the toroidal electric field is restricted less than 0.3 V/m [28]. Additionally, due to the low resistivity of conducting structures to μohm, severe eddy currents makes poloidal field structure difficult to control. These characteristics narrow the operation range for prefill pressure or impurity contents. JT60-SA has an effective level of toroidal electric field of 0.5 V/m, similar to KSTAR or EAST, but eddy currents also too severe up to 600 kA to affect poloidal field configuration.

Summaries of the requirements for a more robust and reliable plasma start-up of KSTAR and ITER;

1. Increase the tolerance of poloidal field error to cover the uncertainties.
2. Widen operation range of prefill pressure for second NBI effect
3. Low toroidal electric field start-up for various physics studies in KSTAR and overcoming the intrinsic limitation of SC solenoid operation in ITER

TPC is likely to overcome the difficulties of KSTAR and ITER, but there are also issues to adopt in KSTAR;

1. Feasibility of TPC in KSTAR due to the intrinsically low magnetic mirror ratio from large aspect ratio (about half mirror ratio than spherical torus)
2. Operation window and limits of TPC for TPC poloidal field strength and prefill pressure
3. Demonstration of ITER-relevant low toroidal electric field operation using TPC

Therefore, this dissertation is consist to four part to achieve the improved ECH-assisted start-up in conventional, SC tokamak. In chapter 2, the background methodology to investigate the start-up is introduced. In chapter 3, efficient and reliable ECH-assisted start-up using TPC in KSTAR is presented. In chapter 4, the characteristics of TPC operation is investigated with experiment and modeling. Chapter 5 shows ITER relevant operation using TPC in KSTAR and propose the ITER start-up scenario using TPC. Chapter 6, conclusion and future work of this dissertation is given.

Chapter 2. Background Theory for Tokamak Start-up Study

For plasma start-up study, Townsend avalanche theory is a basic physics of plasma formation. It is necessary to optimize the vacuum magnetic field in consideration of eddy current distribution and other magnetic materials. Time-dependent plasma density, temperature and current simulations are also required. It is important to optimize preprogrammed plasma start-up scenarios using all of these analyzes.

Townsend avalanche theory is introduced as the basic physics theory of plasma initiation. The theoretical derivation of conditions for electron events from seed electrons has been proposed, and the experiments conducted by Paschen have been verified and compared with the Townsend theory. Based on them, the criteria for tokamak plasma start-up is derived as electric field required as a function of prefill pressure and magnetic connection length.

Optimization of the time-varying magnetic field structure in the plasma startup phase is essential for reliable tokamak plasma initiation. In this phase, the central solenoid coils swing down from the initial charging current for applying the loop voltages in the vacuum chamber. The outer PF coils are also change the current to generate the target magnetic field structure. At the avalanche phase, it is necessary to create a poloidal magnetic field in order to increase the connection length with sufficient toroidal electric field to satisfy the breakdown condition. This phase is evaluated by *Lloyd condition*, described in the previous chapter When

Lloyd conditions are met, a plasma event can occur and plasma currents can start. After the plasma current starts to grow, a vertical magnetic field is required for plasma equilibrium and suitable radial magnetic field is also required for plasma position stability.

The plasma dynamics analysis code is needed to optimize startup scenario development by comparing plasma current evolution and poloidal vertical fields for plasma equilibrium. A simple method is to calculate the current assuming that the plasma is a *RL* (Resistance and Inductance)-*circuit*. However, for more accurate analysis, the methodology is upgraded to solving plasma density, temperature, and plasma current evolution, self-consistently. In this methodology, the plasma resistance is determined by Coulomb collision and electron-neutral collision.

2.1. Townsend avalanche theory

The plasma avalanche is explained by Townsend avalanche theory [29]. In this theory, the seed electrons generated by cosmic ray, natural radiation or ultraviolet are accelerated by external electric field and ionize the background gas. By introducing first Townsend coefficient, α, the density increase along the electric field line is defined as;

$$dn = \alpha n dx \tag{2.1}$$

where α means the number of the produced electron per distance. The density as function of the position is gathered by integrating the equation (2.1);

$$n = n_0 \exp(\alpha x) \tag{2.2}$$

where n_0 is the initial particle number at $x=0$. First Townsend coefficient can be derived by considering the electron energy balance. The electric field is defined by the distance of both electrode and applied voltages;

$$E = V / d \tag{2.3}$$

where E is electric field, V is applied voltage between both electrode, and d is distance between electrodes. For a continuous ionization reaction, it is necessary to obtain sufficient energy for ionization by an external electric field before the other collisions. The distance between collisions is defined by mean free path, λ, and the electron which has long mean free path to get the enough ionization energy is expressed as following;

$$n/N = \exp(-\delta/\lambda) \tag{2.4}$$

where the n is electron density which can contribute to the ionization, N is total particle density, and δ is required distance to get the ionization energy by given electric field. Here, the ionization number α by single particle per distance can be expressed as following;

$$\alpha = \frac{n}{N}\frac{1}{\lambda} = \frac{1}{\lambda}\exp\left(-\frac{\delta}{\lambda}\right) \tag{2.5}$$

In this equations, by replacing the δ/λ as following;

$$\frac{\delta}{\lambda}=\frac{(E\delta)}{(\lambda E)}=\frac{V_I}{(\lambda E)} \tag{2.6}$$

and dividing the equation (2.6) by pressure p, then the final equation is;

$$\frac{\alpha}{p}=\frac{1}{p\lambda}\exp\left(-\frac{V_I/(p\lambda)}{E/p}\right) \tag{2.7}$$

By replacing $1/p\lambda=A$, and $V_I/(p\lambda)=B$, the equation (2.7) is expressed as;

$$\frac{\alpha}{p}=A\exp\left(-\frac{B}{E/p}\right) \tag{2.8}$$

Here, the parameter A and B is determined by background gas species, and the examples of the parameters of hydrogen molecule and helium is presented in table 1.1. The schematic diagram of alpha process of Townsend avalanche is depicted in figure 2.1.

To sustain the plasma avalanche, the secondary electrons comes from the cathode by colliding the ion or photons are essential. The coefficient to represent the secondary electron generation is called by the second Townsend coefficient, γ.

Table 2.1 The parameters A and B in the Townsend theory

Gas	A [cm^{-1} $Torr^{-1}$]	B [$V\,cm^{-1}$ $Torr^{-1}$]	Range of E/p [$V\,cm^{-1}$ $Torr^{-1}$]
H_2	4.8	77	30~250
He	2.8	136	15~600

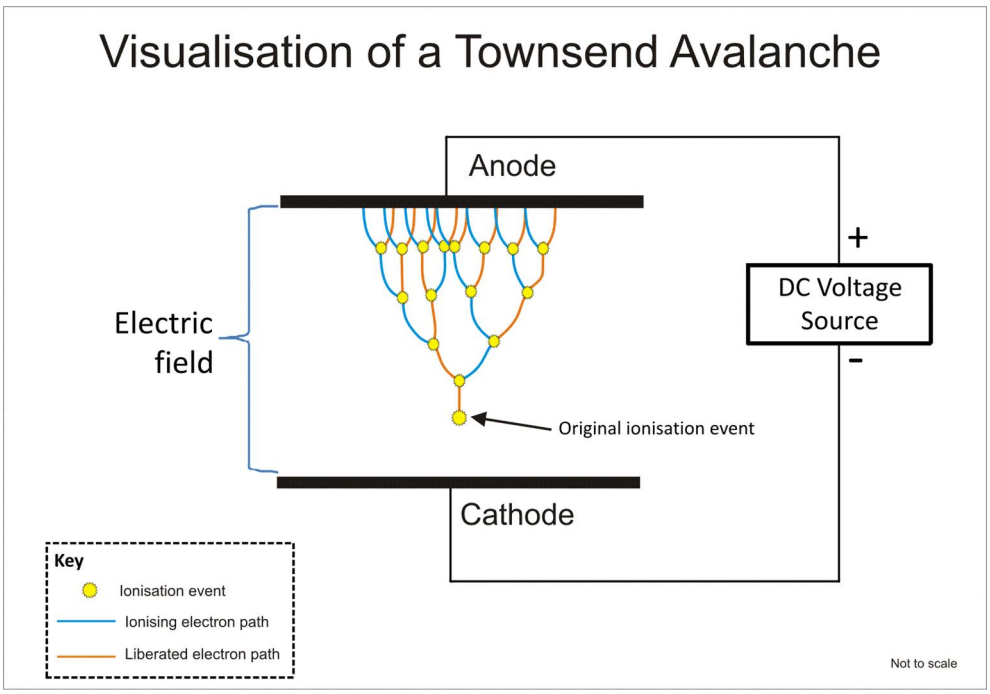

Figure 2.1 Schematic diagram of Townsend avalanche theory. ***Image: https://en.wikipedia.org/wiki/Townsend_discharge***

When the initial current comes to I_0 as the cathode, the current at the anode through the exponentially grown electrons is expressed as;

$$I = I_0 \exp(\alpha l) \tag{2.9}$$

where l is the distance between cathode and anode. The increase of electron current is $I_0 e^{\alpha l} - I_0$ and if we define the multiplication factor $\eta = e^{al} - 1$, then the total electron current can be expressed by the infinite geometrical series;

$$I = I_0 \exp(\alpha l) + \eta I_0 \exp(\alpha l) + \eta^2 I_0 \exp(\alpha l) + \cdots = \frac{I_0 \exp(\alpha l)}{1-\eta} \tag{2.10}$$

From this equation, Townsend makes the discharge condition as;

$$\eta = \gamma \left(e^{al} - 1 \right) = 1 \tag{2.11}$$

The required voltage for plasma formation is studied by Paschen. The relation between the required voltage, the gas pressure and the distance between cathode and anode has been experimentally found. It can be also derived from Townsend avalanche theory. By applying the logarithm to equation (2.11);

$$\alpha l = \ln\left(1 + \frac{1}{\gamma}\right) \equiv \Phi \tag{2.12}$$

Here, Φ is defined by the second Townsend coefficient which is affected by the cathode material. Equation (2.12) multiplied by pl and applied to equation (2.8), the resulting voltage required for plasma breakdown is:

$$V_s = \frac{Bpl}{\ln\left(Apl/\Phi\right)} \tag{2.13}$$

In this equation, constant A, B, and Φ is defined by the gas species and cathode material. The required voltage for breakdown is a function of gas pressure and distance between electrodes.

It has been shown that the Townsend avalanche theory is reliable to explain the initiation of plasmas in tokamak. In tokamak, it has different characteristics such as low loop voltage of few volt, long particle trajectory of thousands meter, and only occurring Townsend first process. For sustain the avalanche process, the ionization rate during the seed electron traveling must be larger than 1;

$$\alpha L_{connection} > 1 \tag{2.13}$$

With consideration of electron drift velocity and gas characteristics related to α, the required electric field according to the prefill pressure with given connection length condition is described as;

$$E_{\min}\left(V \cdot m^{-1}\right) = \frac{1.25\times10^4\, p(Torr)}{\ln\left[510\, p\left(Torr\right) L\left(m\right)\right]} \tag{2.13}$$

For the hydrogen, deuterium, and tritium case. The theoretical derive and the experimental validation are presented in [30] and the plot of equation (2.15) with various connection length and multi-machine experimental results are shown in figure 2.2.

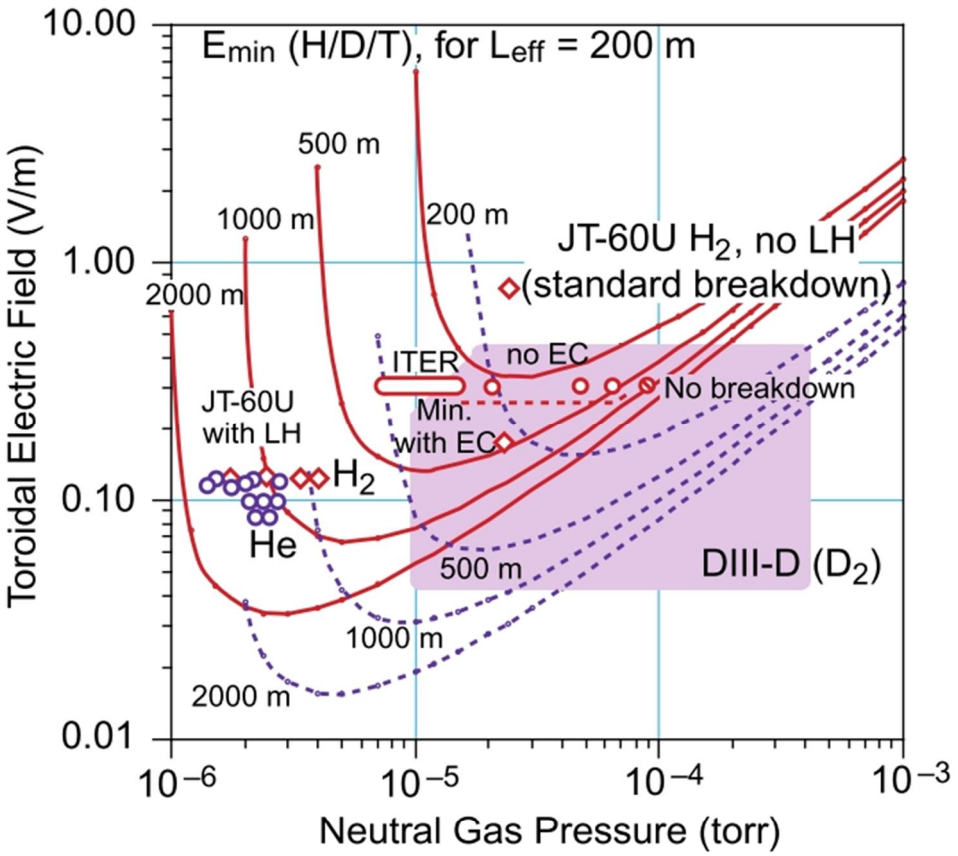

Figure 2.2 Required toroidal electric field for tokamak plasma formation based on Townsend avalanche theory [30].

In tokamak, inductive start-up based on the Townsend avalanche theory has been used. Since the tokamak structure cannot be used with electrodes, the electric field is applied in an induction manner. The electric field is used not only for plasma avalanche, but also for plasma current formation. It makes the tokamak operation as pulse and need to research the non-inductive current drive for the steady state long pulse operation. The configuration of tokamak start-up phase is depicted in figure 2.3.

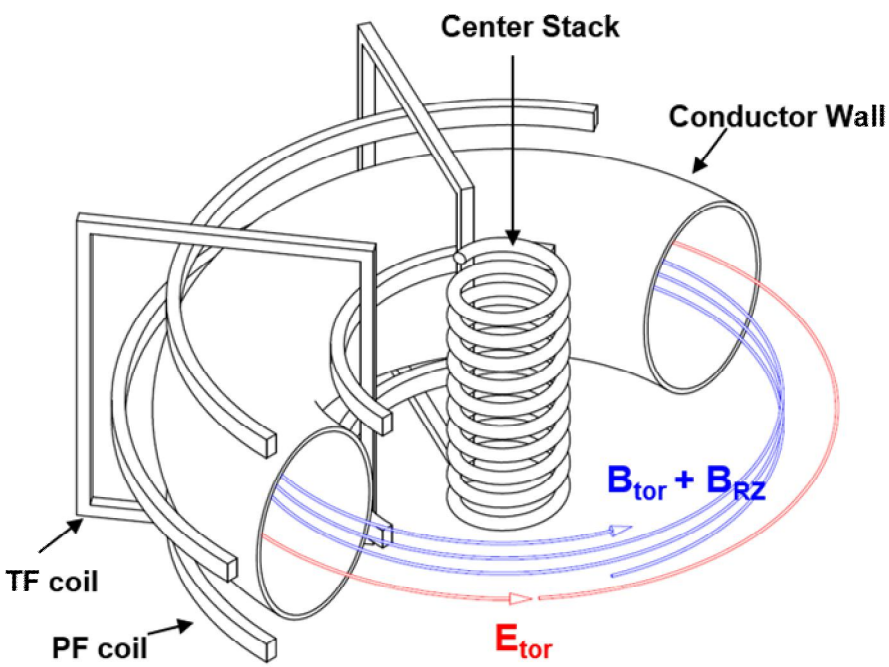

Figure 2.3 Schematic of tokamak and electromagnetic field structure during start-up phase [31].

2.2. Vacuum field structure optimization with eddy current effect

Poloidal magnetic field configuration in the start-up phase is one of the key factors to be analyzed. There are three components that contribute to the poloidal magnetic field: PF coil currents, plasma current, and the eddy currents on the tokamak structure. The poloidal magnetic field by a toroidal current source is calculated by analytic form as followed;

$$\psi(r,z) = I_c G(r,z;r_0,z_0) \tag{2.14}$$

where G is the Green's relation between toroidal current source and arbitrary (r,z) position, ψ is poloidal magnetic flux, and (r_0,z_0) is the position of the toroidal current source. The G is defined as;

$$\begin{aligned} G(r,z;r_0,z_0) &= \frac{\mu}{2\pi k}(rr_0)^{0.5}\left[\left(2-k^2\right)K(k)-2E(k)\right] \\ k &= \frac{4rr_0}{(r+r_0)^2+(z-z_0)^2} \end{aligned} \tag{2.15}$$

where, (r, z) is the target position of magnetic field on poloidal plane. Here, K and E is complete elliptic integral of the first kind and second kind, respectively. The poloidal magnetic flux and poloidal magnetic field have relation as follow;

$$B_r = -\frac{1}{r}\frac{\partial\psi}{\partial z} \text{ and } B_z = \frac{1}{r}\frac{\partial\psi}{\partial r} \tag{2.16}$$

The toroidal electric field is obtained from time derivative of poloidal magnetic flux, ψ. The toroidal magnetic field has $1/R$ dependency and determined by TF coil current. Based on them, the plasma avalanche condition, *Lloyd condition*, is

derived.

During the start-up phase, the eddy currents are major unknown parameters to find magnetic field configuration. The plasma current can also contribute to the poloidal field, but it is neglected for the start-up scenario design. The eddy currents induced in the conductive structure by the PF coils are expressed by the following circuit equation;

$$\mathbf{V} = \mathbf{M}\frac{d\mathbf{I}}{dt} + \mathbf{R}\mathbf{I} \tag{2.17}$$

where **M** is matrix of mutual inductance between toroidally continuous structures and poloidal field coils, and **R** is the resistance of structure, **V** is externally applied voltages and **I** is current at the coil or eddy current elements, respectively.

The circuit equation can be solved by numerical integration like in [32], but the analytic solution of the equation (2.17) described in [33] is helpful to optimize the magnetic field configuration with eddy currents. By defining matrix $\mathbf{A}=-\mathbf{M}^{-1}\mathbf{R}$ and $\mathbf{g}=\mathbf{M}^{-1}\mathbf{V}$,

$$\frac{d\mathbf{I}}{dt} = \mathbf{A}\mathbf{I} + \mathbf{g} \tag{2.18}$$

This is simple 1st order linear differential equation, and the solution **I** is expressed by summation of the homogeneous solution, $\mathbf{I_h}$, and the particular solution, $\mathbf{I_p}$. Here, the $\mathbf{I_p}$ is defined with constant matrix $\mathbf{R^{-1}}$ and **V**;

$$\mathbf{I_p} = \mathbf{R^{-1}}\mathbf{V} \tag{2.19}$$

and the $\mathbf{I_h}$ is expressed as;

$$\mathbf{I_h} = \sum_{j=1}^{N} \mathbf{x_j} \exp\left(\lambda_j t\right) \tag{2.20}$$

Here, $\mathbf{x_j}$ and λ_j are the eigenvector and eigenvalue of matrix A, respectively. The total solution of equation is;

$$\mathbf{I}_i\left(t\right) = I_i^{SS} + \sum_{j=1}^{N} \mathbf{Z_{ij}} \exp\left(\lambda_j t\right) \tag{2.21}$$

where $\mathbf{I_{SS}}=\mathbf{I_p}$, the steady-state currents. To de-normalize the eigenvectors, Z_{ij}, the initial condition is used as;

$$\sum_{j=1}^{N} Z_{ij} = I_i\left(0\right) - I_i^{SS} \tag{2.22}$$

The de-normalized factor χ_j are obtained by $Z_{ij}=Z_{ij}\chi_j$. Finally, the equation (2.21) is expressed as;

$$I_i\left(t\right) = \sum_{l=1}^{N} R_{il}^{-1} V_l + \sum_{j=1}^{N} \hat{Z}_{ij} \exp\left(\lambda_i t\right) \sum_{k=1}^{N} \hat{Z}_{jk}^{-1} \left\{ I_k\left(0\right) - \sum_{l=1}^{N} R_{kl}^{-1} V_l \right\} \tag{2.23}$$

The expression is valid with a constant applied voltage. For example, in the pre-programmed start-up phase, which lasted about 120ms after the solenoid swing down in the KSTAR start-up experiments, the voltage applied to the PF coil remained constant.

To develop the start-up scenario, the magnetic field optimization to minimize the poloidal magnetic field strength at the target positions is performed by Green's relation and analytic eddy current solutions and the cost function is

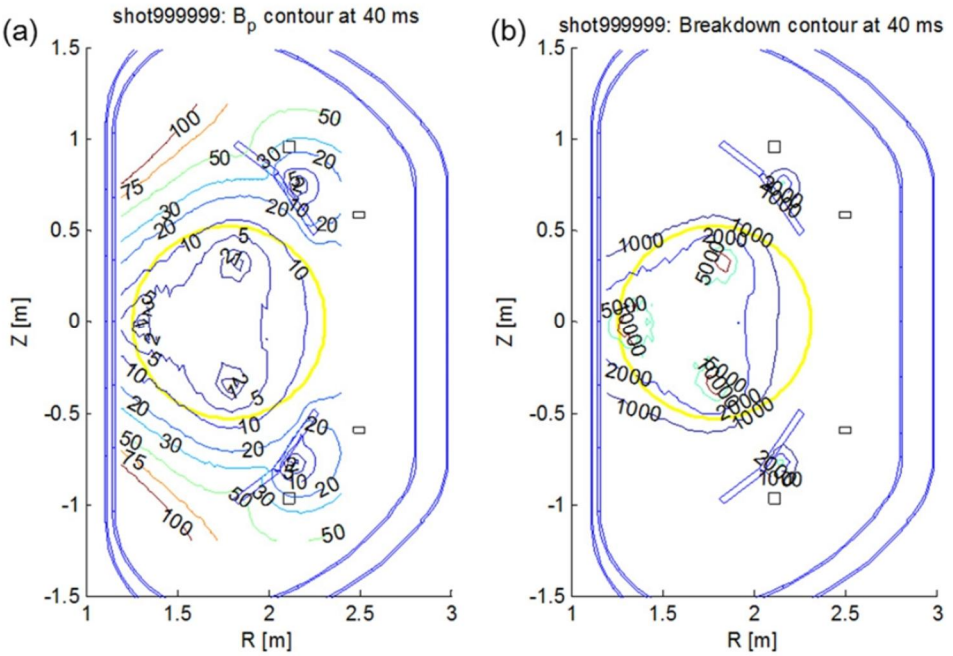

Figure 2.4 Examples of optimized poloidal magnetic field strength (a), and Lloyd breakdown condition (b) in KSTAR. The yellow circle is the target position of minimum poloidal magnetic field [34].

defined as [35];

$$\chi^2 = \sum_{l=1}^{N} \left[\frac{y_i - \sum_{k=1}^{M} V_k x_{k,i}}{\sigma_i} \right]^2 \tag{2.24}$$

where V, σ, M, and N are the applied voltage to the PF coils and the standard deviation used for adjusting weighting factors, number of PF coils, and number of constraints, respectively. The y is target value of the poloidal magnetic field, and the matrix **x** has the relation factors between the applied voltage, eddy currents and the Green relation between current sources and target positions. To find the optimal solution, the singular value decomposition (SVD) method is used. The examples of the conducting structures and the target position for generating field null scenario of KSTAR is depicted in figure 2.4. The yellow circle is the target position to minimize the poloidal magnetic field.

2.2. Plasma dynamics model

A 0-dimensional plasma dynamic simulator during the start-up phase has been studied. Initially the plasma models are proposed in [6] to analyze the effect of ECH-assistance for low loop voltage start-up. To analyze the low toroidal field effect of ITER as a burn-through simulator, a zero-dimensional code was developed in [36]. Based on these researches, many kinds of start-up simulator as SCENPLINT [37], TECHP0D [38, 39], and DYON [40]. As a subroutine of TRANSMAK, SCENPLINT has been used to develop the ITER start-up scenario. TECHP0D has been developed for first plasma study of KSTAR. Finally, DYON is

newly developed burn-through simulator, validated with JET result [41], and applied to the ITER estimation [42].

The basic plasma model of power, particle balance of electron and ion, and plasma current evolution is presented in [36]. The model is based on the plasma state, the initial plasma formation by Townsend avalanche theory or ECH is assumed. The ion particle balance is expressed as;

$$\frac{dn_D}{dt} = \frac{V_n}{V_p} S n_0 n_e - \frac{n_D}{\tau_p} \tag{2.25}$$

where V_n, V_p, S, n_0, and τ_p are neutral volume, plasma volume, ionization rate coefficient, and plasma confinement time, respectively. The ratio between the neutral and plasma volume represent the neutral screening effect. By charge neutrality, the electron density is;

$$n_e = n_D + \sum_I nI \langle Z \rangle_I \tag{2.26}$$

And the neutral density is expressed as;

$$\frac{dn_0}{dt} = \frac{\left(V_p/V_v\right)\left\{\left(\psi n_D/\tau_p\right) - \left(V_n/V_p\right) S n_0 n_e\right\} + \Gamma}{1 - \left\{\left(V_p - V_n\right)/V_v\right\}} \tag{2.27}$$

where ψ, Γ, and V_v are the deuterium recycling coefficient, the external gas influx per unit volume, and the vacuum vessel volume, respectively. The neutral screening regime is defined by the mean free path of a neutral for ionization by electrons.

The electron power balance is presented as;

$$\frac{3}{2}\frac{d\left(n_e \kappa T_e\right)}{dt} = P_{OH} + P_{ECH} - \left(P_{Dion} + P_{Drad}\right) - P_{equil} - P_{brem} - \sum_I \left(P_{ion} + P_{line} + P_{RRE} + P_{DRE}\right) - P_{conv}^e \tag{2.28}$$

Where P_{OH} and P_{ECH} are ohmic and ECH input power. The P_{Dion}, P_{Drad}, P_{equil}, P_{brem}, and P_{conv} are the power loss of ionization, the radiative loss by deuterium, the energy transfer from electron to ion by Coulomb collision, the bremsstrahlung loss, and convective loss, respectively. The power loss by each impurity species are also defined and the P_{RRE} and P_{DRE} are the power loss by radiative recombination and dielectric recombination, respectively. The ion power balance is simpler than electron;

$$\frac{3}{2}\frac{d\left(n_i \kappa T_i\right)}{dt} = P_{equil} - P_{CX} - P_{conv}^i \tag{2.29}$$

where P_{CX} is the charge exchange power loss. Generally the energy confinement time of electron and ion for convective power loss are assumed to be identical.

The plasma current is modeled by RL-circuit approximation;

$$\frac{dI_p}{dt} = \frac{V - R_p I_p}{L} \tag{2.30}$$

Here, the plasma inductance is calculated by plasma geometry and the internal inductance of 0.5 with assumption of flat current density profile, and the plasma resistance is solved with plasma parameters. The externally applied voltage is came from the magnetic field simulation.

The detailed physical models to solve the equation (2.25) to (2.30) are different to each codes. For example, as an energy confinement time after closed

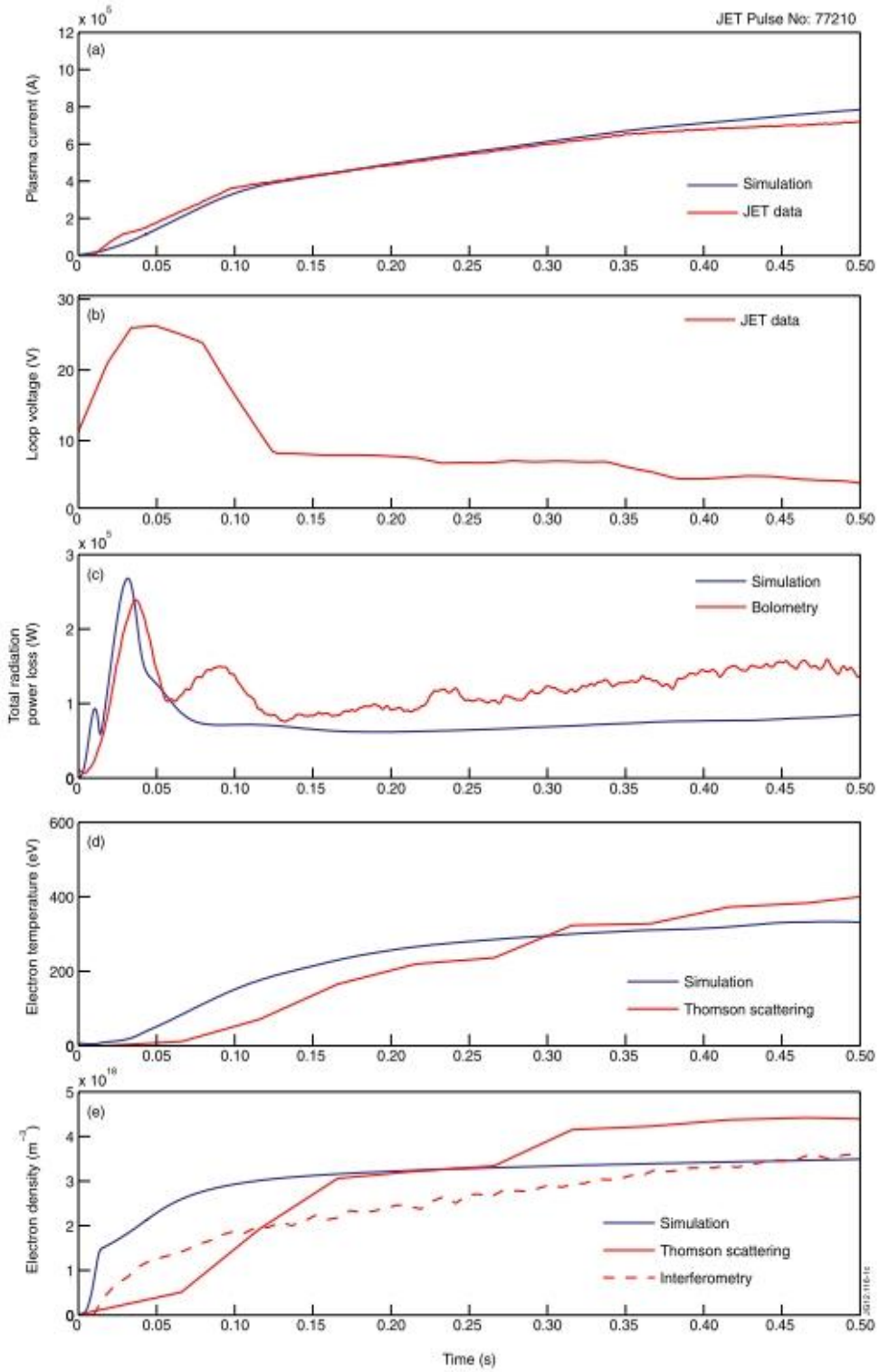

Figure 2.5 Validation of DYON simulator with JET start-up plasma parameters [40].

surface formation, TECHP0D, SCENPLINT, and DYON use Alcator-INTOR scaling [43], combination between the Bohm and the ITER L-mode scaling [30], and the Bohm diffusion model described in [44], respectively. Nowadays, the DYON code was validated with JET ILW (ITER like wall condition) experiments [41] and applied to predict the ITER start-up to estimate the operation window, especially ECH required power [42]. The validation result of DYON with JET experiments are presented in figure 2.5.

TECHP0D, developed for KSTAR initial ECH-assisted start-up. ECH power absorption fraction is calculated with plasma parameters based on[45] and the applied formalism is well described in [39]. The absorbed power to the plasma is;

$$P_{ECH} = P_0\left[1 - f_o e^{-\eta o} - f_x e^{-\eta x}\right] \tag{2.31}$$

where P_0 is injected ECH power, and the η_o and η_x are the dimensionless optical depth of ordinary and extraordinary mode. The f_o and f_x are the fraction of ordinary and extraordinary power. The optical depth of fundamental modes are given by;

$$\eta_o = \frac{\pi^2 R_0}{\lambda}\frac{T_e}{m}\frac{n_e}{n_c}\sqrt{1-\alpha}\left[1 + n_{\parallel}^2\left(0.5-\alpha\right)\right]^{-1} \tag{2.32}$$

$$\eta_x = \frac{\pi^2 R_0}{\lambda}\frac{T_e}{m} n_{\parallel}^2\left(2-\alpha\right)^{1.5}\left(1+\alpha\right)^2\alpha^{-1} \tag{2.33}$$

where λ, m, n_c, α, $n_{\parallel}$ are the free-space wavelength of injected EC, the electron mass, the cutoff density, the ratio of electron density and cutoff density, and the

parallel reflective index, respectively. With N[th]-order harmonic case, the optical depth derived by the quasi-linear Fokker-Planck equation and the cold plasma dispersion relation is expressed as;

$$\eta_{O,X} = \frac{\pi^2}{2}\frac{R}{\lambda}\frac{T_e}{mc^2}\frac{N^3}{(N-1)!}\left(\frac{n_{\perp O,X}^2 N^2 T_e}{2mc^2}\right)^{N-2} \times \alpha n \perp o,x \frac{\left[\left(S-D-n^2\right)\left(P-n_{\perp O,X}^2\right)\right]^2}{D^2\left(P-n_{\perp O,X}^2\right)^2 + n_{\square}^2\left(S-n^2\right)^2} \tag{2.34}$$

where *S*, *D*, *P* are defined as;

$$S = 1-\frac{\omega_{pe}^2}{\omega^2}\left(\frac{\omega^2}{\omega^2-\omega_{ce}^2}\right) = 1-\alpha\left(\frac{N^2}{N^2-1}\right) \tag{2.35}$$

$$P = 1-\frac{\omega_{pe}^2}{\omega^2} = 1-\alpha \tag{2.36}$$

$$D = -\frac{\omega_{pe}^2}{\omega^2}\left(\frac{\omega\omega_{ce}}{\omega^2-\omega_{ce}^2}\right) = -\alpha\left(\frac{N}{N^2-1}\right) \tag{2.37}$$

and the perpendicular reflective index, $n_{\perp}$, is defined by;

$$n_{\perp}^2 = \frac{-B \pm \sqrt{B^2-4AC}}{2A} \tag{2.38}$$

The plus sign is corresponding to the ordinary mode and the minus sign to extraordinary mode.

2.3. Poloidal field structure effect to ECH-assisted start-up

The vertical component of poloidal magnetic field makes improved plasma confinement during the pre-ionization phase before applying the loop voltages. Modeling about the vertical field effect are first derived in [24]. In this research, the particle loss along the magnetic field line and the $E \times B$ drift loss to the outward radial direction are considered.

The applied vertical magnetic field can moderate the $E \times B$ loss, but worsen the magnetic field parallel loss. The electric field E, derived by the charge separation with gradient motion by magnetic field gradient and curvature, can be neutralized by the current flowing along the pitched magnetic field line. But the magnetic connection length is shorten by vertical magnetic field and the plasma loss along the magnetic field line is increased. Therefore, there is optimum vertical magnetic field.

To estimate the optimal vertical field strength, simple particle loss model is applied. With vertical magnetic field, the parallel electric field to magnetic field, $E_{parallel}$ can generate current along the magnetic field line. The terminal velocity of electrons determined by the electric field and collision with background neutral is given by;

$$v_{\square} = \frac{eE_{\square}}{m_e \nu_{ea}} \tag{2.39}$$

where m_e, and ν_{ea} are electron mass and collision frequency of the electron and neutral atoms. With small magnetic pitch of $B_v/B_t \ll 1$, the vertical velocity of the

electron is;

$$v_{Eez} \approx v_{\square} B_v / B_t = \left(eE_z / m_e \nu_{ea} \right) \left(B_v / B_t \right)^2 \tag{2.40}$$

In steady state, the drift motion causing the charge separation is cancelled by the vertical component of parallel motion. Then the vertical electric field is defined as;

$$E_z = \left(T_e m_e \nu_{ea} / e^2 R B_t \right) \left(B_t / B_v \right)^2 \tag{2.41}$$

and then,

$$v_{E \times B} = \left(T_e m_e \nu_{ea} / e^2 R B_t^2 \right) \left(B_t / B_v \right)^2 \tag{2.42}$$

Therefore, the $E \times B$ drift velocity is moderated by the vertical magnetic field.

The loss along the magnetic field is came from the ambipolar diffusion along the magnetic field line. The flow velocity is given by the sound velocity, v_s, and the velocity to the wall is;

$$v_{amb} = v_s B_v / B_t \tag{2.43}$$

Then, the total particle confinement time is roughly given by;

$$\tau_p = \frac{a}{\left(v_{E \times B} + v_{amb} \right)} \tag{2.44}$$

where a is the poloidal distance from plasma to wall. The examples of particle confinement time with typical KSTAR parameters are depicted in figure 2.6.

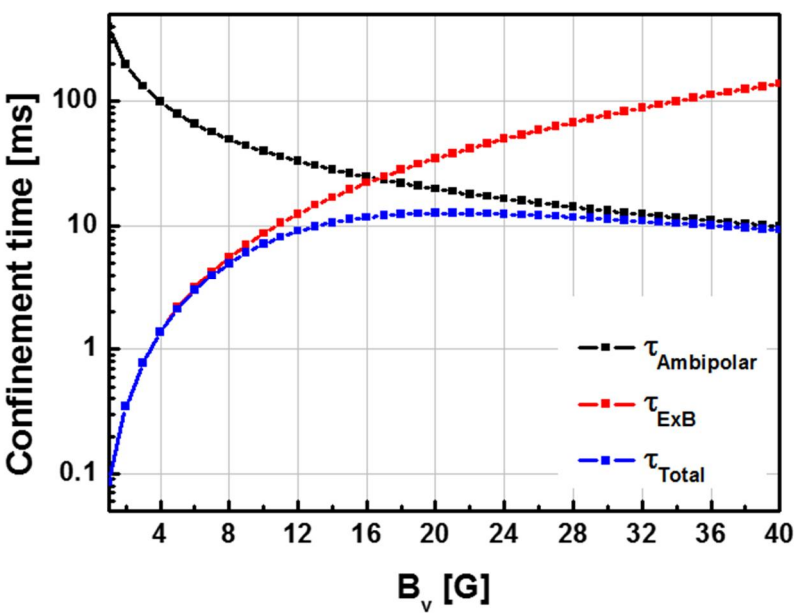

Figure 2.6 Open field confinement time according to the vertical field strength using KSTAR typical condition, B_t=2 T, T_e~20 eV.

Based on the research, more detailed calculation of the equilibrium formation by drift motion cancelation and experimental validation is presented in [25]. With two-fluid calculation, the optimal vertical magnetic field is derived as;

$$\left|B_{z,opt}\right| = \left[\frac{2\bar{\nu}_{\perp}^{e}\left|B_{\varphi}\right| m_e \sqrt{m_i T_{\perp}}}{\mathrm{Re}^2}\left(1+\frac{T_{\perp}}{T_{\perp}}\right)\right]^{1/3} \tag{2.45}$$

And the maximum confinement time is;

$$\tau_{\max} = \frac{\pi}{3}\frac{a}{c_s}\frac{\left|B_{\varphi}\right|}{\left|B_{z,opt}\right|} \tag{2.46}$$

The validation of theoretical model with experiments in TORPEX is presented in figure 3.1.

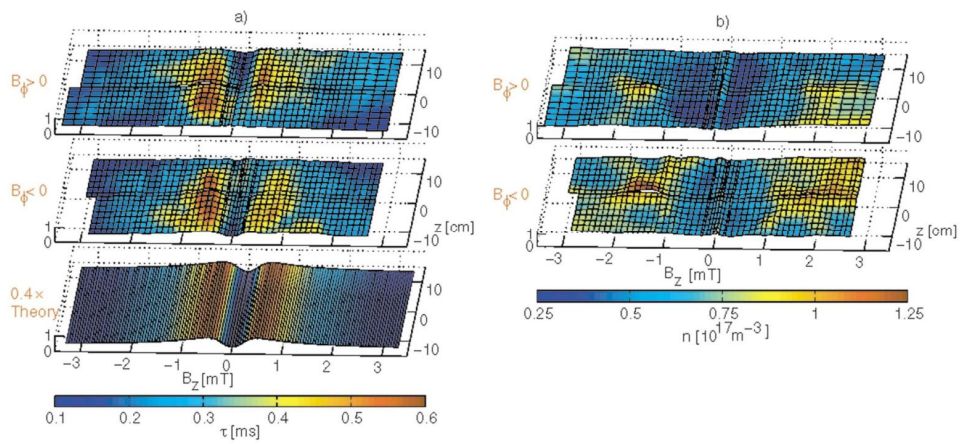

Figure 2.7 The validation of particle confinement time in TORPEX device with theory and experiments [25].

Chapter 3. Reliable and efficient ECH-assisted start-up using TPC in KSTAR

3.1. Development of TPC start-up operation scenario and experimental set-up

The start-up scenario using TPC is developed by the time-transient vacuum magnetic field calculation code [34]. The detailed ferromagnetic effect is studied in [46]. During the start-up phase, the eddy currents on the vacuum vessel or in-vessel conducting components can be induced by externally applied loop voltages. And especially in KSTAR, the ferromagnetic material for the jacket of superconducting solenoid coils can also significantly distort the magnetic field structure. The vacuum magnetic field calculation code solves the problem by considering the specifications of the PF power supply and BRIS circuit [47].

The TPC start-up scenario is developed based on the FNC scenario, overlapping the magnetic field structure generated by PF#5 coils, normally used to make divertor configuration. Three cases are compared in Figure 3.1 (a), (b), and (c) for magnetic field structures of PF#5 only (TPC made by PF#5), conventional FNC, and reference TPC, respectively. TPC exhibits an equilibrium-like magnetic field structure to obtain toroidal force balance during the start-up phase by increasing the poloidal field strength as well as to stable vertical and radial position instability. Due to the initial charging current of other PF coils, the mirror-like TPC structure is formed only in the major radius less than 2.0 m.

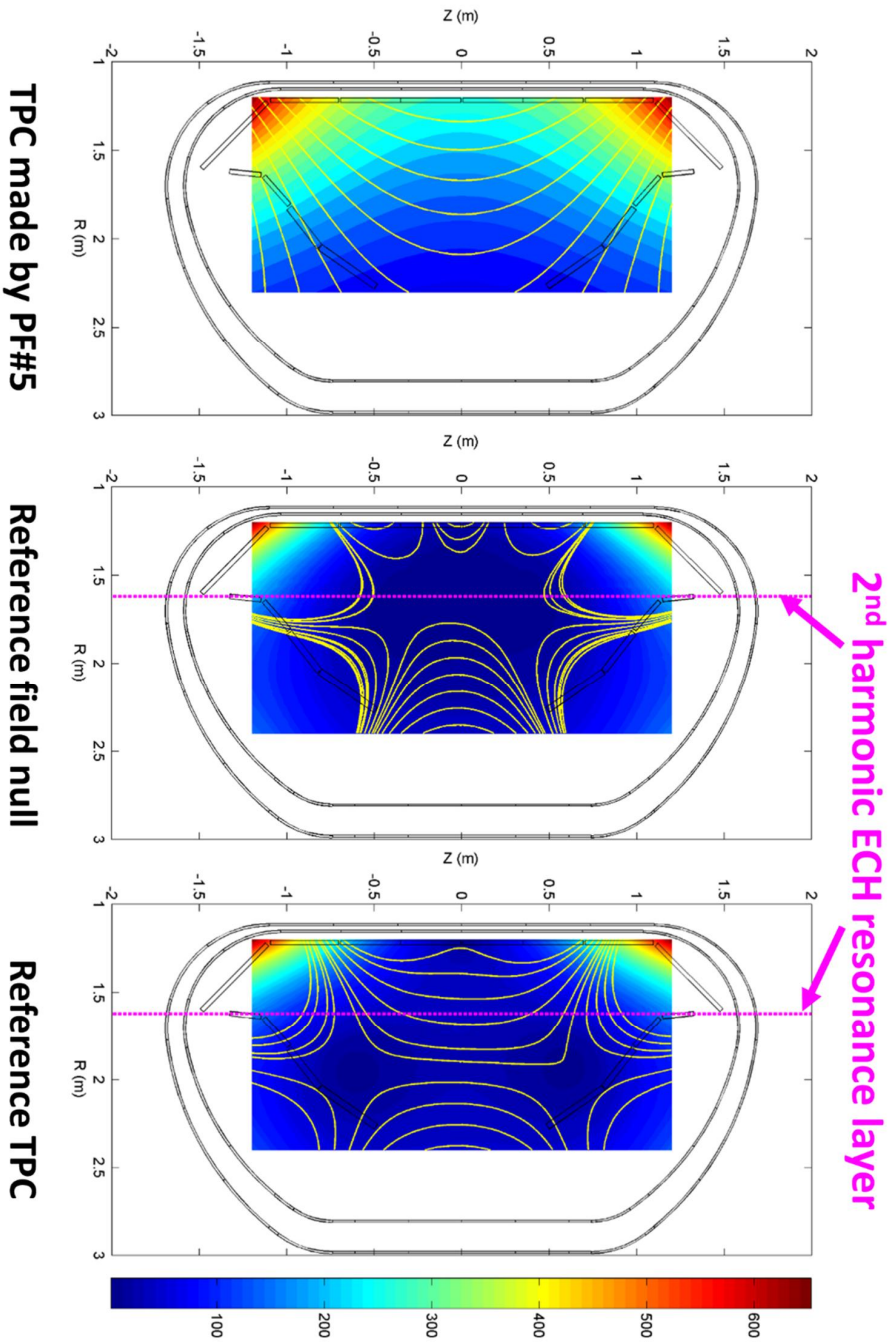

Figure 3.1 The magnetic field configurations of PF#5 only (a), conventional FNC (b), and reference TPC (c). The operation scenario of figure (c) is developed by overlapping the figure (a) on the figure (b). Magenta dot line indicates the X2 EC resonance layer.

The 2nd harmonic, X-mode ECH system is used for pre-ionization of plasmas. The injection power and the frequencies are 600 to 750 kW and 105, 140, and 170 GHz, respectively. The resonance layer is located near the major radius of 1.65 m, to generate the ECH plasmas on TPC. Location of the TPC structure and resonance layer is also depicted in Figure 3.1. Vertical magenta dot line in Figure 3.1 (b) and (c) shows the ECH resonance layer. In this scenario, the magnetic mirror ratio which is close related to particle trapping performance is approximately 1.3 at the ECH resonance layer. Especially, the 170 GHz ECH/ECCD system developed in JAEA (Japan Atomic Energy Agency) is prototype for ITER [48].

To investigate the plasma characteristics during the start-up phase, diagnostic tools are carefully chosen. The basic magnetic diagnostics are adopted such as a Rogowski coil for total plasma current and flux loops for applied loop voltage and plasma effect. The Rogowski coil measures not only the plasma current but also the eddy current inside of the vacuum vessel, the accurate plasma current evolution is gathered by compensating the measured eddy current contributions from without plasma discharge. It is described in figure 3.2. Line averaged electron density is measured by mm-wave interferometry. Line integrated deuterium line and carbon-III line are monitored to show interaction between deuterium molecule and electron and impurity condition. Fast camera shows the 2-D distribution and evolution of plasmas. Finally, the electron cyclotron emission (ECE) is also employed for electron temperature. However with low electron temperature case, for example the pre-ionization plasmas, the ECE need to be carefully compensated due to the violation of black-body assumptions [49]. But it can shows

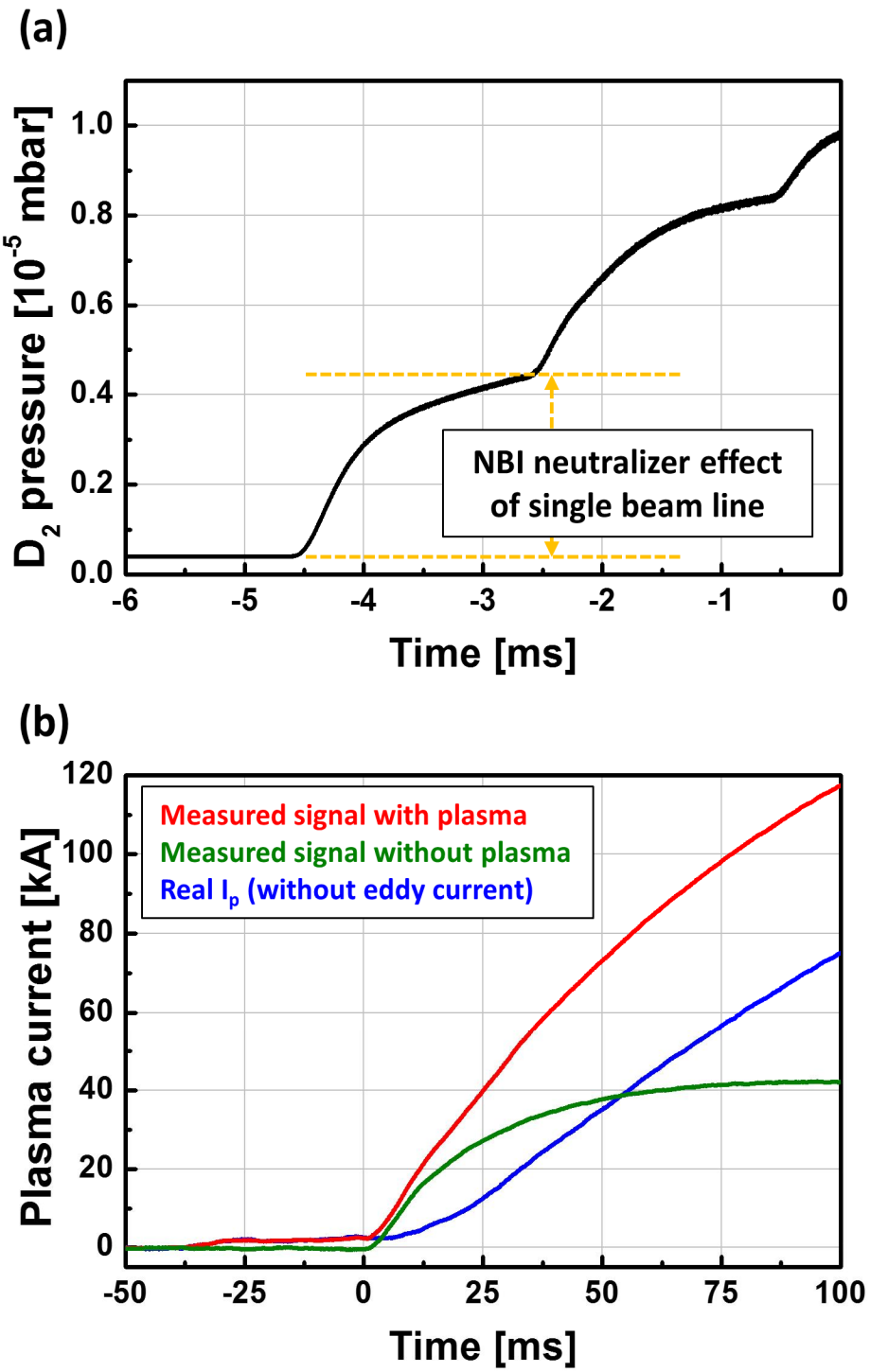

Figure 3.2 Prefill pressure effect by the neutralizer pressure of NBI system (a), and the Rogowski coil signal before and after the eddy current compensation (b).

approximated electron temperature evolution at the given position.

3.2. Demonstration of TPC and comparison with FNC

Efficient ECH-assisted start-up using TPC is demonstrated in KSTAR 2015 experimental campaign. Comparison between the TPC and FNC is conducted and the drastically improved start-up performance is observed with TPC. Start-up scenario based on TPC described in previous chapter is adopted and as an ECH system, 600 kW of 170 GHz, X2 injection with toroidal injection angle of 20 degree is injected 60 ms before the loop voltage onset. Deuterium prefill pressure is $2x10^{-5}$ mbar, which is higher of factor of 2 than stable ohmic discharge chase. All required diagnostics are available.

As a first step, the ECH-assisted effect to FNC is investigated. All conditions are same including start-up scenarios, but the only difference is ECH. Even though the 600 kW of ECH power injection, the plasma parameter evolution is almost same with no evidence of pre-ionization plasmas. Deuterium line peak and electron density rise slightly earlier, but not significant performance improvements. The experimental results are presented in figure 3.3.

The TPC experiments have been performed to demonstrate the feasibility of TPC in conventional tokamak, KSTAR. ECH-assisted FNC, and ECH-assisted TPC are conducted and the results is presented in figure 3.4. The FNC scenario is presented in [34], and the TPC scenario is depicted previous chapter. In these experimental set, ITER-relevant ECH frequency and injection angle are adopted. Resonance layer is R = 1.65 m, and the toroidal magnetic field is 2.7 T at the machine axis. And other parameters are all same such as the loop voltage or the

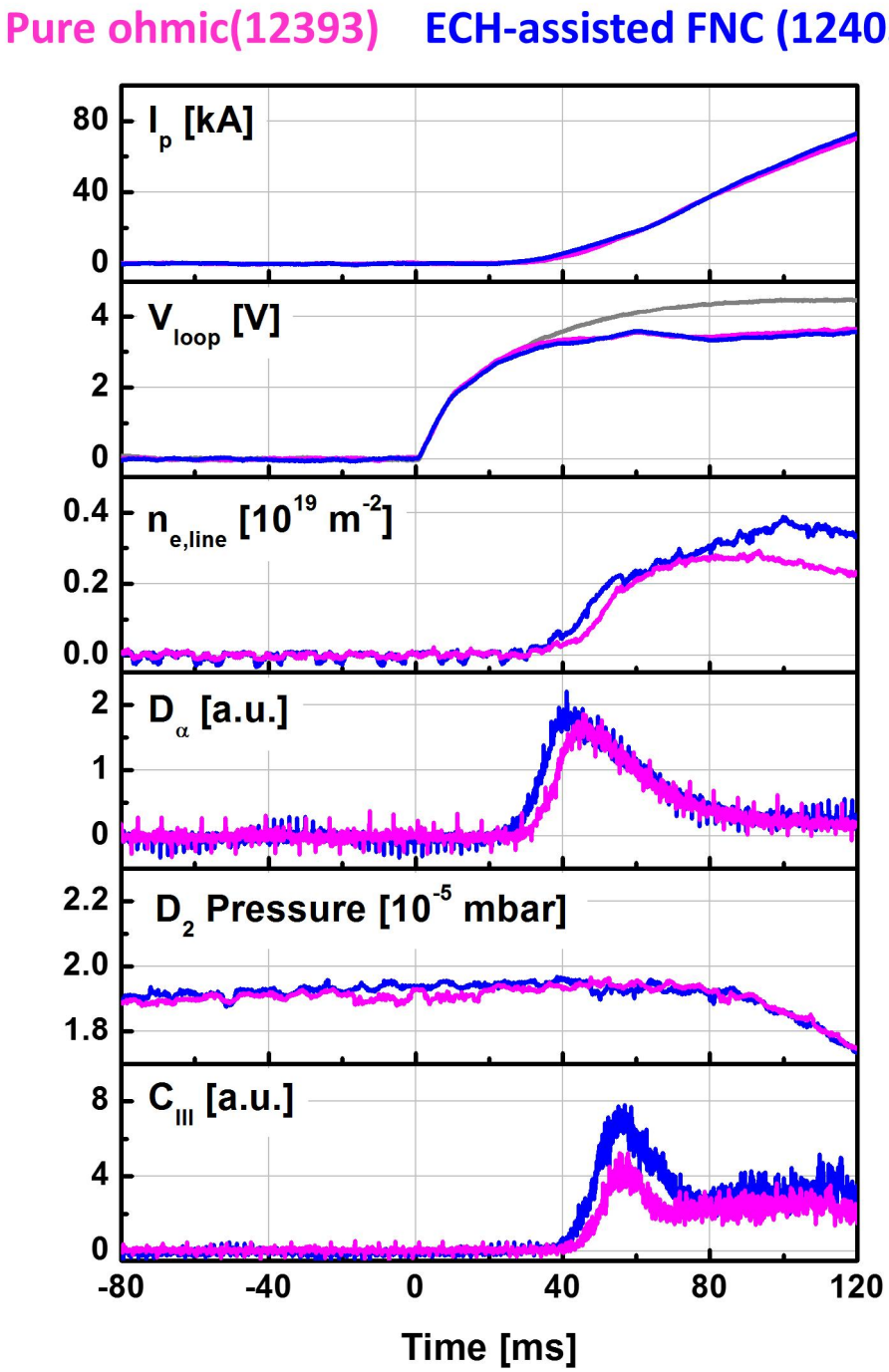

Figure 3.3 Comparison of the plasma start-up performance between the pure ohmic and the ECH-assisted shot using FNC. Plasma current, loop voltage, line averaged electron density, deuterium line radiation, deuterium prefill pressure, and carbon radiation are presented.

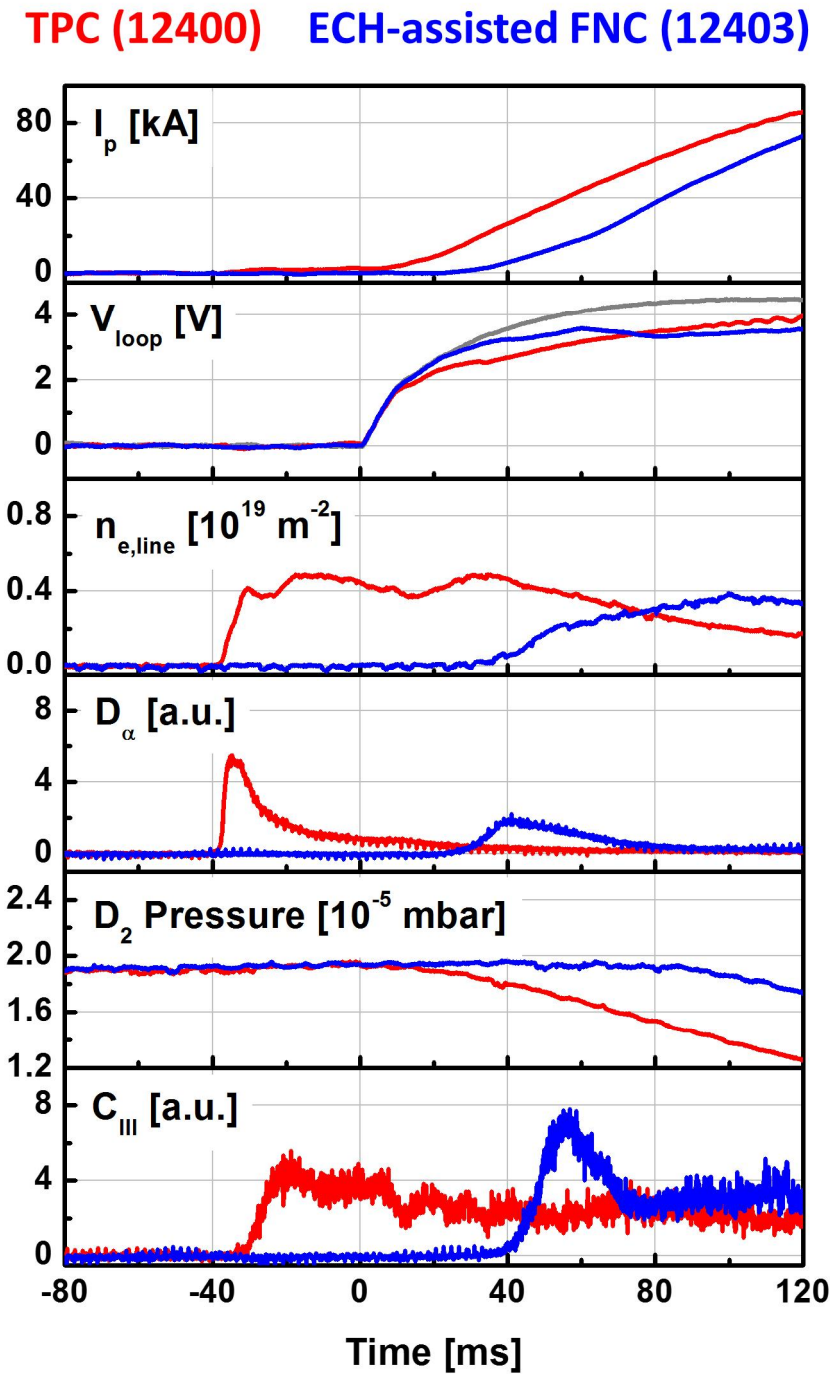

Figure 3.4 Comparison of the plasma start-up performance between TPC and FNC. Plasma current, loop voltage, line averaged electron density, deuterium line radiation, deuterium prefill pressure, and carbon radiation are presented.

prefill pressure.

Comparison between TPC and FNC is performed and the evolution of plasma parameters are described in figure 3.4. The red line and the blue line shows the TPC case and the FNC case, respectively. Plasma currents are formed with a faster current ramp-up rate, much earlier than FNC for TPC. After applying the loop voltage at 0 ms, only 10 ms is required to plasma current formation with TPC, but 30 ms for FNC. By comparing the magnetic measurement data with vacuum shot, it can be seen when the magnetic field caused by the plasma starts to affect the external magnetic field. With TPC, the loop voltage signal is affected at the loop voltage of 2 V, but the 3V with FNC. Pre-ionization plasma is only observed with TPC, line averaged electron density level of 10^{18} m^{-3}. From deuterium line radiation signal, peak observed during the ECH plasma formation phase shows the higher ionization rate. The neutral pressure measured in the pumping duct shows a faster decline than the FNC. Finally, carbon line radiation is kept as low as less than 4 at the entire discharge stage.

The efficient start-up using TPC is also observed with fast camera images. During the pre-ionization phase, not only the various diagnostics, but also the fast camera shows no evidence of ECH plasma with FNC. But with TPC, 20 ms after the ECH injection, the ECH plasma breakdown occurs at the resonance layer and the mirror-like curved magnetic field structure is also identified. With increasing the electron density, the plasma expanded from the resonance layer to the low field side, and fill the whole plasma region. It is presented in figure 3.5. After the loop voltage onset, the pre-ionization plasmas start to generate closed flux surface. The curved magnetic field structure during the pre-ionization phase is affected 8 ms

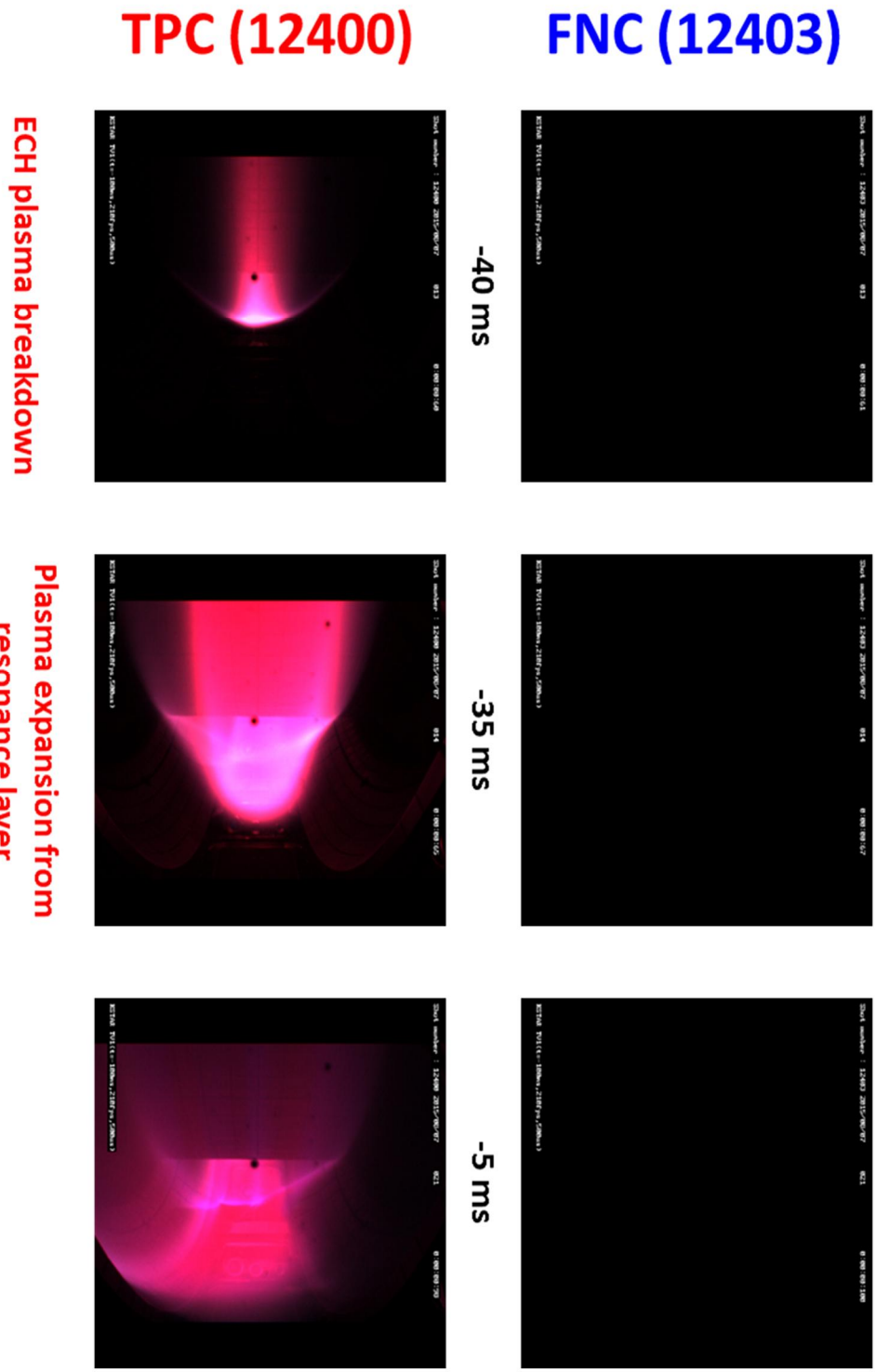

Figure 3.5 Fast camera images of TPC and FNC during the pre-ionization phase.

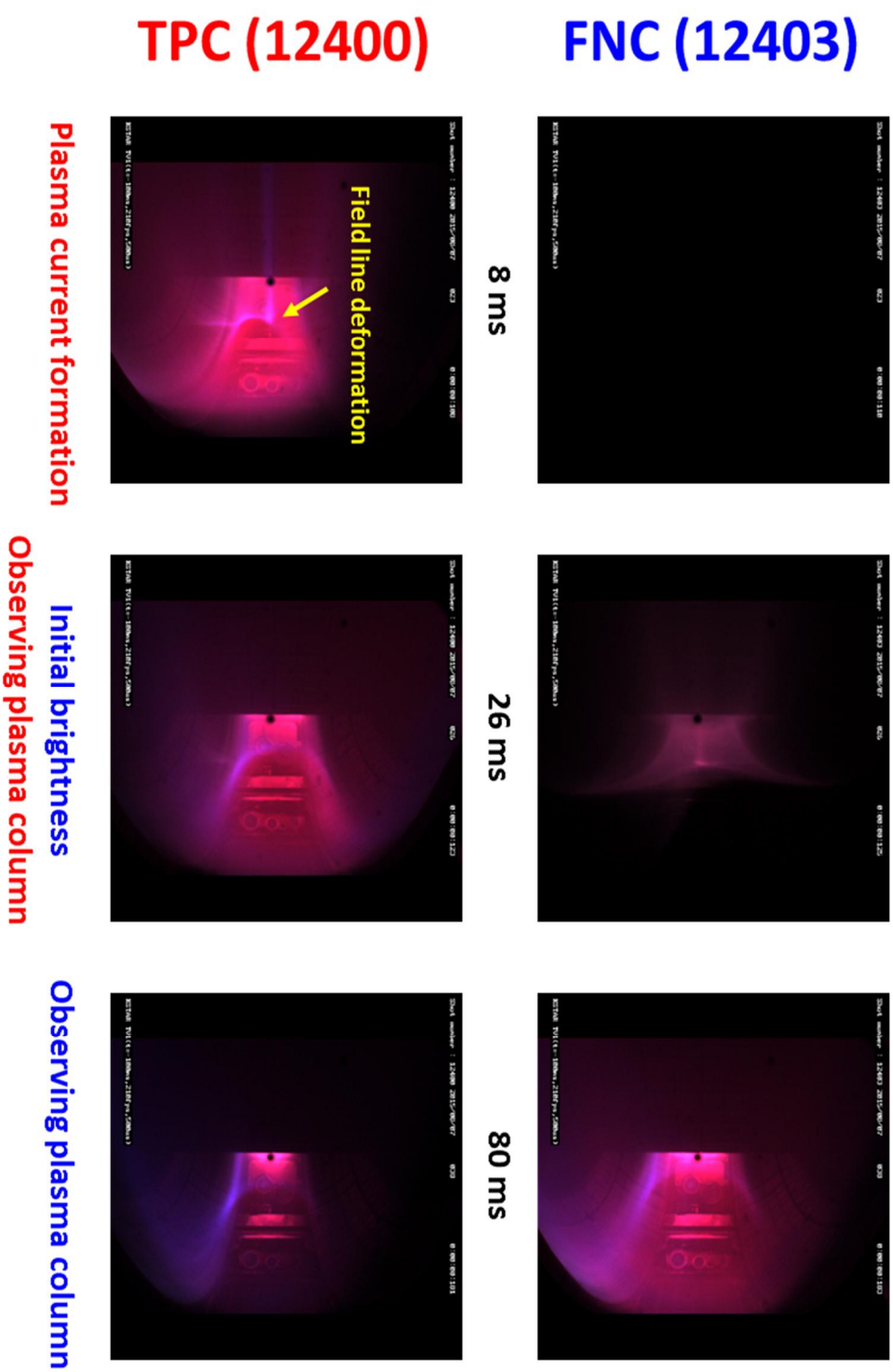

Figure 3.6 Fast camera image of TPC and FNC after applying loop voltage.

after applying loop voltage by the plasma current ramp-up. FNC takes 25 ms to observe the initial brightness from the plasma, but the plasma column is already formed with TPC. Due to the large plasma current of TPC, the plasma column is located at the outboard region. It is because the vertical field strength is tuned to generate equilibrium for plasma current made by FNC. The plasma start-up performance could be more improved with optimized equilibrium field evolution of adopted scenario. It is presented in figure 3.6.

3.3. Benchmarking of TPC experiments with TECHP0D with improved open-field confinement model

The TPC experiment of shot #12400 is benchmarked by 0-dimensional plasma evolution code, TECHP0D. It has been found that the plasma confinement during pre-ionization phase with TPC is improved than FNC by particle trapping effect even though the reduction of connection length by overlapped poloidal magnetic field. To apply the particle trapping effect to the 0-dimensional modeling for TPC analysis, the confinement model during open field phase is upgraded. In TECHP0D, the electron density confinement time during open field phase consists of: 1) the loss along the magnetic field line with sound speed, 2) the loss by curvature and magnetic field gradient drift motion, and 3) the diffusion loss. Among them, the loss along the magnetic field line with sound speed is dominant loss mechanism affected by the particle trapping effect. Such confinement times are also used to the convective electron energy loss.

The parameters to represent the reduction of parallel magnetic field

transport by particle trapping is adopted to TECHP0D model. The particle and energy balance equation is modified as;

$$\frac{dn_D}{dt} = \frac{V_n}{V_p} S n_0 n_e - \frac{n_D}{\left(k_{eff} \tau_{B\square} + \tau_{diff} + \tau_{drift} \right)} \tag{3.1}$$

and

$$\begin{aligned} \frac{3}{2} \frac{d\left(n_e \kappa T_e \right)}{dt} &= P_{OH} + P_{ECH} - \left(P_{Dion} + P_{Drad} \right) - P_{equil} - P_{brem} \\ -\sum_I \left(P_{ion} + P_{line} + P_{RRE} + P_{DRE} \right) &- \frac{3 n_e \kappa T_e / 2}{\left(k_{eff} \tau_{B\square} + \tau_{diff} + \tau_{drift} \right)} \end{aligned} \tag{3.2}$$

where k_{eff} is newly introduced to represent particle trapping effect. To find adequate k_{eff} value, the ionization plasma formation was simulated using experimental conditions. In this case, 170 GHz ECH of 600 kW is applied with 20° of toroidal injection angle. Poloidal error field is 35 G, corresponding to the TPC field strength at the resonance layer.

Without confinement improvement, the ECH plasma is not generated in simulations due to the large plasma loss. By scanning the reduction ratio, the ECH plasma is appears with 35 % reduced parallel loss of electron density and temperature. The pre-ionization plasma density according to the reduction ratio is depicted in figure 3.7 (a). It is notable that the clear confinement enhancement effect is required in TPC experiment even though the mirror ratio of 1.4, less than half of previous researches in spherical torus[26]. In this case, the particle confinement time is about 20 ms.

The particle trapping ration of magnetic field configuration in KSTAR is

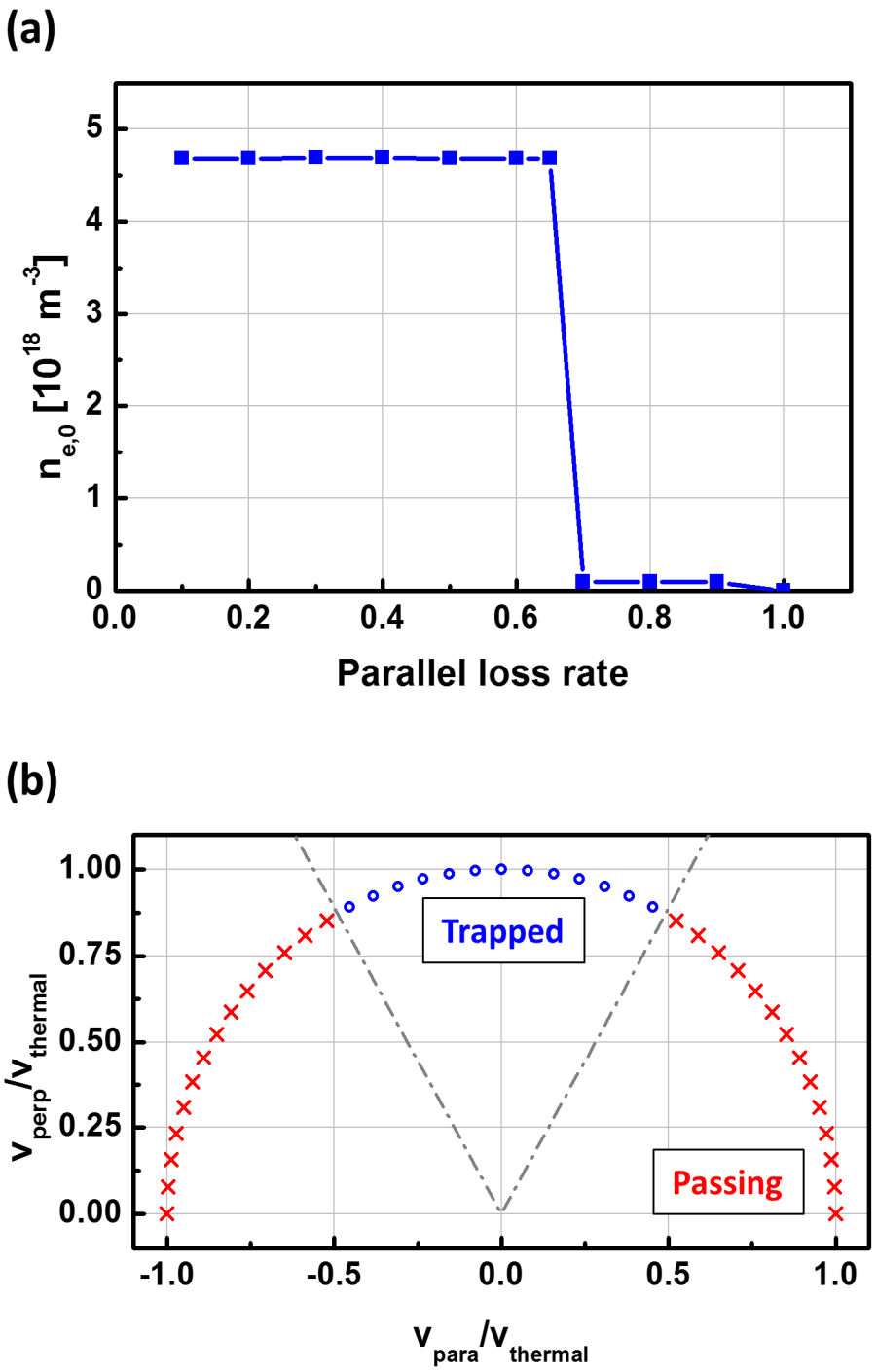

Figure 3.7 Pre-ionization plasma density according to the parallel loss reduction ratio (a), and the particle trapping ratio of KSTAR TPC at the resonance layer (b).

calculated and compared to the reduction rate of plasma convective loss. The single particle calculation using gyro-averaged formalism [50] with magnetic field configuration in KSTAR shows the particle trapping ratio at the EC resonance layer of 30 %, depicted in figure 4 (b). It shows that the parallel loss reduction in experiment is similar to the particle trapping ratio. Based on these results, the open field plasma confinement model of TECHP0D has been improved to be used as a start-up simulator of TPC.

The upgraded TECHP0D is validated with the experimental result of shot #12400. The reference experimental result and TECHP0D result before and after the confinement model improving are presented in figure 3.8. The ohmic and ECH heating condition is identical with experiment and the other input parameters are identical with TPC experiments presented in chapter 2.2. Without confinement model improved, the simulation shows negative result due to the large plasma loss by the short connection length, and delayed closed surface formation due to large poloidal field to generate the closed flux surface. But with upgraded confinement model, the simulation reproduces the experimental results. ECH plasma with density of 4 x 10^{18} m^{-2} is developed, and the plasma current increases up to 70 kA at the end of the start-up phase.

Detailed power balance between $k_{eff}=1$ and $k_{eff}=0.65$ are presented in figure 3.9. TPC like simulation shows the ionization reaction during the pre-ionization phase, but the original one shows no ionization reaction due to low ECH energy absorption ratio and large energy convective loss. The ionization reaction after applying loop voltage makes electron temperature rising delayed. And degraded plasma current formation also make low ohmic heating efficiency. Low

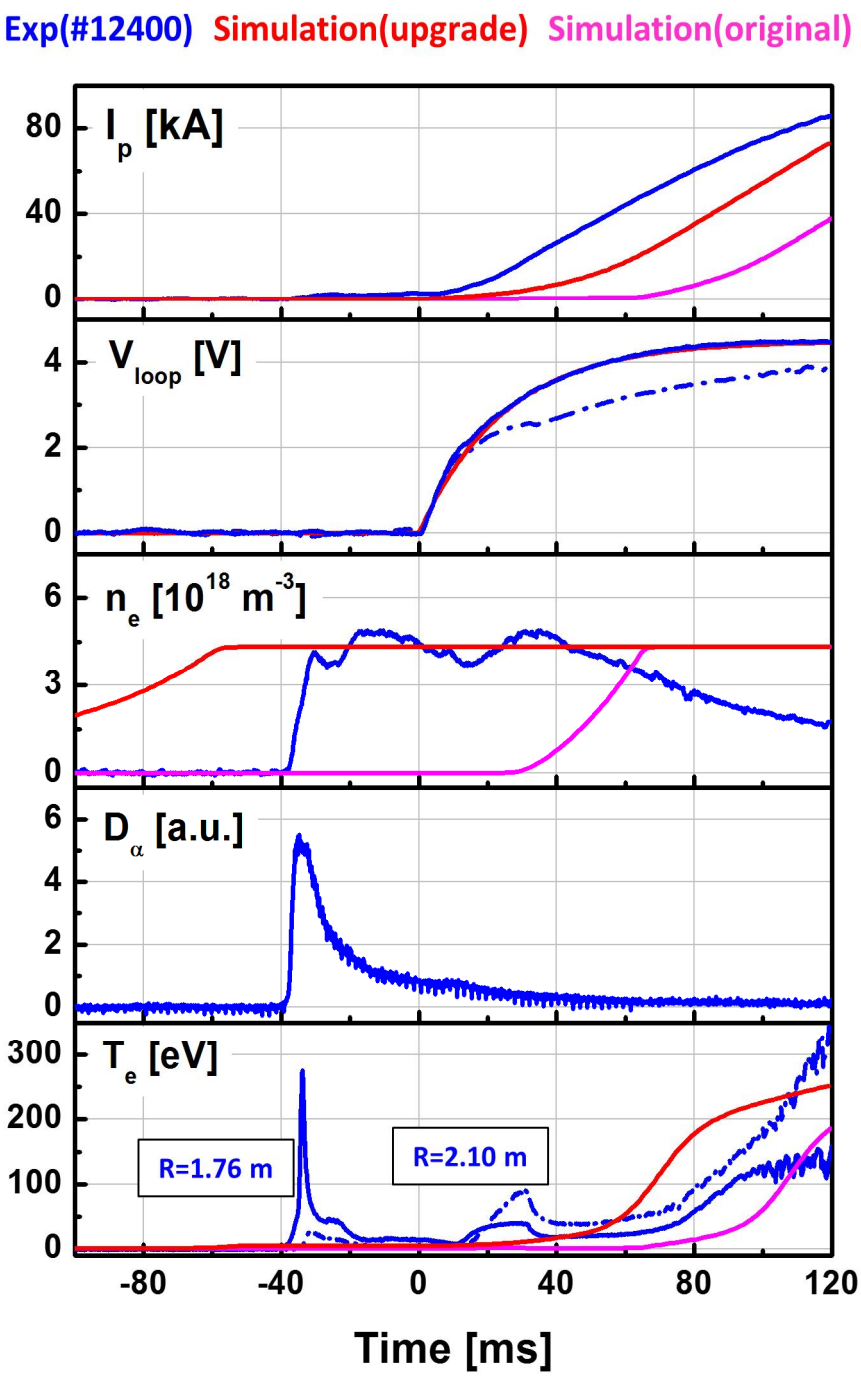

Figure 3.8 Time evolution of plasma parameters of experiment, TECHP0D model before confinement model improving, and with improved model TECHP0D.

plasma density and temperature also makes low ECH absorption efficiency. The TPC like condition has advantages for power balance of reliable plasma start-up.

However, there are obvious difference between simulation and experiment. The clear difference in plasma current evolution is observed. It comes from the lack of plasma shape evolution which can contribute to reduce the plasma resistance by increasing the plasma cross section. And the ECH plasma formation is also not reproduce the experiments, due to the lack of collisionless heating model for 2^{nd} harmonic ECH.

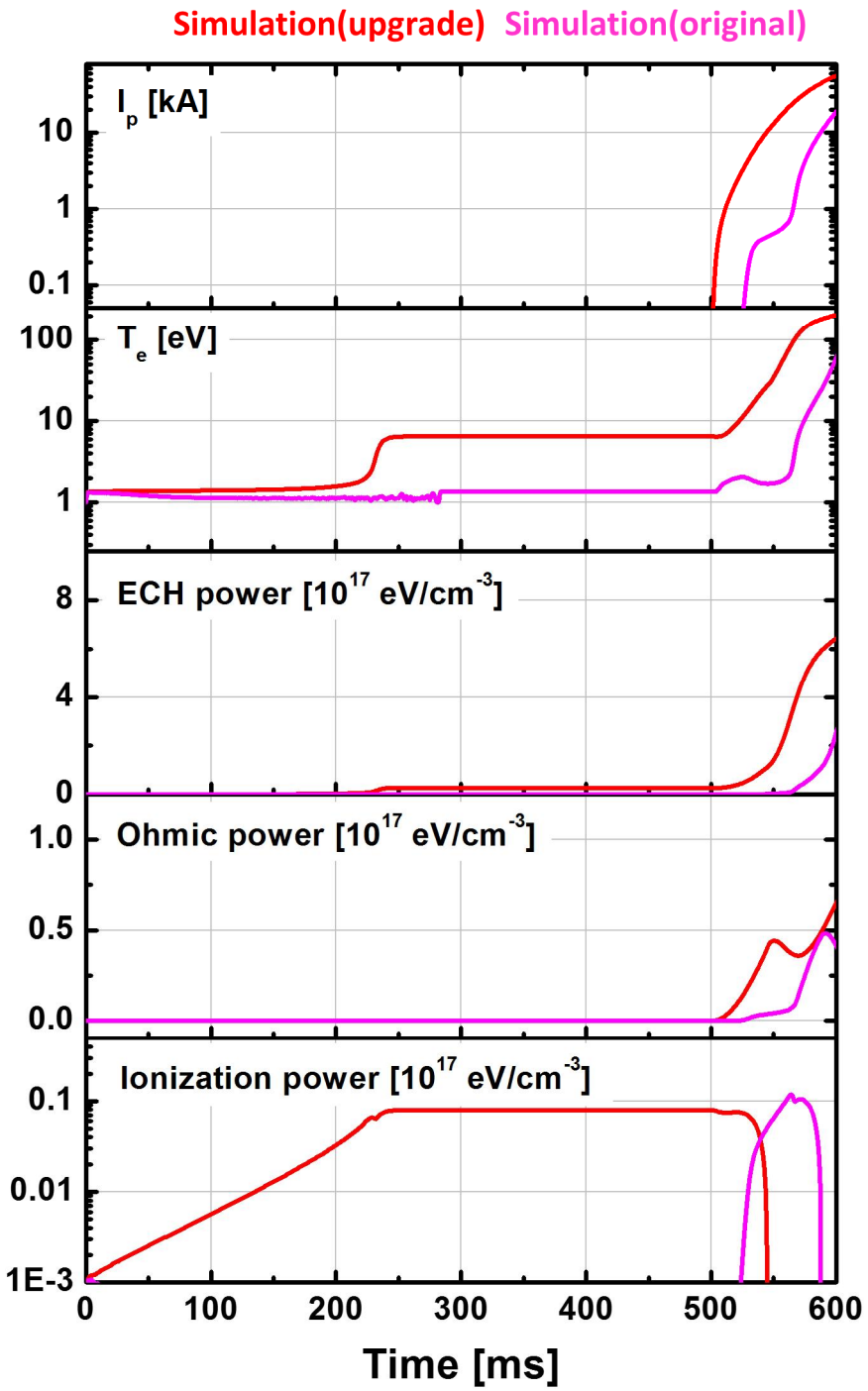

Figure 3.9 Evolution of power balance with and without confinement improvement.

3.4. Reliable start-up with expanded operation window of TPC

Operation window in terms of prefill pressure and magnetic pitch angle is found by 16 KSTAR successful shots dedicated to TPC start-up during 2015 and 2016 experimental campaign. In these experiments, the start-up scenario is identical, depicted in previous chapters. The various ECH/ECCD frequencies of 105, 140 and 170 GHz are applied with extraordinary 2^{nd} harmonic, injection power of 600 to 750 kW, and the toroidal injection angle of 15 to 20°. The toroidal magnetic field strength is adjusted to 1.8, 2.3, and 2.7 T at the machine axis, R = 1.8 m, to match the ECH/ECCD resonance layer at R ~ 1.65 m. The poloidal field strength can be controlled by the variation of the PF#5 charging current.

From the operation window, the TPC shows expanded regime in terms of the magnetic pitch and deuterium prefill pressure than the FNC. With FNC, the magnetic pitch near the resonance layer is normally less than 5×10^{-5}, $B_p < 10$ G and $B_t \sim 2$ T This makes the plasma start-up very sensitive by the magnetic disturbance caused by the ferromagnetic material, increased initial charging current, and the error of eddy current calculation. But with TPC, the magnetic pitch can be increases up to about 30×10^{-4}, it corresponds to the 60 G of poloidal field with KSTAR normal toroidal magnetic field, 2T. The deuterium prefill range is also increases about 1.5 times than FNC, up to 3×10^{-5} mbar. It overcomes the expected prefill pressure disturbance from NBI effect, up to 2.4×10^{-5} mbar.

The magnetic pitch is related to the plasma loss along the magnetic field lines, so the field null configuration thought to be beneficial with its long connection length to the first wall. But the TPC improves the plasma confinement by trapping motion at the open-field phase and shows widen endurance to the short

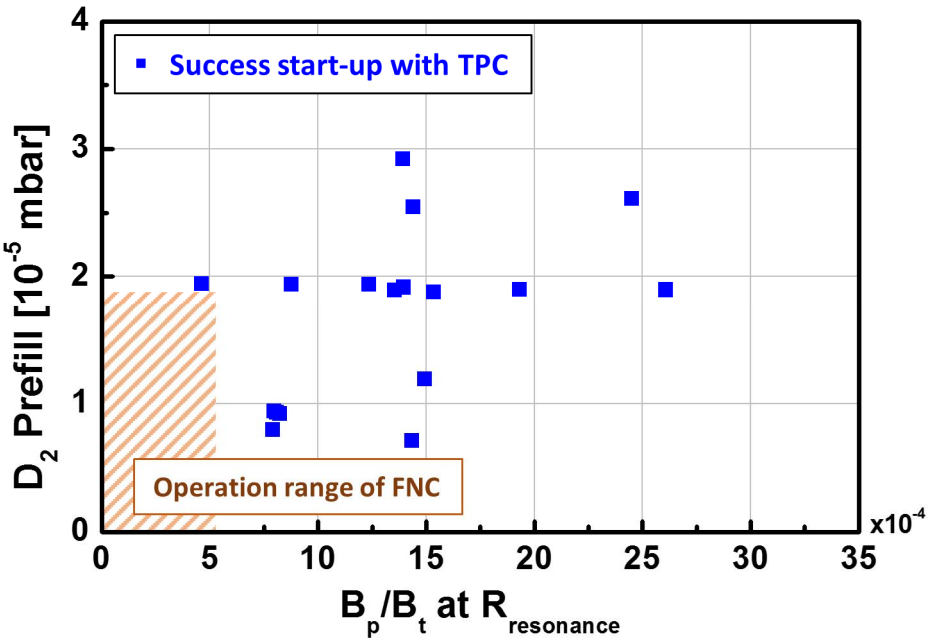

Figure 3.10 Operation range of FNC and TPC for poloidal magnetic field quality and deuterium prefill pressure.

connection length. The enhanced plasma confinement can help to expand the prefill pressure range by covering the increased ionization energy loss.

Chapter 4. Characteristics of TPC start-up

4.1. Operation limits of TPC

With total 27 shots using TPC in 2015 and 2016 campaign, the successful and failure shots plotted on the magnetic pitch and the deuterium prefill window show the different kind of operation limits. One of the operation limit is related to the prefill pressure, too much prefill makes the start-up failure. The other one is related to the lower limit of the prefill with given magnetic pitch. For the robust and reliable start-up with TPC, characteristics of the limits should be identified.

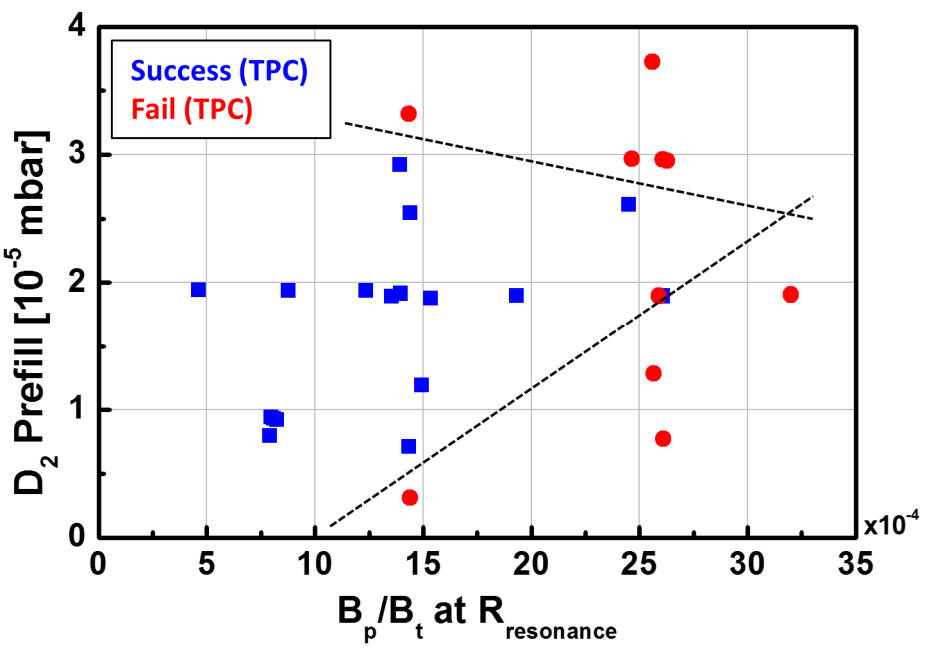

Figure 4.1 Operation window of TPC using 27 shots in KSTAR 2015 and 2016 campaign.

4.2. Parametric dependency of TPC start-up performance

The operation range of TPC start-up is explored with respect to the prefill pressure and the poloidal field strength. The poloidal field strength can be controlled by the variation of the PF#5 charging current from 150 to 750 A/turn, corresponding to the 25 to 75 G at the resonance layer. The prefill pressure is increased up to 2-3 times higher than that of the normal ohmic operation. ECH configuration of 105 and 140 GHz are applied to find the prefill pressure effect. The toroidal magnetic field is adjusted to match the resonance layer at ~1.65 m.

The parameter dependence of start-up performance by the magnetic pitch is studied. The magnetic pitch is defined by the ratio between poloidal magnetic field and toroidal magnetic field at the ECH resonance layer. In this experiments, the toroidal field strength is identical of 1.7 T at KSTAR machine axis, and the magnetic pitch is changed by the charging current variation of PF#5 coil from 150 A to 600 A corresponding to the 25 to 55 G at the resonance layer. 105 GHz, 600 kW of X2 ECH is injected 120 ms before the solenoid swing down for pre-ionization plasmas. The prefill pressure is 1.9×10^{-5} mbar. The experimental results are presented in figure 4.2 (a) for the pre-ionization phase, and (b) for the plasma current formation.

The successful plasma start-up with the magnetic pitch up to 27×10^{-4} is achieved in KSTAR. Such magnetic pitch angle is corresponding to the poloidal field strength of 45 G. It is notable that there is optimal magnetic pitch of 20 to 26×10^{-4} density confinement for density of 4×10^{18} m^{-2}. The low magnetic pitch produces a long connection length, but produces a low plasma density. But the cases with the magnetic pitch less than 27×10^{-4} shows successful plasma current

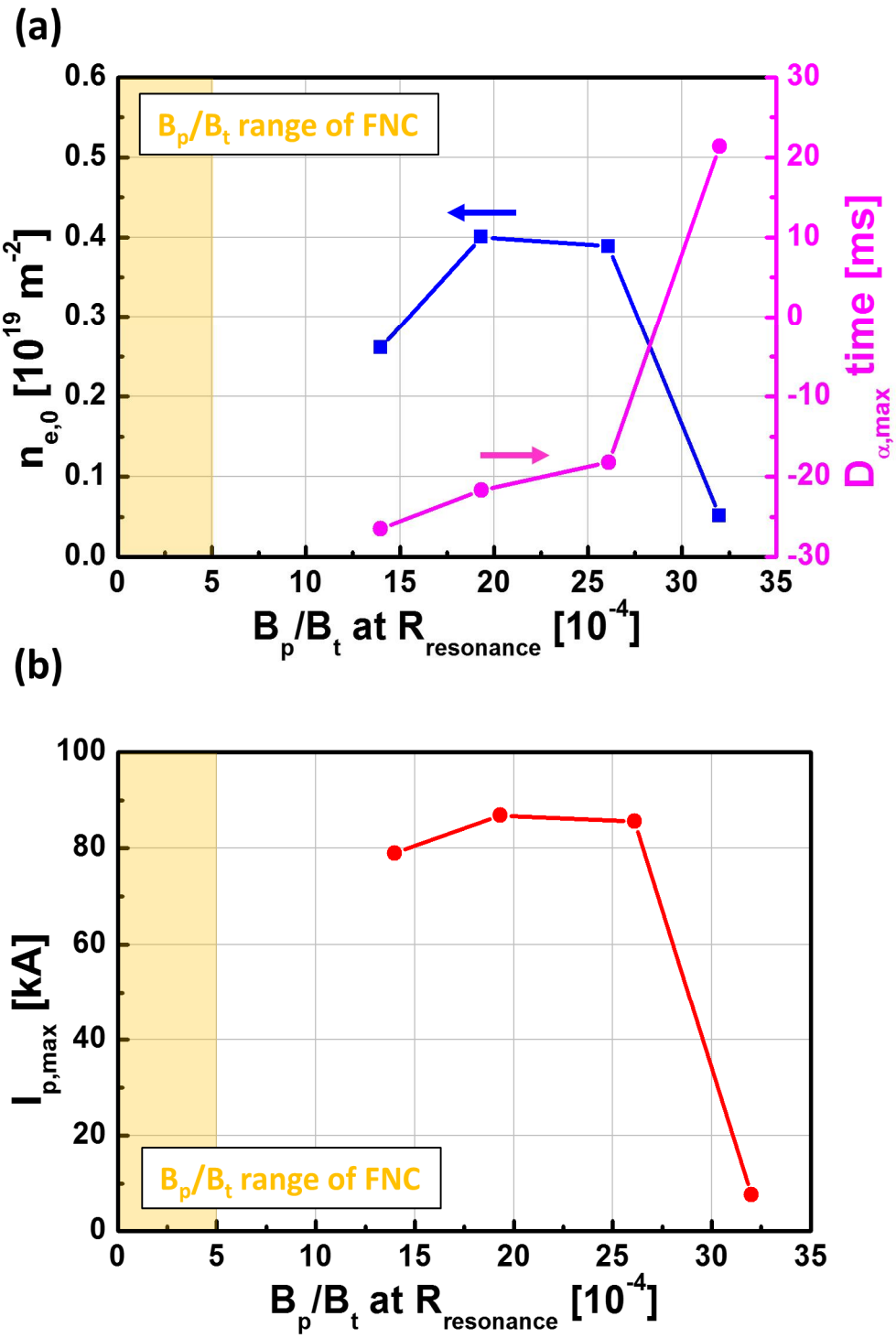

Figure 4.2 Pre-ionization density and peak deuterium line time (a), and maximum plasma current (b) according to the magnetic pitch angle and compared to FNC.

formation up to 80 kA at the end of the start-up phase, and the plasma control system successfully takes over the plasmas.

The result shows that the failure case has low electron density at the pre-ionization phase. Peak signal of deuterium line appeared after applying loop voltage shows that the low ionization rate of ECH plasma. This means that at too high magnetic pitch conditions the plasma loss increases and more power is needed to succeed ionization.

Prefill pressure effect is also explored of TPC start-up and the experimental results are presented in figure 4.3, (a) for the pre-ionization phase, and (b) for the plasma current formation phase. The pressure is varied from 0.3 to 3.5×10^{-5} mbar. 140 GHz of ECH is applied with maximum injection power of 750 kW with injection angle of 20°. The magnetic pitch is fixed of 14×10^{-4}, the poloidal and toroidal magnetic field of 35 G and 2.5 T, respectively. Especially the toroidal field of 2.3 T at the machine axis condition makes the available ECE measurement at the pre-ionization plasma regime and the tendency of electron temperature according to the prefill condition can be identified.

The prefill pressure range of 0.7 to 3.0×10^{-5} mbar show successful plasma current formation up to 80 kA at the end of the start-up phase with pre-ionization density of 1.5 to 0.5×10^{18} m^{-2}. Until the prefill pressure of 3×10^{-5} mbar, the pre-ionization density and the prefill pressure shows linear relation with peak of deuterium line before solenoid swing. The linear relation is depicted in figure 4.3 (a), depicted by the gray dash-dot line. The operation range of prefill pressure is increased 1.5 time higher than FNC. This means that the influence of the second NBI on prefill pressure can be solved through TPC.

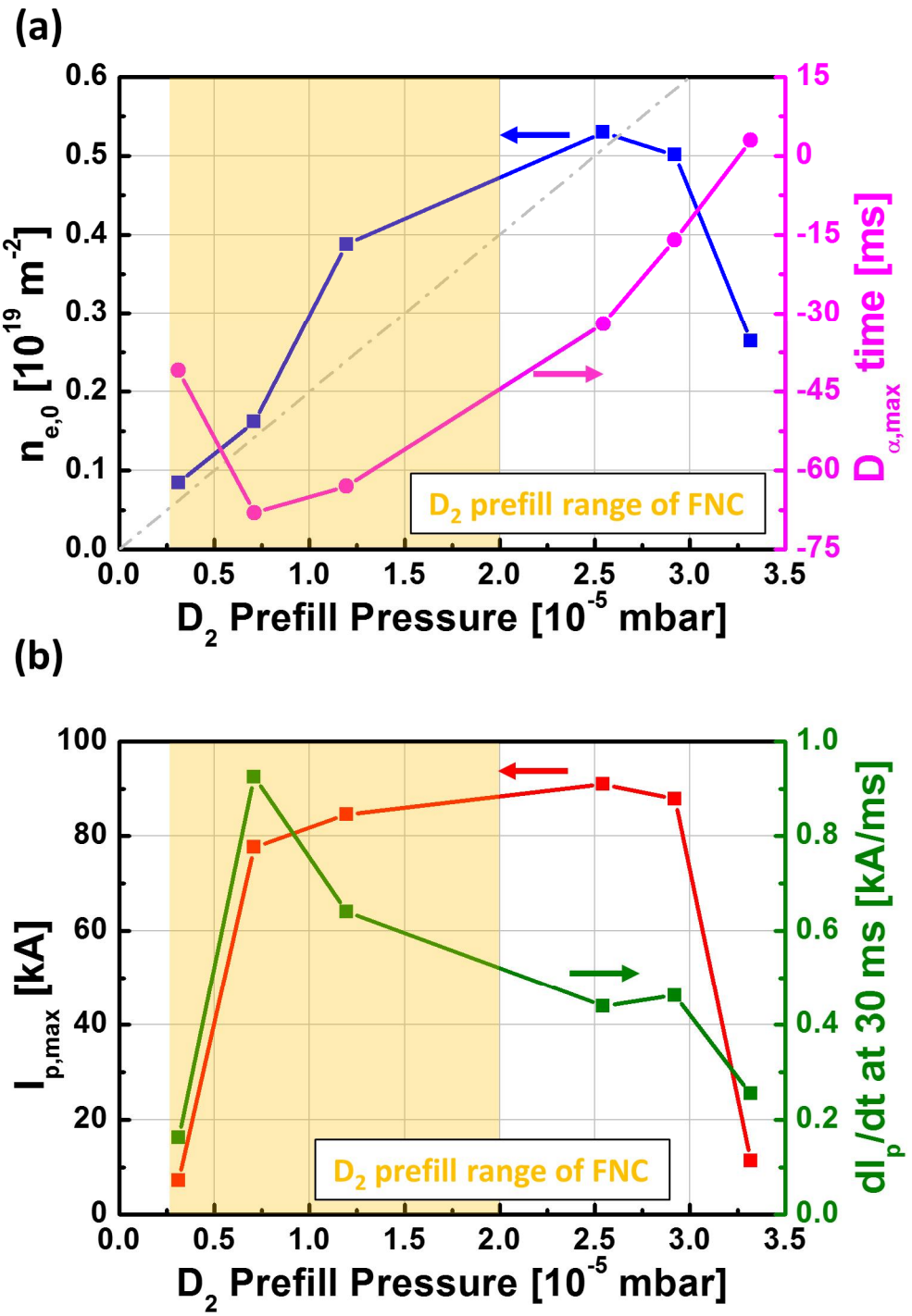

Figure 4.3 Pre-ionization density and peak deuterium line time (a), and maximum plasma current and current ramp-up ratio (b) according to the deuterium prefill pressure and compared to FNC.

Similar to the large magnetic pitch case, the large prefill pressure of $3.3x10^{-5}$ mbar shows delayed peak of deuterium line signal with low pre-ionization density of $2.5x10^{18}$ m^{-2}. Too much prefill pressure to be ionized with given ECH power makes low ionization rate and make start-up failure. And there are another start-up failure case, with low pre-ionization density even though high ionization rate, identified by deuterium line signal. In this case the plasma current does not rising with low current ramp-up rate. With successful shots, the low pre-ionization density makes fast plasma current ramp-up rate. This is because, for a given external heating power, the lower the density, the more favorable the electron temperature rise.

We can summarize the operation characteristics of TPC: there are two kinds of start-up failure case. The first one is the low pre-ionization density even though high ionization rate, and the second one is the low ionization rate driven by too much prefill pressure or too short magnetic connection length. Detailed analysis of both operation limits with upgraded TECHP0D code will be followed.

4.3. Interpretation of operation limits with upgraded TECHP0D and its validation

To analyze the characteristics of both operation limits, upgraded TECHP0D code is adopted with modified input parameter. The low ionization boundary simulates the loop voltage application time while the generation of ECH plasma. The lower pre-ionization density boundary is simulated by reducing the prefill pressure so that the density is low even at high ionization rates. The

simulation results are compared to the experimental results.

For the low density limit case, impurity burn-through can be achieved by ECH only due to the low impurity radiation loss. The plasma facing component of KSTAR is made of carbon, mainly considering the carbon impurity effect. The impurity radiation is defined as;

$$P_{IRAD} \propto n_e n_I f\left(T_e\right) \tag{4.1}$$

where n_e, n_I, and $f(T_e)$ are electron density, impurity density, and reaction rate according to the electron temperature from [51]. Thus, low density can reduce impurity radiation loss, and below a certain density, plasma burn-through conditions can be achieved only through ECH power. In this state, the electron temperature could be increased over 100 eV. This phenomenon can be found in 0D calculations by changing the pre-ionization plasma density with high ionization rate. The electron temperature with electron density in pre-ionization phase is shown in figure 4.4 (a). Without impurity content, then the ECH plasma temperature is always larger than 100 eV. With finite impurity contents, the electron temperature reduces from few hundreds of eV to near 10 eV at the critical density. The critical electron density reduces as the impurity ratio increases.

However, the high electron temperature has a negative effect to the plasma confinement. It makes strong convective loss along the magnetic field line by increasing the sound speed. The fast sound speed due to the high temperature result in the short confinement time, which is shorter than the closed flux surface formation time where sufficient plasma current can overcome the external error field. Therefore in low prefill density case, the convective loss of the plasma is too

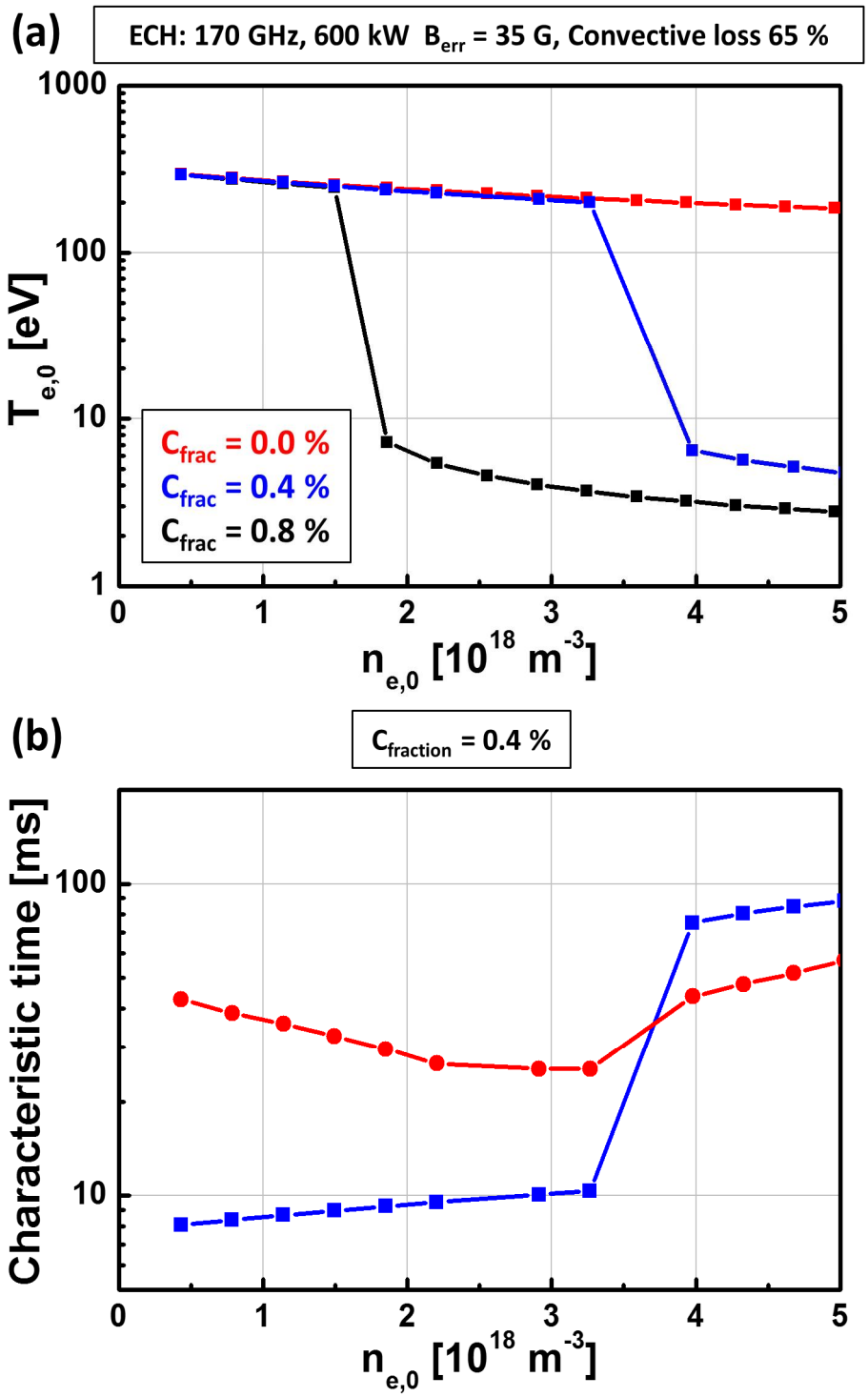

Figure 4.4 Electron temperature according to the electron density of pre-ionization phase under different impurity condition (a), and comparison of convective loss time and closed surface formation time (b).

fast to sustain the plasma until the closed surface formation. Plasma convective loss time along the magnetic field line and closed surface formation time are presented in figure 4.4 (b). Due to the inductance of plasma column, plasma current ramp-up rate is not increased as followed to the high electron temperature. Since the plasma loss time is represented by the characteristic time of the exponential function, 5 times the characteristic time corresponding to the 99 % loss time.

The low electron density effect is validated by the experiments, shot #15888 and #15889. The two shots are located near the lower prefill limits and the success and failure of the plasma start-up are divided by the lower total ionization density difference. The ECE measurements near the machine axis and resonance layer show a trend similar to the electron temperature calculated from the simulation. The comparison of two shots are presented in figure 4.5.

During the pre-ionization phase, the low density shot #15889 shows the electron temperature higher than 200 eV at the 10 cm away from the resonance layer, and also the ECE raw signal is clearly higher. But the pre-ionization density of $2x10^{18}$ m^{-2} case, shot #15888, shows obvious very low temperature and low raw signal. The absolute temperature value could have some error due to its black body assumptions for ECE data processing, but the drastic temperature difference shown in TECHP0D results is also appeared in to experimental condition, the only density difference of less than $1x10^{18}$ m^{-2}. Since the peaks of deuterium line radiation appear in the pre-ionization phase of the shots, it can be seen that both shots have a high ionization rate. The low density shot fails to plasma current formation. The

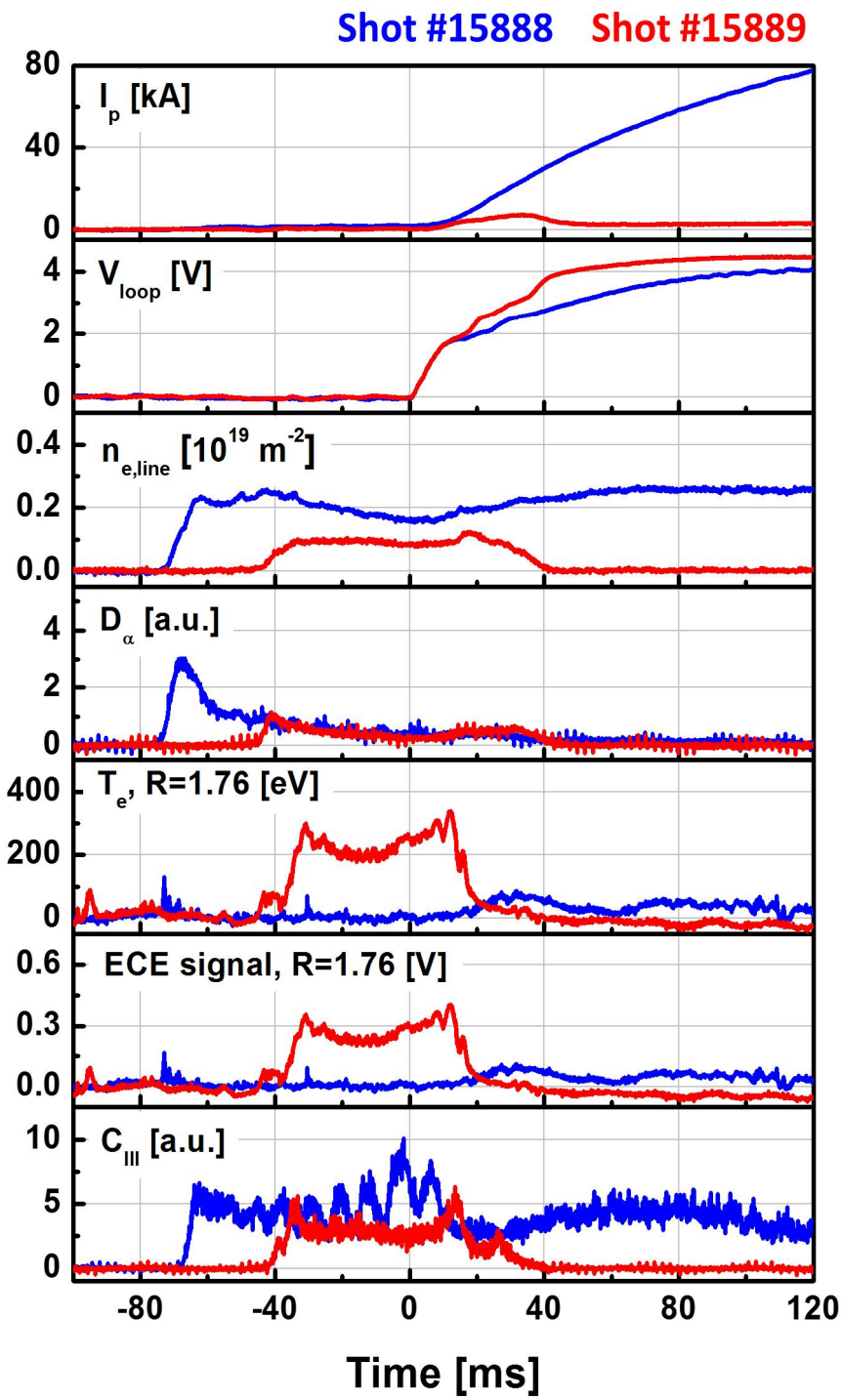

Figure 4.5 Plasma parameters of start-up success (#15888) and failure (#15889) case in KSTAR.

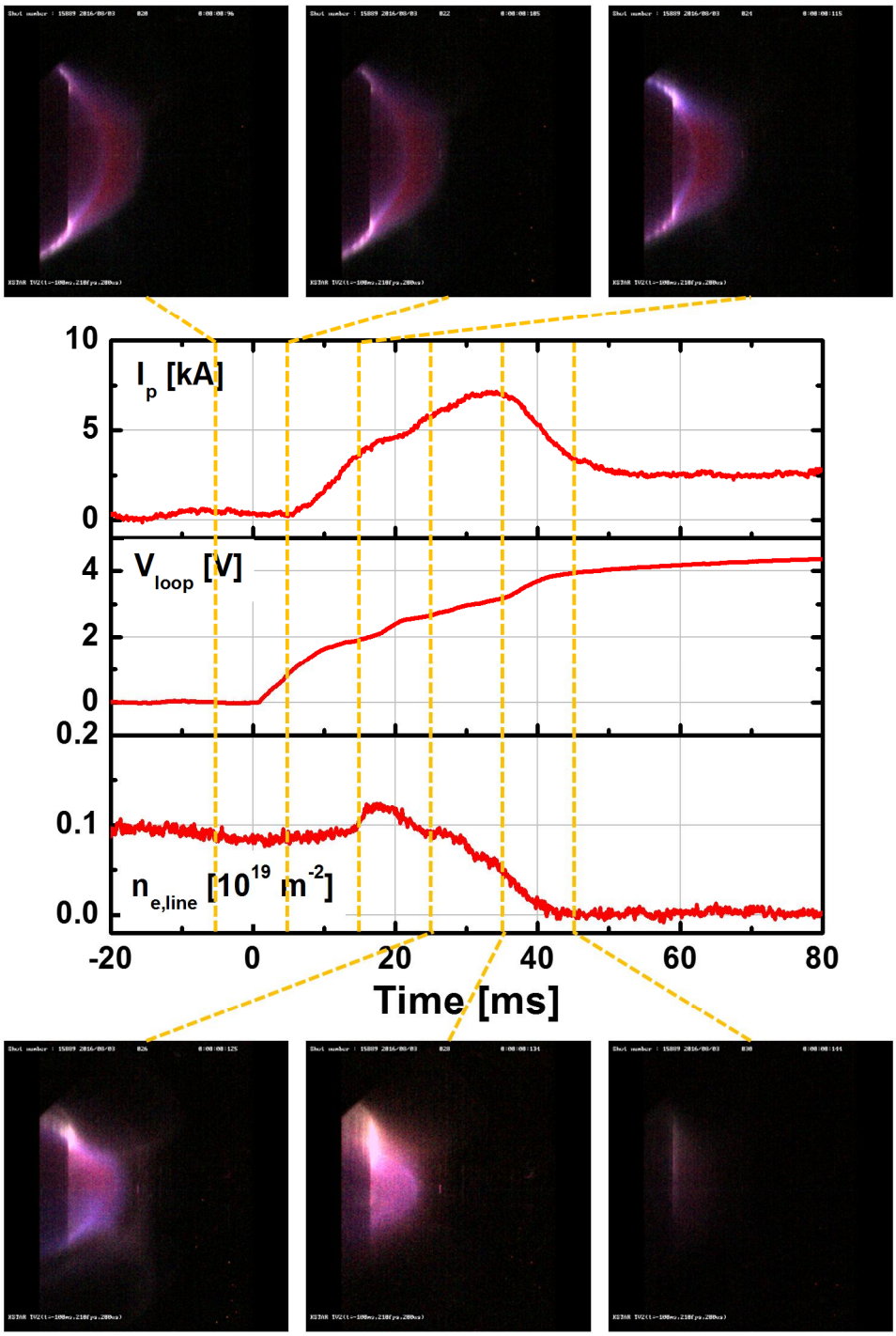

Figure 4.6 Plasma parameters and fast camera images of the start-up failure case.

characteristics of low density failure case is also found by the fast camera images. In failure case, the pre-ionization plasmas with curved magnetic field is identified at the camera images. However, no plasma column is formed after the solenoid swing down, and all the plasma is lost through the vacuum wall for about 50 ms. From 5 ms before the loop voltage is applied, the camera image at 10 ms intervals is shown in Figure 4.6 with different plasma factor changes. The image shows the clear plasma loss without plasma column formation. This is consistent with the plasma density and current measurement results.

To simulate the case of low ionization rate limits, plasma start-up performance with different ohmic power application times is studied. A plasma start-up simulation with three different ohmic power injection timings is shown in figure 4.7. The simulation shows a delayed electron temperature rise with a low ionization rate. A lower electron temperature increases the plasma resistance and slowly increases the plasma current. The delayed temperature rise is caused by an ionization reaction with a low ionization rate and convection loss without forming a closed surface. Figure 4.8 shows the closed flux formation time due to the ionization speed in the solenoid swing-down. Early closed magnetic surfaces are formed at high ionization rates.

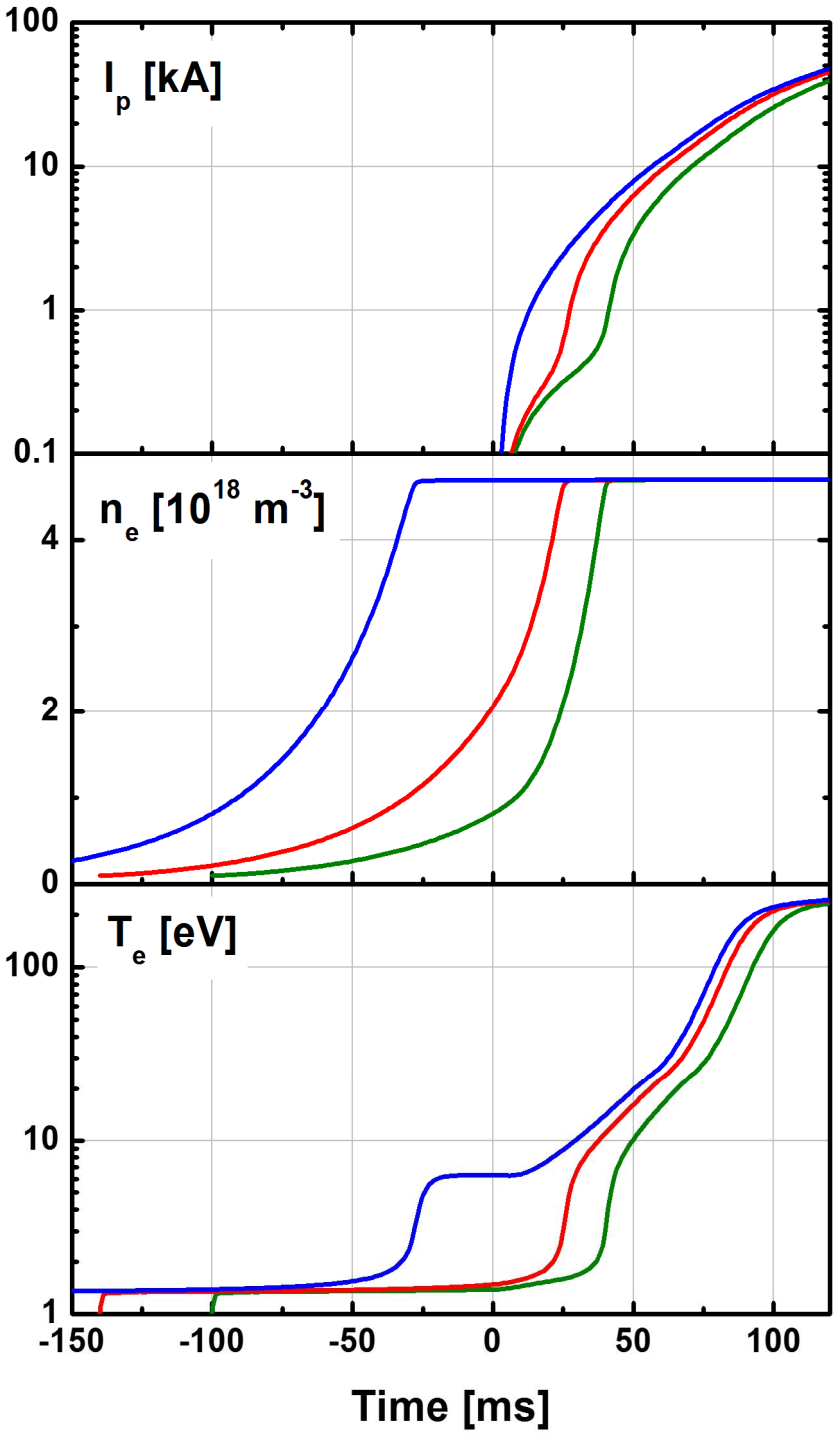

Figure 4.7 Start-up simulation with different ionization rate at solenoid swing down.

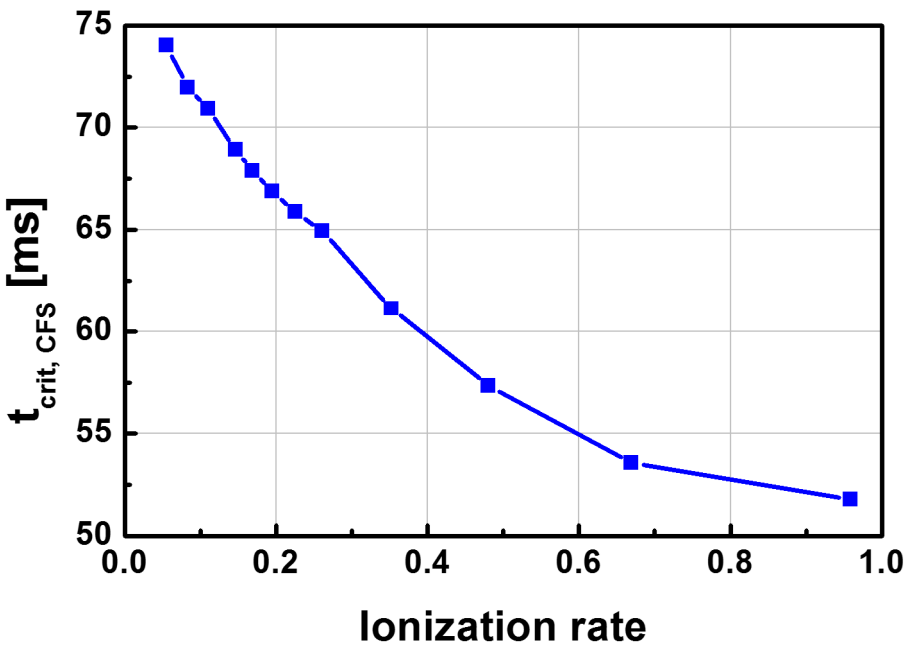

Figure 4.8 Simulation results of closed surface formation time according to the initial ionization rate.

4.4. ECH power effect to the operation limit

The ECH power effect to the TPC start-up is identified with TECHP0D modeling, because the experiments with various ECH power is impossible. The ECH power affect the both operation limits, the simulation results are depicted in figure 13. First, the low ionization limit is moved to higher prefill due to the increased input ECH power. The ionization rate can be increases with much higher ECH input power. But the low pre-ionization density limit is moved to higher prefill regime simultaneously, because the higher ECH power can make impurity burn-through with higher impurity radiation. Therefore, the ECH power does not extend the reliable operation range but moves to the high prefill pressure region.

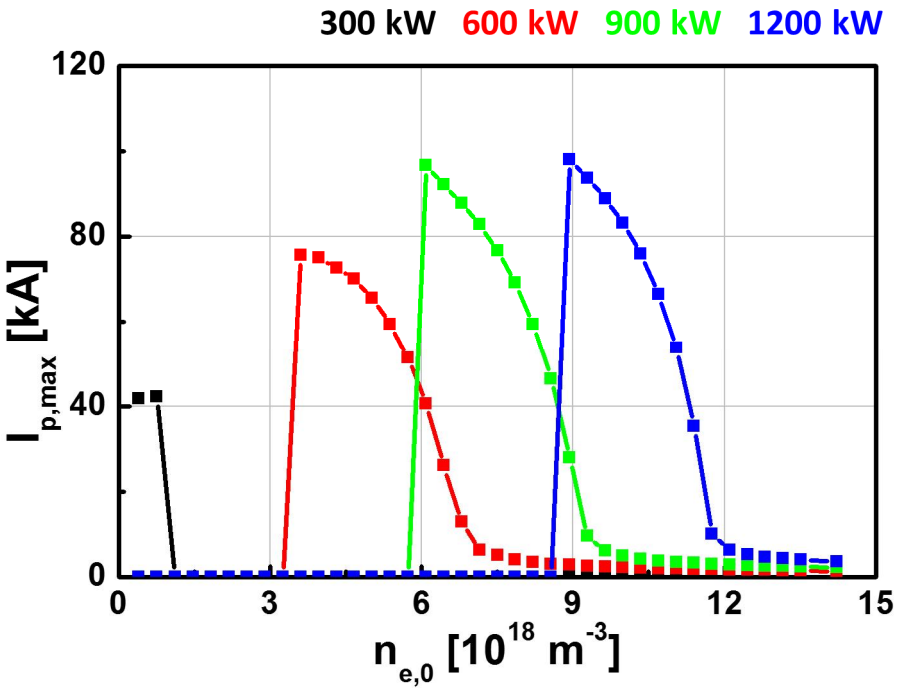

Figure 4.9 Simulation of operation window according to the ECH power.

Chapter 5. Feasibility study of TPC start-up for ITER

A low toroid field start-up for the development of a new baseline scenario of KSTAR as well as for the verification of ITER design parameters was demonstrated using the TPC method in KSTAR. ITER PF coil geometry and ECH conditions are considered to predict start-up of ITER based on the TPC. Particularly, since the 2^{nd}-harmonic collisionless heating characteristics are closely related to the machine safety problem, they are discussed based on the KSTAR results. ITER's TPC-based transient start-up scenarios with eddy currents calculation have been developed and compared with existing FNC based scenarios.

5.1. ITER-relevant toroidal electric field start-up experiments in KSTAR

Stable low loop voltage start-up using TPC is achieved in KSTAR. BRIS-less low loop voltage start-up has been tried for reversed plasma current operation until 2012 campaign based on FNC, but the start-up was very unstable. After employing TPC, the start-up has been significantly improved. One of the experimental results are depicted in FIG. 4. In this scenario, the toroidal electric field is 0.26 V/m less than 0.3 V/m, relevant to ITER [28]. 140 GHz, X2 ECH power up to 750 kW is injected for 90 ms with toroidal angle of 15° before the loop voltage onset. Prefill pressure of 0.7×10^{-5} mbar is applied for successful deuterium ionization with reduced ohmic power. As a result, the pre-ionization density of 1×10^{18} m^{-2} is formed. Peaked deuterium line signal shows high pre-ionization rate during pre-ionization phase and the carbon impurity signal is kept low level during

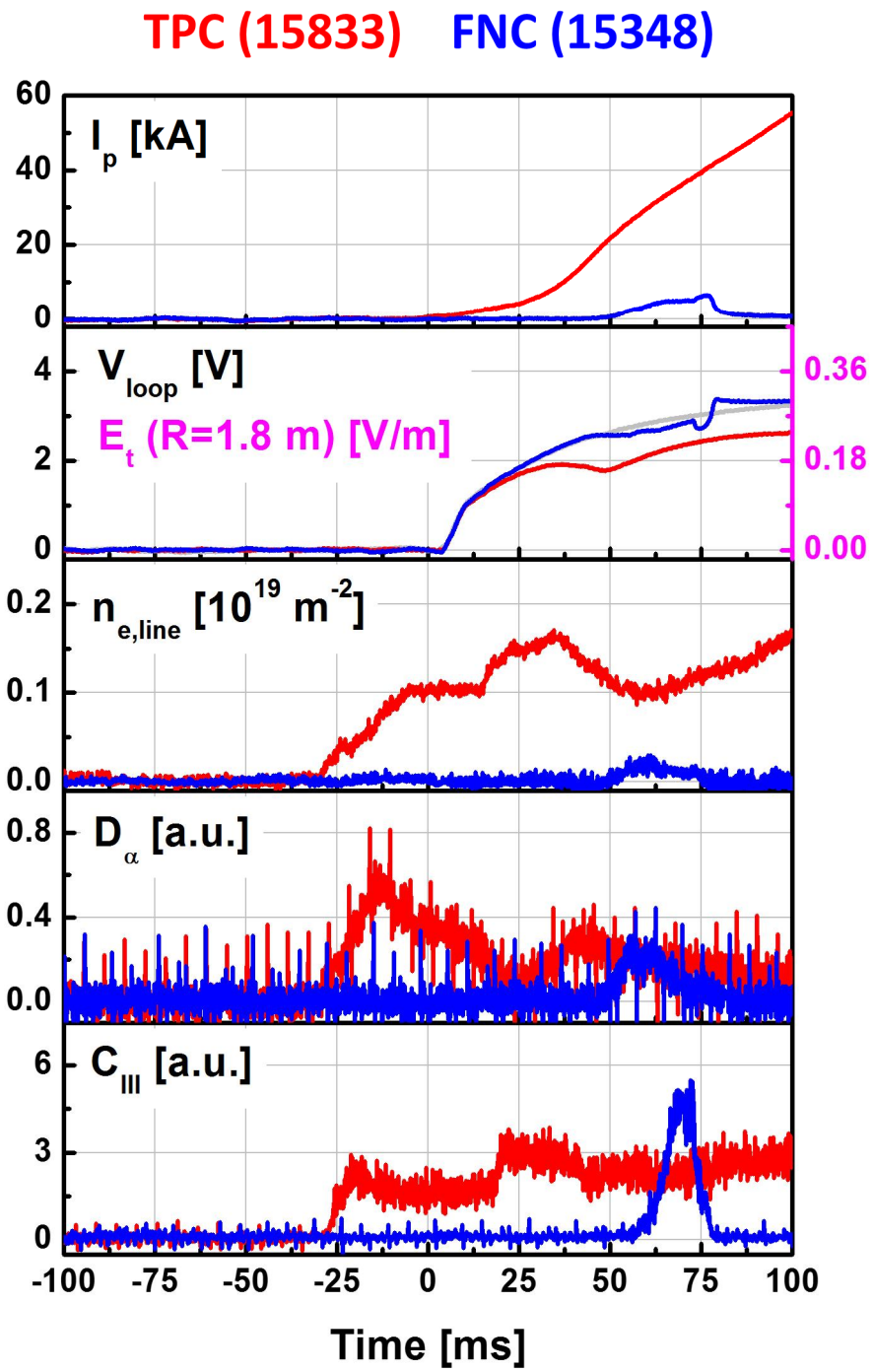

Figure 5.1 Comparison of low toroidal electric field start-up using FNC (#15348) and TPC (15833) in KSTAR.

the whole start-up phase. The poloidal field strength at the resonance layer is 27 G.

Low electric field start-up is major issues of both KSTAR and ITER. In KSTAR, the reversed plasma current operation has been tried as a new reference scenario for various physics studies related to the resonant magnetic perturbation, the plasma rotation, and so on. But such low toroidal field makes rarely successful plasma start-up even though the assistance of ECH. In ITER, it has been noticed that the low toroidal electric field due to the engineering limitation of superconducting solenoids operation makes difficulties for reliable plasma start-up.

The low toroidal electric field start-up experiments using TPC is presented in figure 4.1, with comparison of FNC. The applied toroidal electric field is less than 0.3 V/m during whole start-up phase, relevant to the ITER level. With FNC, there is no pre-ionization plasmas and failure to plasma current formation. But with TPC, the pre-ionization plasma with density of $1x10^{18}$ m^{-2} is formed. Peak deuterium line signal shows high ionization rate during the pre-ionization phase. The plasma current of 60 kA is achieved at the end of the pre-programmed start-up phase. The carbon line radiation monitor shows no severe carbon influx during start-up. This result shows not only the promising results for ITER TPC, but also the expansion of the capability to various physical experiments for KSTAR. The experimental results of TPC and FNC are presented in figure 4.1.

5.2. PF geometry for mirror-like magnetic field structure and ECH/ECCD condition of ITER

The PF coil must be carefully determined to make the TPC structure because the ITER has an up-down asymmetric structure. In the ITER configuration, PF# 1 and PF# 6 correspond to the coil positions used to make the TPC in KSTAR. However, the number of turns of PF # 6 is twice that of PF # 1. Therefore, coil current of both coils are determined by considering the difference of turn number.

Figure 4.2 shows the magnetic configuration generated by 500 A of PF#1 and 250 A of PF#6. In this case, the TPC structure is formed with 20 G of poloidal field near the machine axis. The poloidal flux contour depicted by yellow solid lines shows clear TPC structure generated with ITER geometry. The mirror ratio of ITER is 1.5, which is slightly higher than KSTAR because the aspect ratio of ITER is 3.1, which is lower than 3.6 of KSTAR.

The toroidally inclined ECH/ECCD of ITER also need to be considered due to its low heating efficiency than pure perpendicular injection. The multi-machine compassion research shown that the toroidally inclined injection of 20° in ITER makes the increased threshold power for pre-ionization plasma factor of 2 [52]. Also in DIII-D, it was observed that the maximum D_α was influenced by the ECH angle of incidence as shown in figure 4.3. In KSTAR TPC experiment, the ITER-relevant ECH/ECCD configuration of 170 GHz, X2 with toroidal injection angle of 20° successfully makes $4x10^{18}$ m^{-2} pre-ionization plasmas. In this case, the injection power is 600 kW and it takes 20 ms for collisionless heating.

ECH pre ionization has issues related to machine safety. Injected ECH

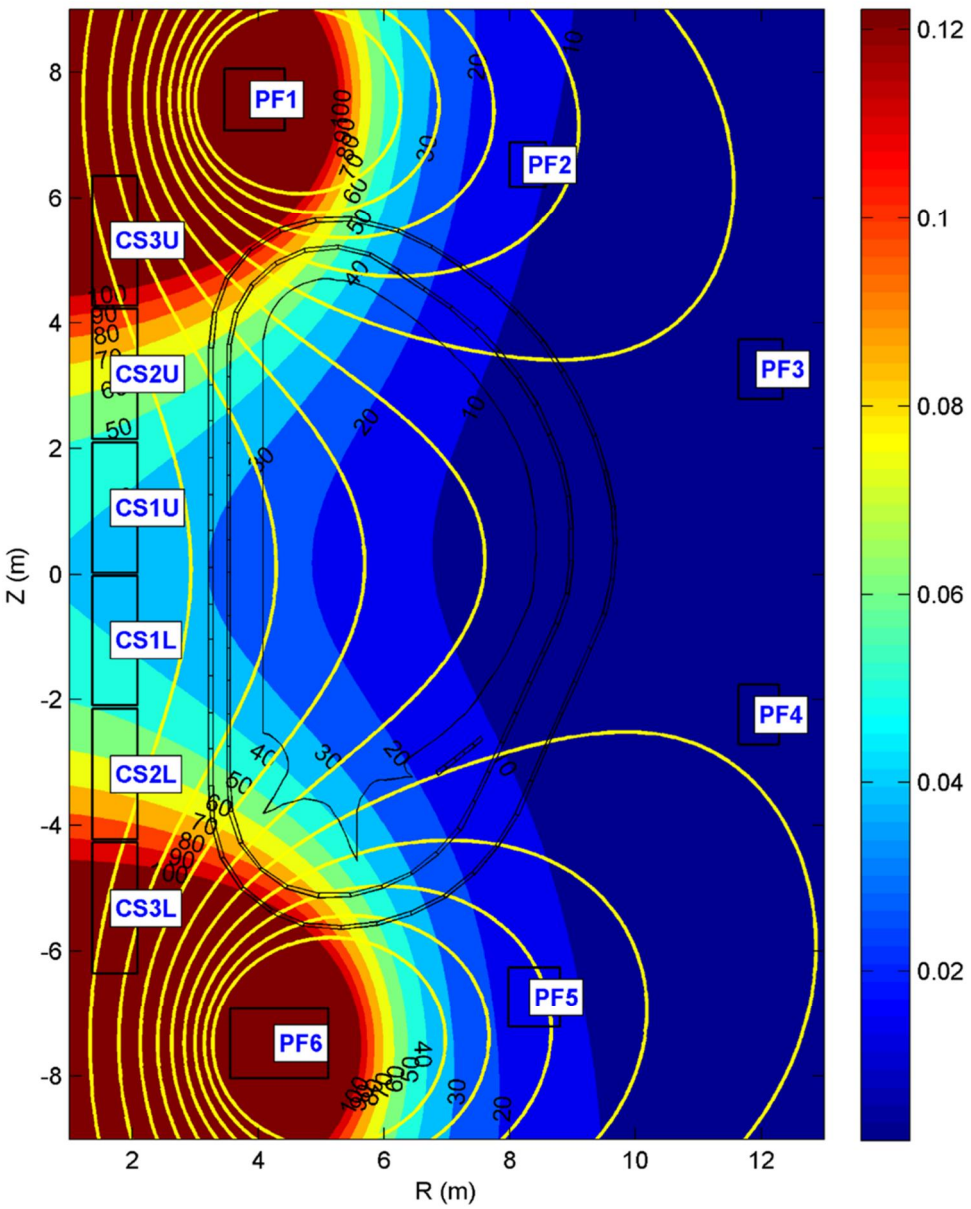

Figure 5.2 Mirror-like poloidal magnetic field structure made by PF#1 and PF#6 in ITER.

power can damage the in-vessel components because there is no target plasma to absorb the ECH power at the collisionless heating phase. Unabsorbed power can be reflected in the chamber and damage the in-vessel component. By comparing the energy growth rate during the collisionless heating phase derived in [22], the required time for ECH plasma formation can be estimated. With identical ITER ECH configuration of 600 kW, 170 GHz and toroidally inclined launch, it takes 20 ms delay for collisionless heating in KSTAR with TPC structure. The ratio of $\beta_{ITER}/\beta_{KSTAR}$ according to ECH injection power in ITER is presented in figure 4.4. With this ratio and the 20 ms delay time measured in the KSTAR experiment, the delay time in the ITER can be predicted. For example, with 1 MW injection shows the heating efficiency ratio of ~0.3 and the delay time in ITER can be estimated to ~ 60 ms.

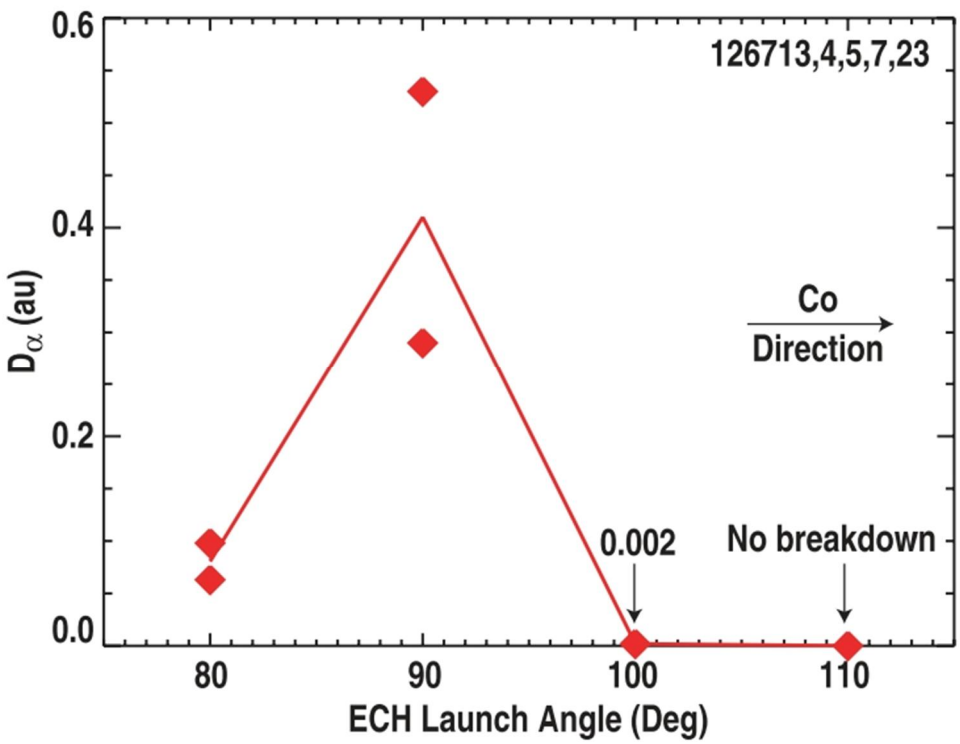

Figure 5.3 ECH plasma formation according to the ECH injection angle in DIII-D [16].

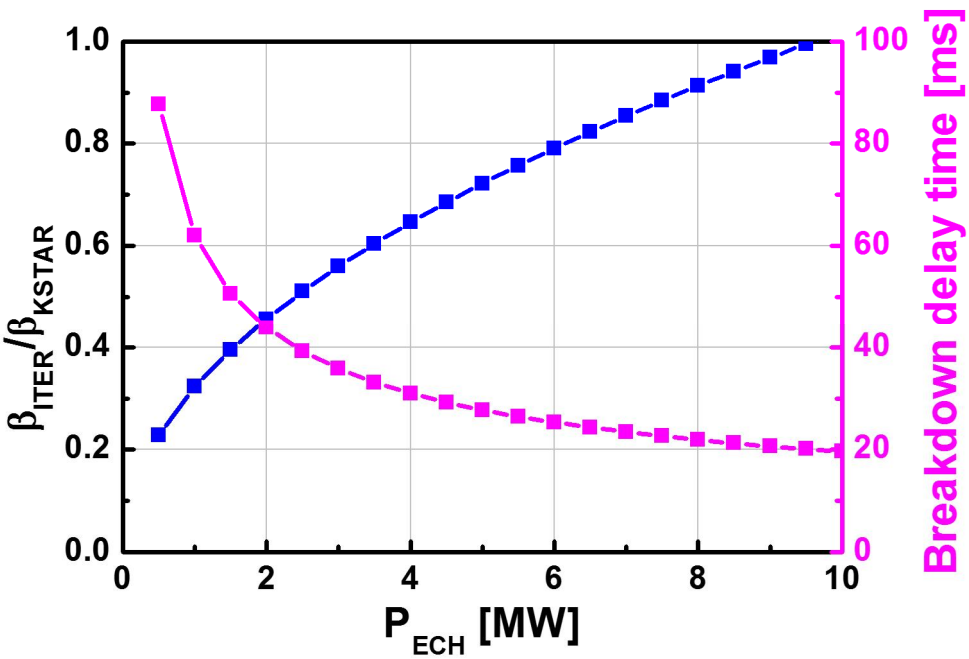

Figure 5.4 Ratio of collisionless energy growth rate between KSTAR and ITER.

5.3. Start-up scenario development based on TPC in ITER and comparison with FNC

The start-up scenario using TPC is developed using time dependent poloidal magnetic field calculation with eddy currents induced on the toroidally continuous conducting structure of ITER. The reference scenario is based on ITER_c_33NHXN_v3_4, half charging CS and power supply configuration B. The solenoid operation is identical but the initial charging current of CS3L and CS3U is changed to 23.5 kA/turn with up-down symmetricity. Current waveforms of the outer PF coils are newly developed.

The magnetic properties of original FNC is proposed in figure 4.5. In original FNC scenario, due to the large eddy current and SC solenoid operation, the target toroidal electric field of 0.3 V/m is achieved 0.8 s after the solenoid swing down. To maximize the electromagnetic condition, the poloidal field structure is optimized to make field null structure at 0.8 s. It is assumed that a plasma is generated at that time, and then simulates the rise of the plasma current by the applied loop voltage. The magnetic field configuration is also changed to plasma equilibrium with satisfying position stability, described by decay index.

The TPC method can further improve the plasma start-up scenario. Based on the KSTAR results, the minimum toroidal electric field for initiating the plasma current is achieved in 0.2 s after the solenoid swing down. This not only reduces the amount of wasted solenoid flux, but also reduces the AC losses to enable stable superconducting coil operation. In TPC scenario, it is assumed that the plasma current evolution phase is identical to original FNC.

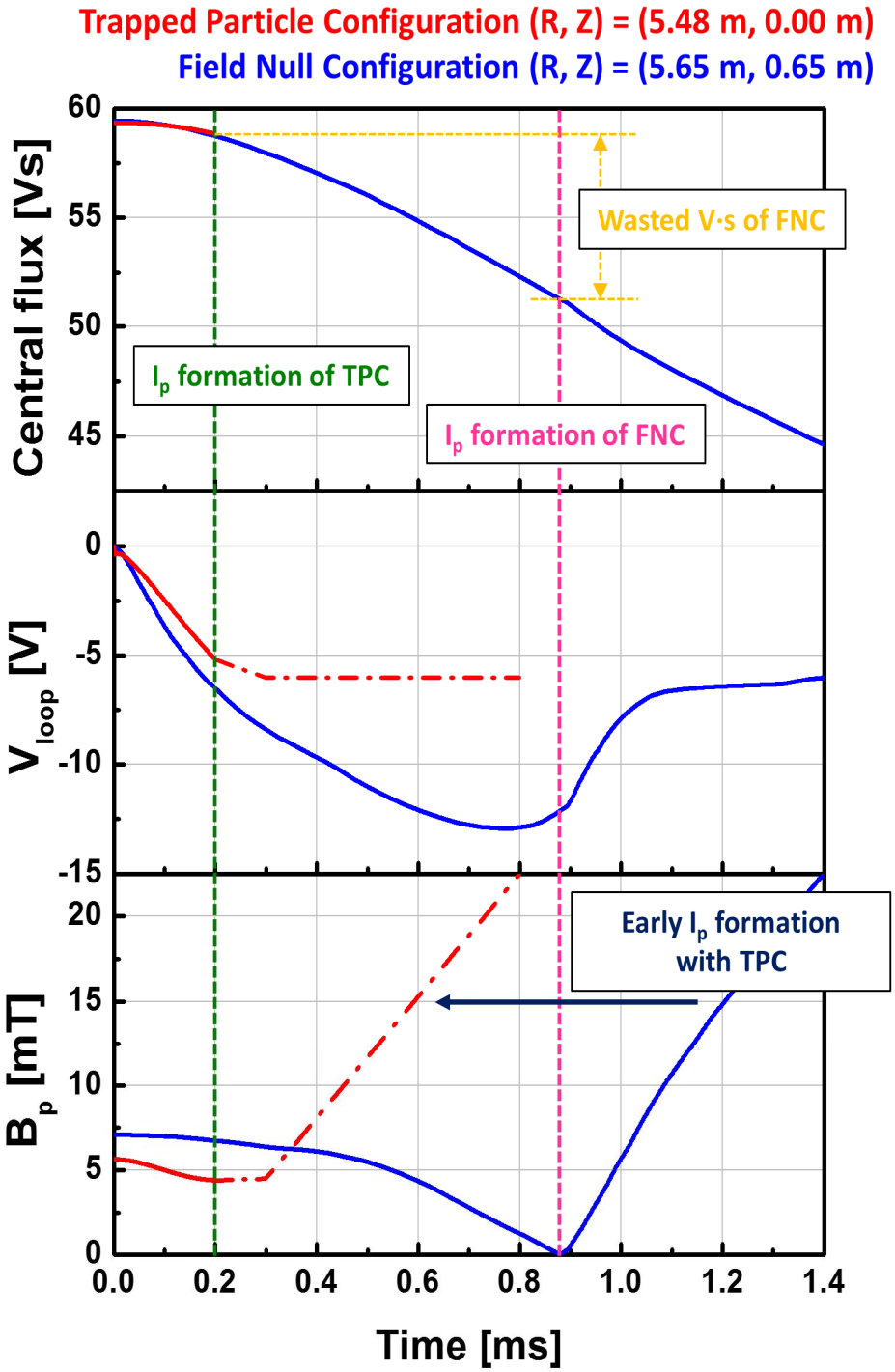

Figure 5.5 Time trace of magnetic characteristics of FNC based scenario and newly developed TPC based scenario to ITER.

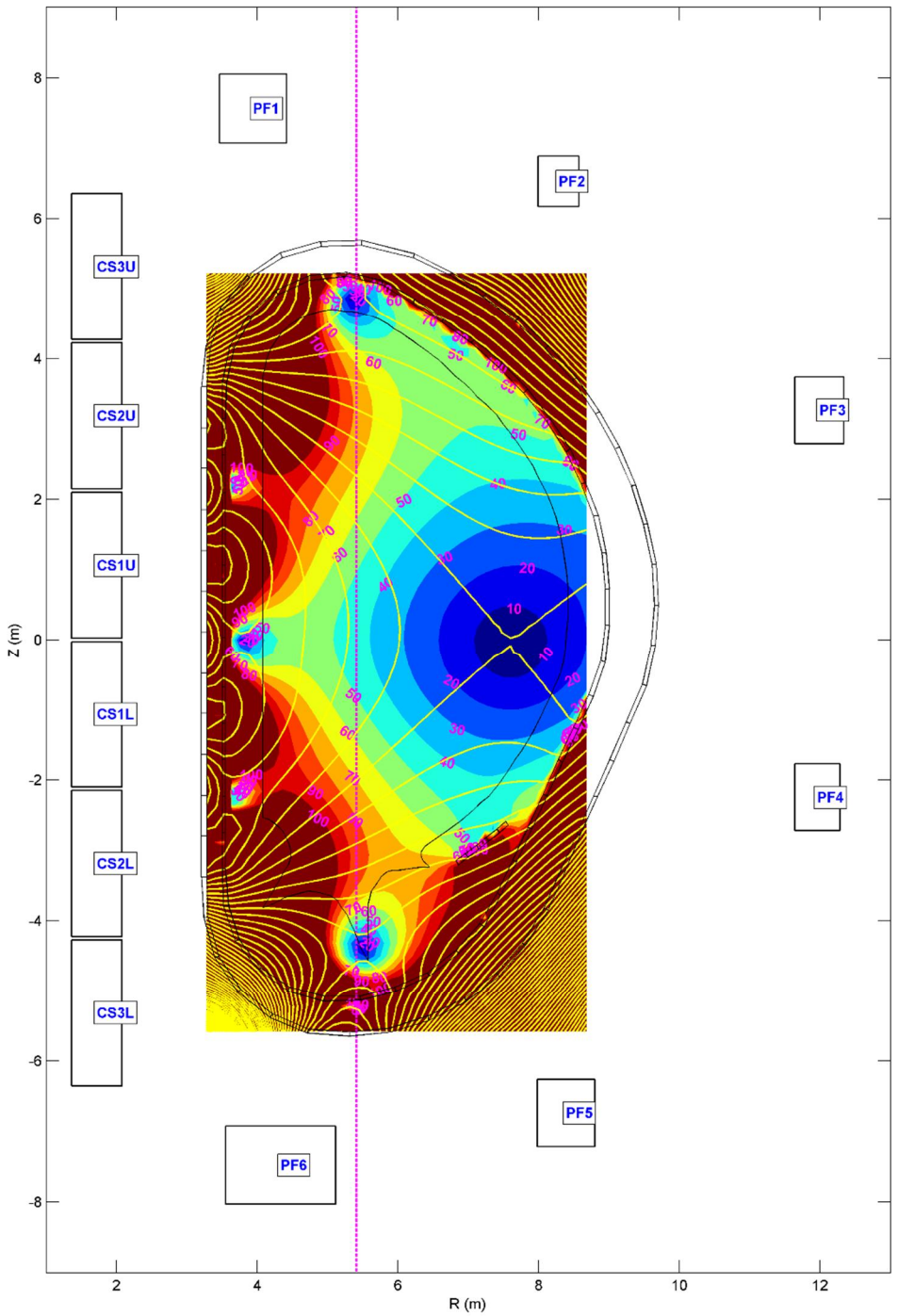

Figure 5.6 Poloidal field structure of TPC based scenario at 0.2 s to ITER.

The poloidal field strength and the flux contour at the 0.2 s on newly developed scenario is proposed in figure 4.6. The PF#1 and PF#6 currents are modified to generate the TPC structure. Due to the other PF coils, there are some field null structure, but it is not relevant to plasma formation because it is too close to the first wall so the connection length is not enough. The ECH resonance layer is located on the TPC configuration, and the ECH plasma can be confined by the trapping motion. The magenta vertical dashed line in figure 4.6 indicates the 170 GHz ECH resonance layer. The strength of the poloidal field in the midplane, resonance region is 40 Gauss, which is a proven value in KSTAR that start-up can be improved.

Chapter 6. Conclusion and future work

The plasma start-up using TPC is successfully demonstrated in KSTAR. Owing to improved confinement of ECH pre-ionization plasmas, the experiments show the earlier and the faster plasma current formation can be obtained with wider operation range in terms of the deuterium prefill pressure and the magnetic pitch at the identical loop voltage for TPC compared with FNC. Such efficient plasma start-up with ECH plasmas is also confirmed by the start-up modeling code, TECHP0D where the open-field confinement model is newly improved in this work. It is shown that the confinement is enhanced by the particle trapping motion. TPC is helpful to overcome the limitation of FNC such as the poloidal magnetic field and prefill pressure control issues in KSTAR, and also expected in ITER.

Efficient plasma start-up using TPC is demonstrated in KSTAR with a broad operation range in terms of the error field strength, prefill gas pressure, and the toroidal electric field. Especially the toroidal electric field could be reduced lower than the ITER target value. The operation window is found from experiments which provides the experimental guideline for stable start-up using TPC. The physics background of the operation limits are investigated with TECHP0D which reveals that the low and the upper prefill limit result from the convective loss of plasmas before the closed flux formation and the loss of electron energy by ionization during the plasma current formation phase, respectively.

Based on these results, feasibility study of ITER start-up scenario by using TPC is done under the ITER-relevant conditions established in KSTAR. The TPC scenario shows advantages of early current initiation without delicate

magnetic field control. ITER-like ECH/ECCD configuration is also tested in KSTAR of 170 GHz X2 frequency and 20° of toroidal injection angle. In these experiments, efficiency of plasma start-up using TPC is validated. Finally, it is confirmed that the TPC structure can be produced by using the ITER PF coil system.

The ITER-relevant low loop voltage start-up is also achieved in KSTAR with a drastic increase of the plasma start-up success rate using TPC. Using these results, the start-up scenario TPC is proposed in ITER and preliminary predictive simulations are performed with the eddy current calculation on the toroidally conducting structures. The critical toroidal electric field using TPC can be achieved at 0.2 s after the solenoid swing down in ITER while the PF#1 and PF#6 can generate the mirror-like field structure at the 2^{nd} harmonic ECH resonance layer. Using TPC, not only severe volt-second savings but also stable superconducting operations with a reduced required toroidal electric field are achieved which is promising for a reliable and stable plasma start-up in ITER. The time delay of 2^{nd} harmonic pre-ionization for the collisionless heating phase is also estimated based on the KSTAR results, which is a machine safety issue of the ECH-assisted start-up.

An efficient and reliable start-up with TPC can significantly resolve the start-up related issues in KSTAR, and expected to be one of main start-up methods for future superconducting tokamaks, such as JT60-SA, ITER, and beyond. Such efficient start-up schemes are also helpful to plasma initiation in the spherical torus with solenoid-free start-up methods like outer PF coil start-up or helicity injection.

Appendix A. TPC experiments in VEST

In VEST device, the study of ECH-assisted plasma start-up has been conducted with the Electron Bernstein Wave (EBW) physics study. The basic characteristic of plasma start-up is presented in [26]. But additional start-up studies with magnetic mirror-ratio effect is conducted. Based on the previous results, the reference plasma start-up scenario using TPC with full solenoid flux capability is developed.

A1. Magnetic mirror ratio effect to plasma start-up

The plasma current formation researches with different magnetic mirror ratio is conducted in VEST devices using various PF coil combination. In previous work, the pre-ionization plasma qualities according to the magnetic mirror ratio is presented, but the plasma current initiation result is not shown.

To generate the different magnetic mirror ratio condition, different PF coil sets are applied. VEST has one long solenoid and 9 up-down symmetric PF coil sets for various magnetic field control. For conventional TPC, serially connected PF#3 and #4 are used, and PF#5 and PF#9 are used to make low mirror ratio configuration. By controlling the applied current to PF coils, the poloidal field strength at the resonance layer is determined as about 10 G at the solenoid swing down. The magnetic field configuration of both mirror ratio case with EC resonance layer is presented in figure A.1.

For pre-ionization, 6 kW, 2.45 GHz of EC wave is injected with extraordinary, fundamental condition. Toroidal magnetic field is 0.1 T at the

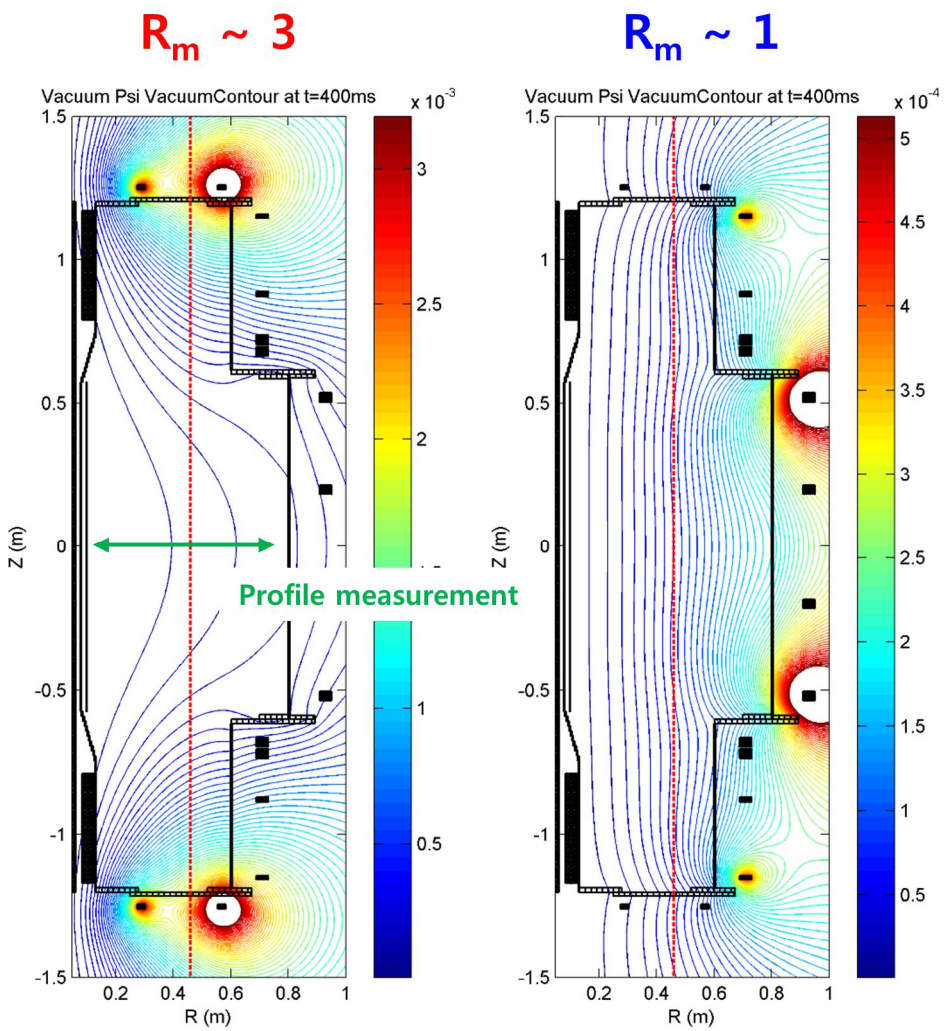

Figure A.1 Magnetic field configuration of different mirror ratio in VEST. Rm~3 case and Rm~1 case.

machine center, major radius at 0.4 m, and the resonance layer is major radius of 0.43 m. Wave is injected perpendicular for efficient plasma heating, not current drive. The prefill pressure is $2x10^{-5}$ Torr, and the diagnostics as movable triple Langmuir probe and basic magnetic diagnostics are applied.

The electron density and temperature profiles at the pre-ionization phase is presented in figure A.2. The low mirror ratio case, $1x10^{17}$ m^{-3} of pre-ionization density is formed near the EC resonance layer. The density diffuses to the low magnetic field side from resonance layer, but the density is negligible at the high field side. Electron temperature profile also shows that the heated plasma over 10 eV at the low field side, but the low temperature at the high field side. But with higher mirror ratio case, the plasma is formed at the broaden region, both low field side and the high field side. Especially, level of 10^{16} m^{-3} electron density is formed at the high field side, which is about one order higher than the low magnetic mirror case.

The plasma start-up experiment with identical loop voltage is conducted to both mirror ratio case. In high mirror ratio case shows the successful plasma current formation up to 16 kA, but the start-up is failed with low mirror ratio case. The plasma resistivity profile using Spitzer's formulation shows that the resistivity of high mirror ratio case is less than half than the low mirror ratio case, especially at the high field side. Due to the low aspect ratio, the toroidal electric field at the high field side is higher than the low field side. Therefore, the pre-ionization plasma quality at the high field side is much important to reliable start-up.

The experiments show that the open field confinement can be improved

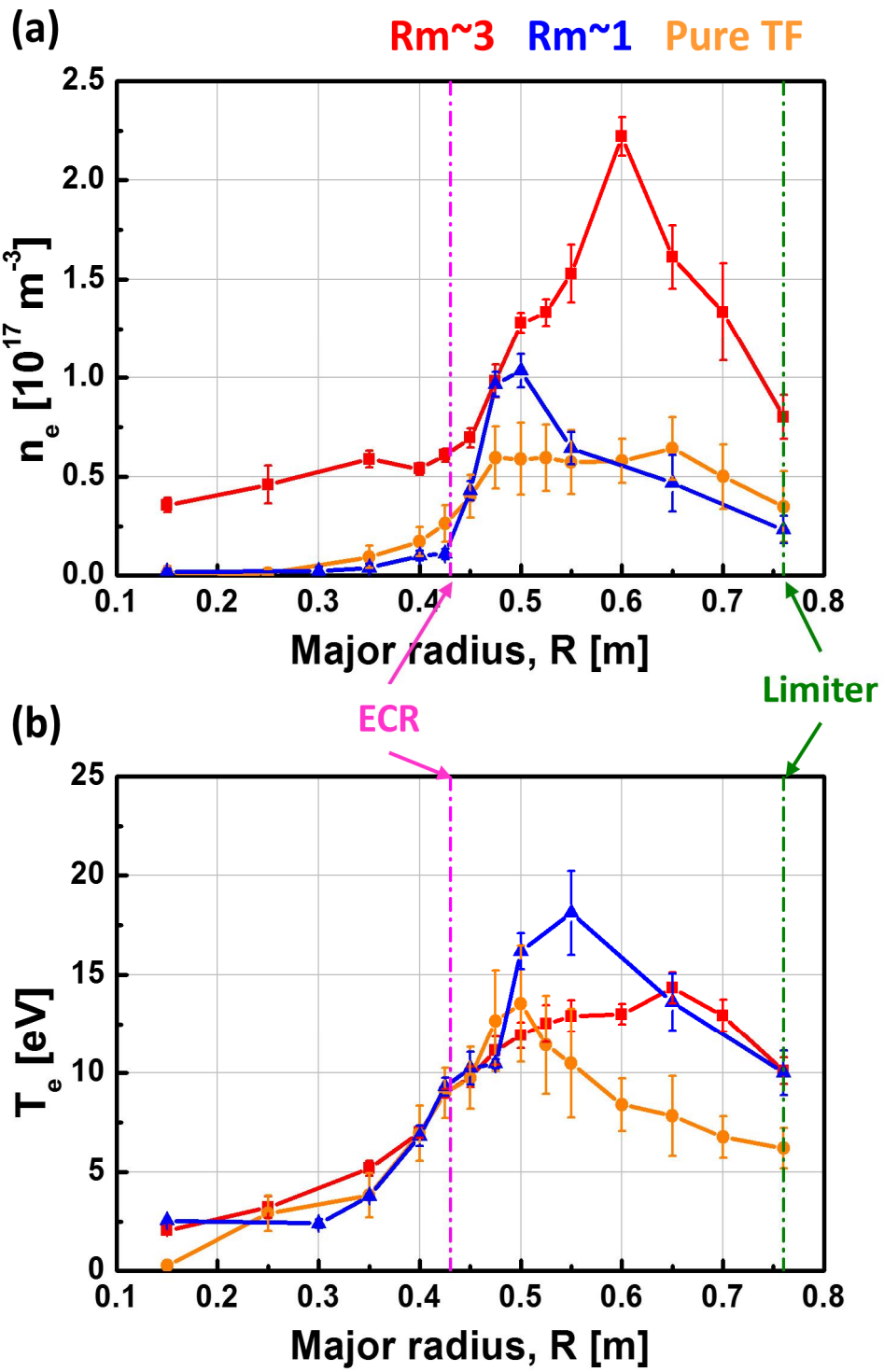

Figure A.2 Pre-ionization density (a) and temperature (b) profile with different mirror ratio case.

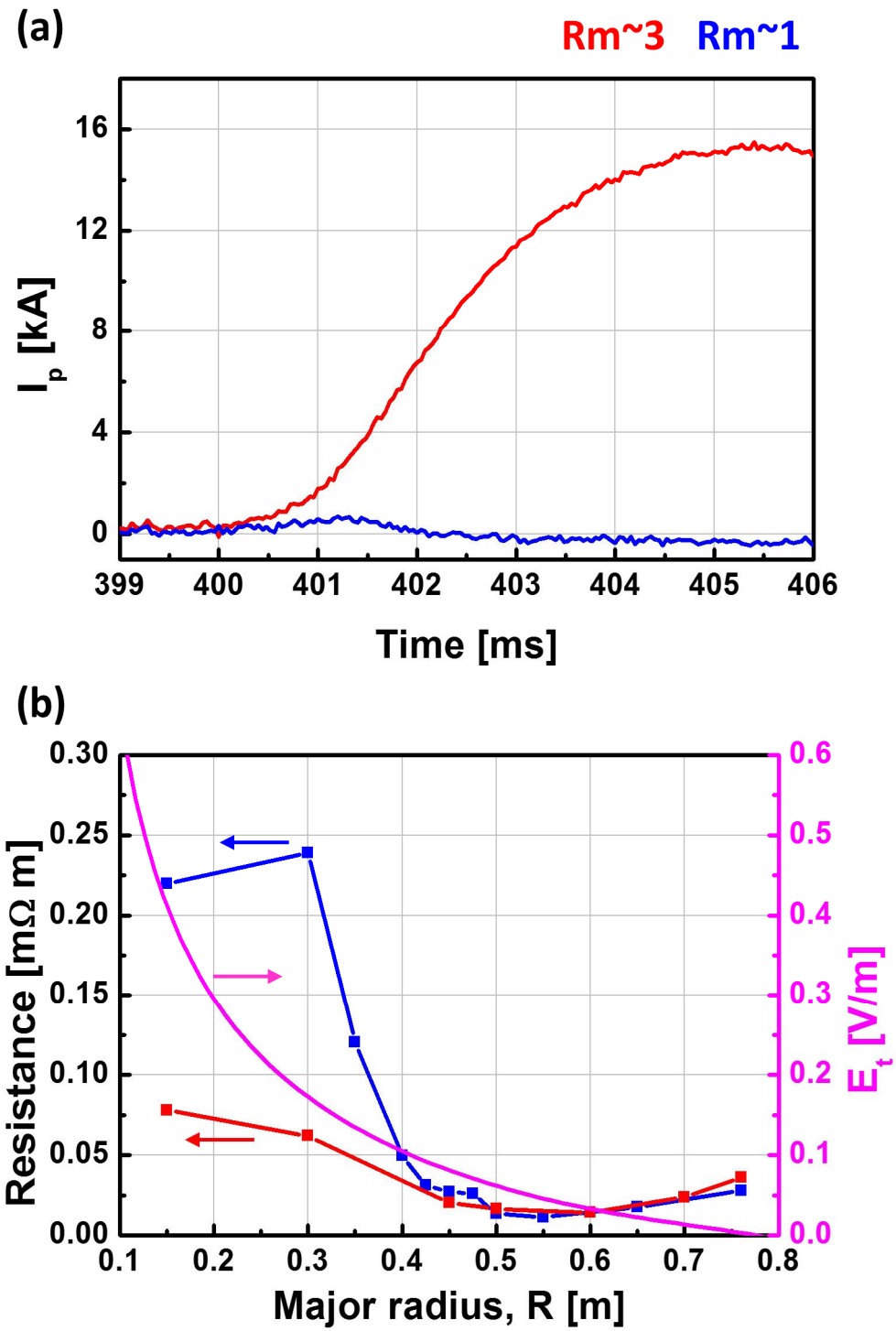

Figure A.3 Plasma start-up performance with different mirror ratio (a), and radial profile of pre-ionization plasma properties at the loop voltage applied time (b).

with the combination of radial and vertical component of poloidal magnetic field. The particle trapping effect by curved magnetic field structure makes more improved plasma confinement. The figure A.4 shows the connection length of both low and high magnetic mirror ratio experiments. The connection length of low mirror ratio case at the resonance layer is much longer than high mirror ratio case, but the plasma confinement is poor. Additionally, the curved structure makes broaden distribution of pre-ionization plasmas than low mirror ratio. The pre-ionization plasma at the high field side is essential for reliable start-up with high toroidal electric field.

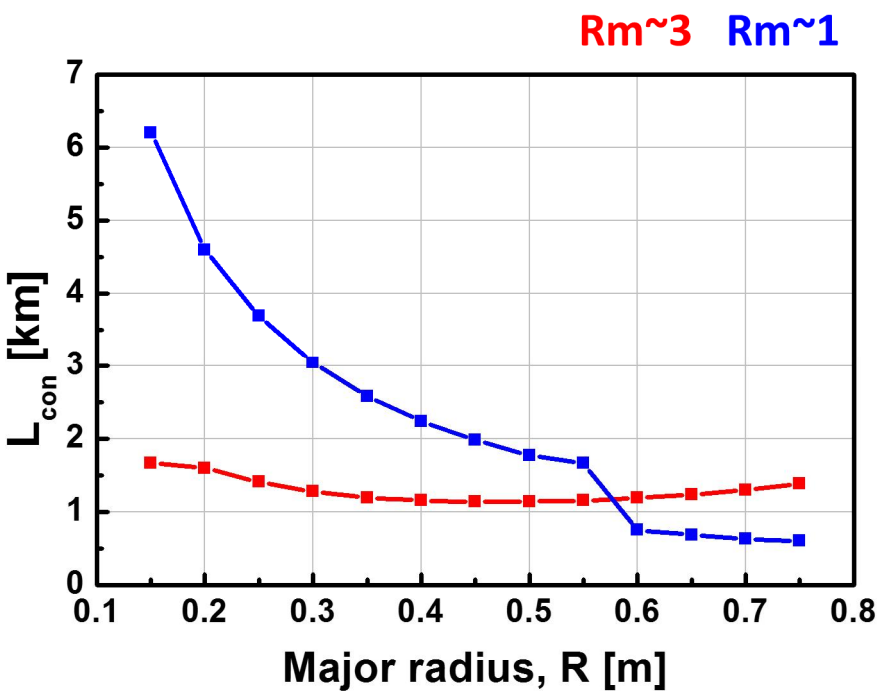

Figure A.4 Magnetic connection length of different magnetic mirror ratio scenario.

A2. Development of reference start-up scenario using TPC with full solenoid flux capability

The reference plasma start-up scenario using TPC is developed in VEST. The FNC-based scenario of VEST is not well suited for using the same method as KSTAR because of its strong stray magnetic field. Start-up scenario of KSTAR generates multipole null structure to maximize the low poloidal field region. And this is the same with other devices, like DIII-D [53]. But field configuration of VEST is monopole null, it is difficult to ignore the stray field. Furthermore, due to the low toroidal magnetic field, the poloidal field strength for the TPC cannot be raised to the KSTAR level.

However, VEST has advantages to generate TPC. Due to the elongated chamber for various researches related to plasma merging [54] or innovative divertor, VEST has a solenoid coil that is much longer than the main plasma chamber [55]. Thus, the solenoid initial charge current can create a TPC structure and only the poloidal magnetic field intensity can be controlled by the external coil. PF#5 is selected to compensate the too strong poloidal field strength generated by PF#1 and not to distort the TPC structure. Poloidal field structure of PF#1, PF#5, and TPC scenario (shot #14584) are depicted in figure A.5. The magnetic structure is calculated with eddy current effect [32].

Comparison of the plasma start-up performance between conventional FNC scenario and newly developed TPC scenario is conducted. With identical loop voltage, the TPC shows efficient plasma start-up according to the current ramp-up ratio and maximum achieved current.

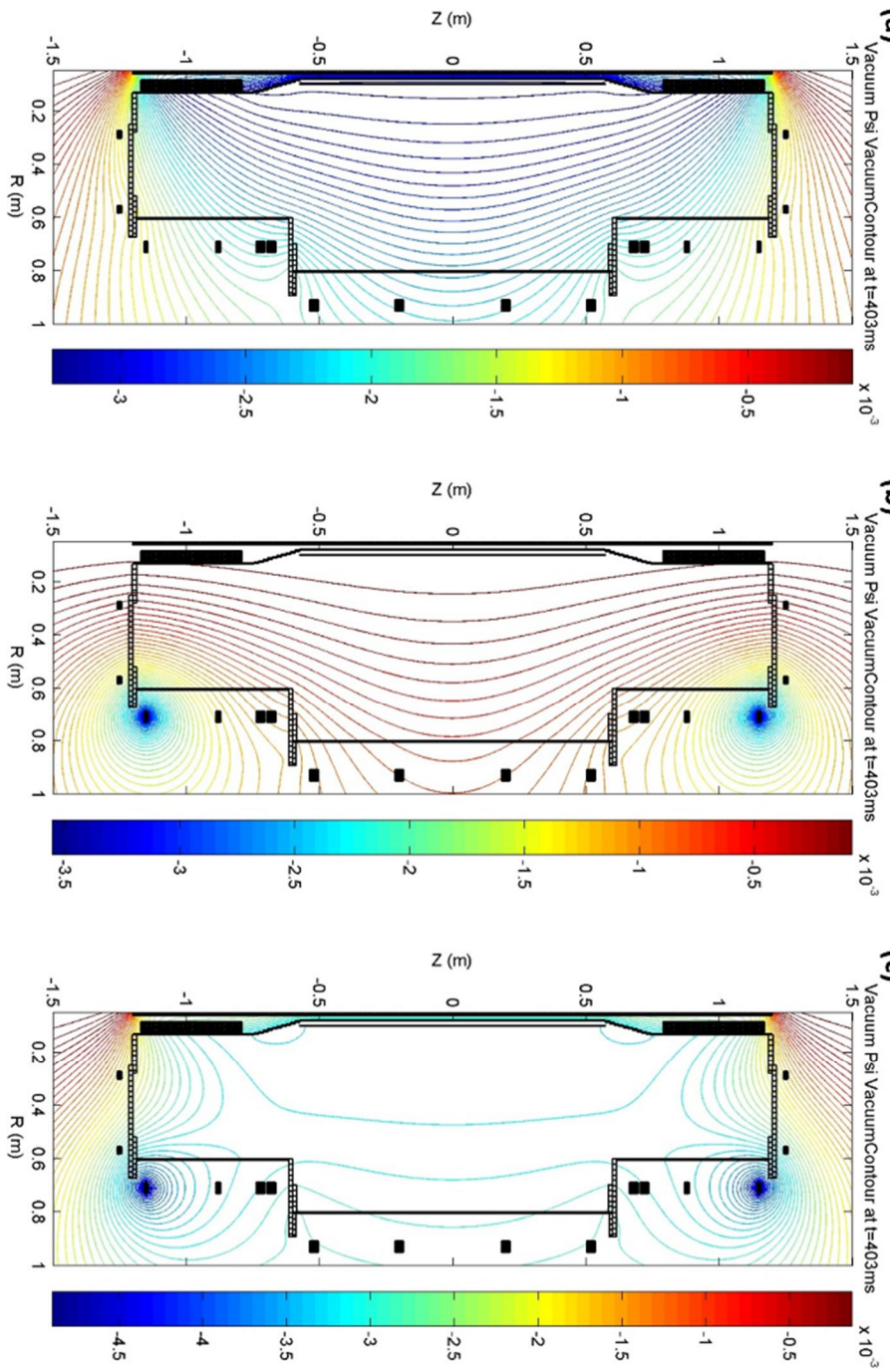

Figure A.5 Poloidal magnetic flux contour of PF#1 (a), PF#5 (b), and PF#1 and PF#5(c).

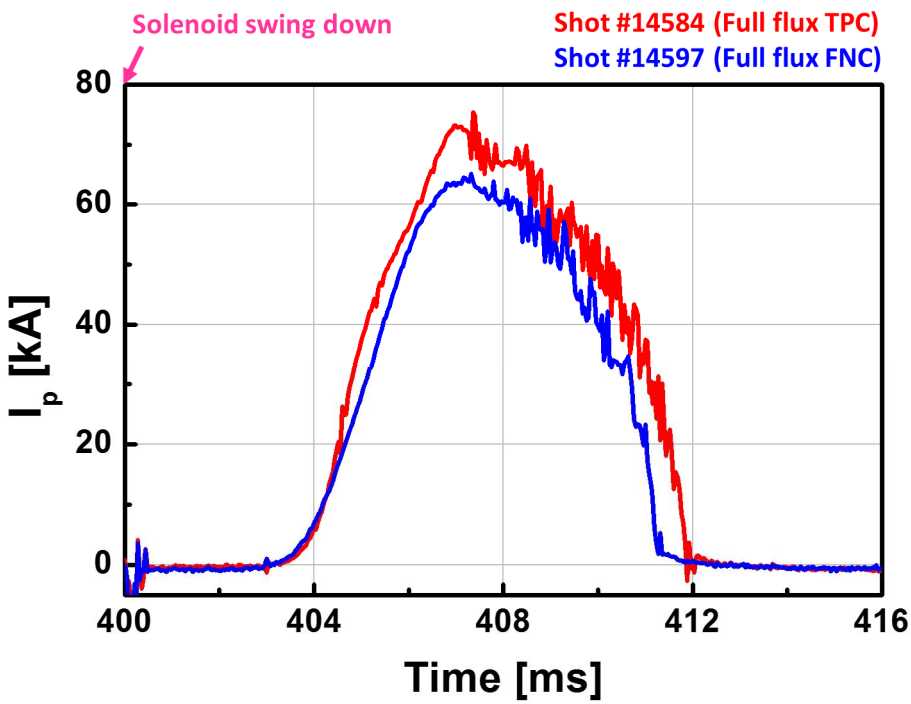

Figure A.6 Plasma current formation of FNC (#14597) and TPC(#14584).

Bibliography

[1] J. Wesson, "Tokamaks", *Clarendon Press Oxford*, (2004).

[2] L. Spitzer Jr, "The stellarator concept", *Physics of Fluids (1958-1988)*, **1,** 253 (1958).

[3] Y.M. Peng and D.J. Strickler, "Features of spherical torus plasmas", *Nuclear Fusion*, **26,** 769 (1986).

[4] M. Yoo, Y.-S. Na, J. Kim, Y. An, B. Jung, Y. Hwang, S. Shim, H. Lee, and T. Hahm, "On Ohmic Breakdown Physics in a Tokamak", (2014).

[5] W. Jiang, Y. Peng, Y. Zhang, and G. Lapenta, "Numerical modeling of tokamak breakdown phase driven by pure Ohmic heating under ideal conditions", *Nuclear Fusion*, **56,** 126017 (2016).

[6] Y.M. Peng, S. Borowski, and T. Kammash, "Microwave start-up of tokamak plasmas near electron cyclotron and upper hybrid resonances", *Nuclear Fusion*, **18,** 1489 (1978).

[7] D. Bulyginskii, M. Larionov, L. Levin, O. Miklukho, A. Tokunov, and N. Shustova, "Effect of the preionization method on the discharge in a tokamak", *Soviet Journal of Plasma Physics*, **6,** 11 (1980).

[8] T. Ocho, S. Kubo, M. Ikeda, T. Saito, Y. Terumichi, Y. Hamada, and S. Tanaka, "Microwave preionization of the tokamak discharge at the electron cyclotron resonance", *Physics Letters A*, **77,** 318 (1980).

[9] S. Tanaka, K. Hanada, T. Minami, S. Ide, M. Iida, H. Tanaka, T. Maekawa, and Y. Terumichi, "Initiation of plasma current with the assistance of electron cyclotron waves in the WT-3 tokamak", *Nuclear fusion*, **33,** 505

(1993).

[10] R. Gilgenbach, M. Read, K. Hackett, R. Lucey, V. Granatstein, A. England, C. Loring, J. Wilgen, R. Isler, and Y.M. Peng, "Electron cyclotron/upper hybrid resonant pre-ionization in the ISX-B tokamak", *Nuclear Fusion*, **21,** 319 (1981).

[11] K. Hoshino, T. Yamamoto, A. Funahashi, N. Suzuki, T. Matoba, T. Yamauchi, H. Matsumoto, T. Kawakami, H. Kimura, and S. Konoshima, "Electron cyclotron heating and pre-ionization in the JFT-2 Tokamak", *Journal of the Physical Society of Japan*, **54,** 2503 (1985).

[12] B. Lloyd and T. Edlington, "Low voltage start-up in the CLEO Tokamak using ECRH", *Plasma physics and controlled fusion*, **28,** 909 (1986).

[13] D. Holly, S. Prager, D. Shepard, and J. Sprott, "Tokamak start-up with electron-cyclotron heating", *Nuclear Fusion*, **21,** 1483 (1981).

[14] B. Lloyd, G. Jackson, T. Taylor, E. Lazarus, T. Luce, and R. Prater, "Low voltage ohmic and electron cyclotron heating assisted startup in DIII-D", *Nuclear Fusion*, **31,** 2031 (1991).

[15] K. Kajiwara, Y. Ikeda, M. Seki, S. Moriyama, T. Oikawa, T. Fujii, and J.-. Team, "Electron cyclotron heating assisted startup in JT-60U", *Nuclear Fusion*, **45,** 694 (2005).

[16] G.L. Jackson, M.E. Austin, J.S. deGrassie, A.W. Hyatt, J.M. Lohr, T.C. Luce, R. Prater, and W.P. West, "Plasma Initiation and Start-up Studies in the DIII-D Tokamak with Second-Harmonic EC Assist", *Fusion Science and Technology*, **57,** 27 (2010).

[17] J. Bucalossi, P. Hertout, M. Lennholm, F. Saint-Laurent, F. Bouquey, C.

Darbos, E. Traisnel, and E. Trier, "First experiments of plasma start-up assisted by ECRH on Tore Supra", *Nuclear Fusion*, **48,** 054005 (2008).

[18] H. Zohm, J. Adamek, C. Angioni, G. Antar, C. Atanasiu, M. Balden, W. Becker, K. Behler, K. Behringer, and A. Bergmann, "Overview of ASDEX Upgrade results", *Nuclear Fusion*, **49,** 104009 (2009).

[19] M. Joung, Y. Gorelov, S. Park, J.H. Jeong, Y.S. Bae, H.L. Yang, J.H. Kim, S.H. Han, J.G. Kwak, and J. Lohr, "Second Harmonic 110 GHz ECH-assisted Start-up in KSTAR", *EPJ Web of Conferences*, **32,** 02012 (2012).

[20] G. Granucci, S. Garavaglia, D. Ricci, G. Artaserse, F. Belli, W. Bin, G. Calabro, M. Cavinato, D. Farina, L. Figini, A. Moro, G. Ramogida, C. Sozzi, O. Tudisco, and F. Team, "Experiments and modeling on FTU tokamak for EC assisted plasma start-up studies in ITER-like configuration", *Nuclear Fusion*, **55,** 093025 (2015).

[21] Y.S. Bae, J.H. Jeong, S.I. Park, M. Joung, J.H. Kim, S.H. Hahn, S.W. Yoon, H.L. Yang, W.C. Kim, Y.K. Oh, A.C. England, W. Namkung, M.H. Cho, G.L. Jackson, J.S. Bak, and K. Team, "ECH pre-ionization and assisted startup in the fully superconducting KSTAR tokamak using second harmonic", *Nuclear Fusion*, **49,** 022001 (2009).

[22] G.L. Jackson, J.S. deGrassie, C.P. Moeller, and R. Prater, "Second harmonic electron cyclotron pre-ionization in the DIII-D tokamak", *Nuclear Fusion*, **47,** 257 (2007).

[23] A. Bruschi, R. Bozzi, S. Cirant, F. Gandini, G. Granucci, S. Mantovani, V. Mellera, V. Muzzini, A. Nardone, and S. Nowak, "ECRH antenna at 140 GHz on FTU tokamak", *Fusion engineering and design*, **53,** 431 (2001).

[24] S. Nakao, K. Ogura, Y. Terumichi, and S. Tanaka, "Particle loss from an electron cyclotron resonance discharge plasma in the WT-2 device", *Physics Letters A*, **96,** 405 (1983).

[25] S.H. Muller, A. Fasoli, B. Labit, M. McGrath, M. Podesta, and F.M. Poli, "Effects of a vertical magnetic field on particle confinement in a magnetized plasma torus", *Phys Rev Lett*, **93,** 165003 (2004).

[26] Y. An, J. Lee, J. Jo, B.-K. Jung, H. Lee, K.-J. Chung, Y.-S. Na, T. Hahm, and Y. Hwang, "Efficient ECH-assisted plasma start-up using trapped particle configuration in the versatile experiment spherical torus", *Nuclear Fusion*, **57,** 016001 (2017).

[27] K. Itami, S.-H. Hong, Y.-S. Bae, M. Matsukawa, and W.-C. Kim, "Wall-conditioning plasmas by ECRF heating in KSTAR", *Journal of Nuclear Materials*, **438,** S930 (2013).

[28] Y. Gribov, D. Humphreys, K. Kajiwara, E.A. Lazarus, J.B. Lister, T. Ozeki, A. Portone, M. Shimada, A.C.C. Sips, and J.C. Wesley, "Chapter 8: Plasma operation and control", *Nuclear Fusion*, **47,** S385 (2007).

[29] D. Mueller, "The physics of tokamak start-up", *Physics of Plasmas*, **20,** 058101 (2013).

[30] P.C. ITER Physics Expert Group on Disruptions, and MHD, "Chapter 8: Plasma operation and control", *Nuclear Fusion*, **39,** (1999).

[31] M.-G. Yoo, J. Lee, Y.-G. Kim, J. Kim, T.S. Hahm, Y.S. Hwang, and Y.-S. Na, "New understanding of the ohmic breakdown mechanisms in KSTAR", *KSTAR Conference 2017, Parallel Oral 3A-5*, (2017).

[32] Y. An, J. Lee, H. Lee, J. Jo, B.K. Jung, K.J. Chung, Y.G. Kim, J. Jo, J.H.

Yang, Y.S. Na, T.S. Hahm, and Y.S. Hwang, "Plasma start-up design and first plasma experiment in VEST", *Fusion Engineering and Design*, **96-97,** 274 (2015).

[33] R. Pillsbury and J. Schultz, "Modelling of plasma start-up in ITER", *IEEE transactions on magnetics*, **28,** 1462 (1992).

[34] J. Kim, S.W. Yoon, Y.M. Jeon, J.A. Leuer, N.W. Eidietis, D. Mueller, S. Park, Y.U. Nam, J. Chung, K.D. Lee, S.H. Hahn, Y.S. Bae, W.C. Kim, Y.K. Oh, H.L. Yang, K.R. Park, H.K. Na, and K. Team, "Stable plasma start-up in the KSTAR device under various discharge conditions", *Nuclear Fusion*, **51,** 083034 (2011).

[35] J. Kim, W. Choe, and M. Ono, "Time-dependent optimization of initiation phase of the outer PF coil-only inductive start-up of NSTX plasmas", *Plasma physics and controlled fusion*, **46,** 1647 (2004).

[36] B. Lloyd, P. Carolan, and C. Warrick, "ECRH-assisted start-up in ITER", *Plasma physics and controlled fusion*, **38,** 1627 (1996).

[37] V. Belyakov, K. Lobanov, L. Makarova, A. Mineev, and V. Vasiliev, "Plasma initiation stage analysis in tokamaks with TRANSMAK code", *Plasma Devices and Operations*, **11,** 193 (2003).

[38] Y.-s. Bae and W. Namkung, "Study of the effects of ECH power and pulse length on preionization in the KSTAR tokamak", *IEEE Transactions on plasma science*, (2003).

[39] Y.S. Bae and A. Engl, "Study on pre-ionization using second-harmonic electron cyclotron waves for the KSTAR first plasma", *Journal of Korean Physical Society*, **51,** 1313 (2007).

[40] H.T. Kim, W. Fundamenski, A.C.C. Sips, and E.-J. Contributors, "Enhancement of plasma burn-through simulation and validation in JET", *Nuclear Fusion*, **52,** 103016 (2012).

[41] H.T. Kim, A.C.C. Sips, and E.-J. Contributors, "Physics of plasma burn-through and DYON simulations for the JET ITER-like wall", *Nuclear Fusion*, **53,** 083024 (2013).

[42] H.T. Kim, A.C.C. Sips, P.C. de Vries, and J.-E. Contributors, "Plasma burn-through simulations using the DYON code and predictions for ITER", *Plasma Physics and Controlled Fusion*, **55,** 124032 (2013).

[43] P. Efthimion, M. Bell, W. Blanehard, N. Bretz, J. Cecchi, J. Coonrod, S. Davis, H. Dylla, R. Fonck, and H. Furth, "Initial confinement studies of ohmically heated plasmas in the tokamak fusion test reactor", *Physical review letters*, **52,** 1492 (1984).

[44] E. de la Cal, "Theoretical modelling of deuterium ICRF wall conditioning discharges", *Plasma physics and controlled fusion*, **48,** 1455 (2006).

[45] O. Eldridge, W. Namkung, and A. England, *Electron cyclotron heating in tokamaks*. 1977, Oak Ridge National Lab., Tenn.(USA).

[46] S. Yoon, A. England, W. Kim, H. Yonekawa, J. Bak, B. Park, J. Kim, K. You, Y. Jeon, and S. Hahn, "Effect of magnetic materials on the in-vessel magnetic configuration in KSTAR", *Fusion Science and Technology*, **65,** 372 (2014).

[47] S.-H. Hahn, K. Kim, J. Choi, H. Ahn, D. Lee, K. Park, N. Eidietis, J. Leuer, M. Walker, and H. Yang, "Controls on KSTAR Superconducting Poloidal Field (PF) Magnets", *Progress in Superconductivity and Cryogenics*, **10,**

23 (2008).

[48] J. Jeong, K. Sakamoto, M. Joung, S. Park, H. Kim, W. Han, J. Kim, Y. Bae, H. Yang, and J. Kwak. *Commissioning of 170 GHz, 1 MW EC H&CD in KSTAR*. in *EPJ Web of Conferences*. 2012. EDP Sciences.

[49] N. Luhmann Jr, H. Bindslev, H. Park, J. Sanchez, G. Taylor, and C. Yu, "Microwave diagnostics", *Fusion Science and Technology*, **53,** 335 (2008).

[50] A. Ejiri and Y. Takase, "Toroidal current initiation in low aspect ratio tokamaks based on single-particle orbit analysis", *Nuclear fusion*, **47,** 403 (2007).

[51] P. Carolan and V. Piotrowicz, "The behaviour of impurities out of coronal equilibrium", *Plasma Physics*, **25,** 1065 (1983).

[52] J. Stober, G.L. Jackson, E. Ascasibar, Y.S. Bae, J. Bucalossi, A. Cappa, T. Casper, M.H. Cho, Y. Gribov, G. Granucci, K. Hanada, J. Hobirk, A.W. Hyatt, S. Ide, J.H. Jeong, M. Joung, T. Luce, T. Lunt, W. Namkung, S.I. Park, P.A. Politzer, J. Schweinzer, A.C.C. Sips, A.U. Team, T.-I. Team, and I.I.O. Scenar, "ECRH-assisted plasma start-up with toroidally inclined launch: multi-machine comparison and perspectives for ITER", *Nuclear Fusion*, **51,** 083031 (2011).

[53] E. Lazarus, A. Hyatt, G. Jackson, and D. Humphreys, "Using a multipole expansion for startup in the DIII-D tokamak", *Nuclear fusion*, **38,** 1083 (1998).

[54] K.J. Chung, Y.H. An, B.K. Jung, H.Y. Lee, J.J. Dang, J.W. Lee, J. Yang, J.G. Jo, D.H. Choi, Y.G. Kim, Y.S. Na, and Y.S. Hwang, "Initial plasma start-up using partial solenoid coils in Versatile Experiment Spherical Torus

(VEST)", *Fusion Engineering and Design*, **88,** 787 (2013).

[55] K.J. Chung, Y.H. An, B.K. Jung, H.Y. Lee, C. Sung, Y.S. Na, T.S. Hahm, and Y.S. Hwang, "Design Features and Commissioning of the Versatile Experiment Spherical Torus (VEST) at Seoul National University", *Plasma Science & Technology*, **15,** 244 (2013).

Abstract in Korean

입자가둠 구조를 활용한 효율적이고 효과적인 전자공명가열 플라즈마 시동이 초전도 토카막인 KSTAR에서 증명되고, 플라즈마 시동 전산 모사를 통해 분석되었다. 자기장 성능과 중수소 압력에 따른 입자가둠 구조의 특성이 연구되었다. ITER와 같은 조건에서 입자가둠 구조를 이용한 안정적인 플라즈마 시동이 가능함이 KSTAR에서 확인되었고, 기존 널 자기장 구조를 이용한 ITER 시나리오를 대신하여 입자가둠 구조를 이용한 시나리오가 제시되었다.

전자공명가열 도움을 이용한 플라즈마 시동은 JT60-SA 혹은 IITE와 같은 미래 토카막 장치들의 플라즈마 시동 단계의 어려움을 극복하기 위해 제안되었다. 초전도 코일의 운전 한계로 인하여 유도적 방법으로 인가되는 전기장이 현재 토카막 장치보다 낮다. 또한 큰 맴돌이 전류와 자성 구조체로 인해 폴로이달 자기장을 정확히 제어하기가 어렵다. 전자공명가열을 이용한 플라즈마 시동은 이러한 제한된 유도적 인가 파워와 폴로이달 자기장 조건을 완화하기 위해 연구되어 왔다.

많은 연구들이 전자공명가열 도움을 통한 플라즈마 시동 시 기존의 널 자기장 대신 자기장 구조가 있을 때 효율성이 증가될 수 있음을 보여 왔다. 가장 최근 VEST 장치에서 개발된 입자가둠 방법은 기존에 비해 강화된 전이온화 플라즈마의 가둠 성능과 이로 인해 넓은 운전 영역에서 효율적인 플라즈마 시동이 가능함을 보여주었다.

입자가둠 구조의 특성이 큰 초전도 토카막에서 확인되어야 한다. 입자가둠 방법은 JT60-SA 혹은 ITER와 같은 미래 토카막에서 예상되는 플라즈마 시동의 문제점을 해결할 수 있을 것으로 기대되지만, 추가적인 연구를 통한 확인이 필요하다. 입자가둠 구조를 KSTAR에 적용할 때 고려한 점들은 다음과 같다. 우선 입자가둠 구조를 만들기 위한 코일을 초기 PF 코일들의 충전 전류를 고려하여 신중하게 선택되었다. 두 번째로 높은 종횡비로 인한 낮은 입자 가둠 비율임에도 불구하고 플라즈마 시동에 도움을 줄 수 있는지 확인해야 한다. 세 번째로, 입자가둠 구조의 운전 영역을 알아야 하고, 마지막으로 ITER와 같은 조건에서도 유효한지 확인해야 한다.

입자가둠 구조를 이용한 플라즈마 시동이 KSTAR에서 시도되었다. 입자가둠 구조를 이용한 시나리오는 기존의 널 기반 시나리오에 미러와 같은 구조를 덮어 씌우는 방식으로 개발되었다. 600 kW의 170 GHz, X2의 전자공명가열이 이용되었고, 토로이달 방향으로 20도의 각도를 가지고 입사되었다. 입자가둠 구조의 유효성과, 기존 필드 널에 비해 효율적인 시동이 가능함이 실험적으로 증명되었다.

낮은 입자가둠비 조건에서 입자가둠 구조가 유효한지를 0차원 플라즈마 시동 모사 코드인 TECHP0D 코드를 통해 분석하였다. 플라즈마 가둠 모델에서 전도 손실을 줄일 수 있도록 개선되었다. 입자가둠 구조를 이용한 실험 결과를 모사해 본 결과 대략 35 %의 전도 손실 감소가 있을 때 실험 결과가 재현되었다. 이 비율은 단일입자 계산을 통해

도출된 입자 가둠 비율과 유사한 값을 가진다.

입자가둠 구조의 운전 영역이 KSTAR의 2015년과 2016년 실험 결과를 통해 확인되었다. 입자가둠 구조를 이용하여 플라즈마 시동이 성공한 16샷을 통해, 폴로이달 자기장 성능과 중수소 압력에 대한 운전 영역이 기존의 널 구조보다 확장되어, 폴로이달 자기장은 5배, 중수소 압력은 1.5배 증가할 수 있다.

KSTAR에서 수행된 전체 27개의 입자가둠 구조를 이용한 실험 샷을 통해 입자가둠 구조의 운전 한계를 확인할 수 있다. 폴로이달 자기장 성능과 중수소 압력에 대한 운전 영역에서, 자기장 성능과 무관한 높은 중수소 압력 한계와, 자기장 성능과 선형적 관계를 가지는 낮은 중수소 압력 한계가 발견되었다. 폴로이달 자기장 성능과 중수소 압력에 대한 의존성 실험에서, 두 가지 종류의 플라즈마 시동 실패 조건이 확인되었다. 하나는 전이온화 플라즈마의 이온화율이 낮을 때 이고, 다른 하나는 전이온화 플라즈마의 밀도가 낮을 때 이다.

이러한 운전 한계가 TECHP0D 코드를 통해 확인되었다. 낮은 전이온화 밀도의 경우, 감소한 복사 손실로 인해 높은 전자온도가 달성될 수 있다. 복사 장벽이 전자공명가열만을 통해 극복될 수 있다. 그러나 이러한 높은 전자 밀도는 닫힌 자속면 형성보다 빠른 전도 손실 시간을 유발하고, 따라서 플라즈마 시동이 실패한다. 낮은 이온화율의 경우 토로이달 전기장 인가 후 이온화 반응에 의한 에너지 손실이 발생한다. 이러한 손실은 전자 온도 상승을 방해하고, 플라즈마 저항을 높게 만들어 플라

즈마 시동을 실패하게 만든다.

입자가둠 구조의 ITER 적용 가능성을 연구하였다. ITER 수준의 낮은 토로이달 전기장 상황에서 입자가둠 구조를 이용한 플라즈마 시동 실험이 KSTAR에서 성공적으로 수행되었다. 700 kW의 전자공명가열 파워가 인가되었고, 전체 플라즈마 시동 단계에서 토로이달 전기장이 ITER 목표보다 낮게 유지되었다. 입자가둠 구조가 ITER PF 코일 구조를 이용해서 형성될 수 있음이 확인되었다. 상하 비대칭 구조를 고려하여, PF#1과 PF#6의 인가 전류를 조절함으로써 입자가둠 구조가 형성될 수 있다. 새롭게 개발된 입자가둠 구조를 통한 ITER 시동 시나리오가 제시되었고, 기존의 널 기반 시나리오와 비교되었다. 솔레노이드 코일의 자속 절약과, 안정적인 초전도 코일 운전이 가능할 것으로 기대된다.